Chromium Stable Isotope Variations in the Early Solar System and Deep Earth

Matthew Jerram
St. Edmund Hall
University of Oxford

A thesis submitted for the degree of
Doctor of Philosophy
Trinity Term 2019

Supervisors: A.N. Halliday & P. Bonnand

Abstract

Chromium Stable Isotope Variations in the Early Solar System and Deep Earth

A thesis submitted for the degree of Doctor of Philosophy

Trinity Term 2019

Matthew Jerram

This study uses high precision chromium (Cr) isotope measurements to provide insights into the composition of the mantle, and constraints on the material from which Earth accreted. This involved achieving a deeper understanding of Cr isotope fractionation, facilitating the determination of a more precise δ^{53}Cr for the bulk silicate Earth (BSE). This in turn leads to a comparison with different classes of chondrites as representatives of distinct types of disk material.

The δ^{53}Cr composition of the mantle is unaffected by partial melting, but is perturbed by different metasomatic processes, which has created a δ^{53}Cr heterogeneous mantle. An accurate δ^{53}Cr BSE value cannot be acquired using mantle peridotites due to the widespread metasomatic variations they record. An alternative method to calculate the δ^{53}Cr BSE composition is to use komatiites, as they sample a large volume of the mantle. The δ^{53}Cr of komatiites varies during fractional crystallisation, which must be considered when calculating the initial composition. Different methods were used to determine the initial composition of the komatiite liquid. A weighted average is best able to account for the variations to the δ^{53}Cr during crystallisation, and produces a well-constrained BSE composition, -0.12 ± 0.03 ‰.

Enstatite chondrites are meteorites that may have made up a significant proportion of the material that formed the Earth. The δ^{53}Cr isotopic composition of the enstatite chondrites are within error of the BSE, with the closest match provided by EH chondrites.

Extended abstract

Chromium Stable Isotope Variations in the Early Solar System and Deep Earth

A thesis submitted for the degree of Doctor of Philosophy

Trinity Term 2019

Matthew Jerram

The chromium (Cr) isotope composition of the Bulk Silicate Earth (BSE) provides insights into the early history of the Earth, including the material from which it formed (as represented by chondritic materials) and the conditions of core formation. Past studies have been unable to provide a precise value for the composition of the BSE using traditional approaches; even fertile and seemingly unaltered peridotites have a large range in Cr stable isotope compositions. BSE values calculated using this method are poorly constrained, -0.12 ± 0.10 ‰ (Schoenberg et al., 2008) and -0.14 ± 0.12 ‰ (Xia et al., 2017). These BSE values are of limited use in providing constraints on the formation of Earth, as the range encompasses the composition of most extra-terrestrial bodies.

The Cr behaviour in mantle peridotites was explored first, in order to ascertain whether a selection of mantle peridotites could be used to calculate a more precise isotope composition of the Earth. A total of 42 ultramafic samples were measured, and considered alongside measurements from previous studies. Samples measured included spinel and garnet lherzolites, harzburgites, dunites, one wehrlite and one pyroxenite. The effects of partial melting and metasomatism were of particular interest as both had previously been used to explain the $\delta^{53}Cr$ variations of the mantle. Past studies disagreed on the effect of partial melting on the $\delta^{53}Cr$ value of the mantle (Schoenberg et al., 2008; Xia et al., 2017; Shen

et al., 2018). We find no evidence that the $\delta^{53}Cr$ of the mantle is affected by partial melting. This is expected, as only small fractionations occur during melting (<0.1 ‰), and the compatible behaviour of Cr in the mantle means that the change this will create in the $\delta^{53}Cr$ of the mantle is insignificant (<< 0.1 ‰).

Metasomatism has previously been used to explain extreme Cr isotope compositions (Xia et al., 2017). Metasomatic alterations are identified in high $\delta^{53}Cr$ peridotites, which show trace element compositions indicative of carbonatite metasomatism such as high La/Yb combined with low Ti/Eu. Carbonatites have low concentrations of Cr. Therefore, for carbonatite metasomatism to lead to large isotope fractionation in the mantle, disequilibrium loss of Cr into the carbonatite melt, due to Cr undersaturation of these melts is required. This process may not be limited to carbonatite melts, with high $\delta^{53}Cr$ compositions possibly caused through interactions with a range of Cr deficient melts. Chromium stable isotope ratios in the mantle are widely affected by this, hard to identify, metasomatism. Therefore, it is not possible to use peridotites to calculate an accurate estimate of the BSE.

An alternative method for calculating the $\delta^{53}Cr$ composition of the BSE is to use komatiites. Their high degree of melting means that they have compositions similar to the mantle from which they formed. Komatiites form by melting large volumes of the mantle, such that localised heterogeneities caused by metasomatism are of no consequence. Komatiites can only be used to estimate the BSE if the melts are not fractionated during melting. The amount of $\delta^{53}Cr$ fractionation during melting between the mantle and basaltic liquids is small (<0.1 ‰), with any variations further reduced in komatiite due to the high temperatures of their formation. The BSE has previously been estimated using a compilation

of komatiites and other peridotites, with an improved accuracy, -0.11 ± 0.06 ‰ (Sossi et al., 2018a).

The second part of the research project was a detailed study of the $\delta^{53}Cr$ behaviour within komatiite flows in order to calculate a new $\delta^{53}Cr$ BSE value. Komatiite suites from three localities were studied, each of which showed different $\delta^{53}Cr$ behaviour. One komatiite flow displays an increase in $\delta^{53}Cr$ as the liquid evolves, while another has no variation in $\delta^{53}Cr$. Isotopically light olivine excesses and deficits can explain the $\delta^{53}Cr$ variations. The isotopic composition of olivine depends on the temperature controlled $Cr^{2+}/\Sigma Cr_{TOT}$ ratio, which is why some flows show $\delta^{53}Cr$ variations while others do not. The $\delta^{53}Cr$ variation during crystallisation must be taken into account when calculating the initial flow composition. Different methods for calculating the initial komatiite liquid composition were used, with the weighted average providing a reproducible value across all flows, and one that was best able to account for the variations from crystallisation. Using the initial komatiite liquid composition of the komatiite localities in this study, as well as two well sampled flows measured in Sossi et al. (2018a), a new value of the BSE of -0.12 ± 0.03 ‰, is proposed.

The $\delta^{53}Cr$ BSE value can be used to identify the type of material from which Earth accreted. Different types of chondrites have been proposed as the building blocks of the Earth. Ordinary chondrites have a chemical composition closest to Earth, while enstatite chondrites have the closest match to the isotopic composition. Heterogeneous Earth formation models use a mixture of these two groups of chondrites forming at different stages (Dauphas, 2017). Only two previous $\delta^{53}Cr$ measurements of enstatite chondrites have been made, and so further investigation is required to constrain this possibly major contributor to the composition of the Earth.

The final section of this work provides the $\delta^{53}Cr$ isotopic composition of 11 enstatite chondrites from both the EH and EL enstatite parent bodies. Different behaviour of Cr is identified in the two groups, however this is due to the higher petrological types of the EL6 chondrites, allowing isotopic equilibrium to be reached. Variations in the EL enstatite chondrites occur due to heterogeneous sampling of isotopically light troilite. The EH chondrites measured in this study were of lower petrological grade, and $\delta^{53}Cr$ variations within this class show relic fractionations from the solar nebula. The composition of EL chondrites (-0.05 ± 0.10 ‰ 2 s.d.) shows no signification difference to the composition of the EH chondrites (-0.09 ± 0.04 ‰ 2 s.d.) (at the 95% confidence interval using a two tailed t test). The BSE isotope composition is best achieved with accretion of ordinary chondrites and EH chondrites.

ACKNOWLEDGEMENTS

To begin with, I would like to thank my supervisors Alex Halliday and Pierre Bonnand for all of their support and guidance throughout. Many thanks to Alex for the discussions on the working of the solar system through the years, and ensuring that I was well watered at all pub meetings. Pierre was an excellent teacher, challenging me on my data and interpretations, as well as teaching me all I know in the lab. Finally, it was much appreciated that you both gave me the freedom to cycle to my heart's content, which I'm sure helped me complete my thesis.

Thanks to the rest of the cosmotope group with all of its different members throughout the years for being a great bunch of people. A special mention must be given to Jane Barling, for providing cake at coffee time along with some more exotic offerings, for her kindness in proof reading my often impenetrable writing, and for her time spent aiding in a wide range of problems in the lab. I should also mention Sean Hopkins and Naomi Saunders, my fellow students over the past many years, for your friendships and discussions on isotopes.

I would not have been able to complete any of my lab work without the help of the technical staff in the department. Alan, for teaching me all of the correct ways to turn the TIMS off and on again. Phil, for providing me with top quality chemical data. Thanks to Steve for providing excellent assistance within the labs.

The fellow inhabitants of office 20.16, past and present, have made working in department more pleasurable, even if not more productive. Thanks for putting up with my mess, and maybe one day, some of you will come to the pub with me for lunch.

Lastly I need to thank my family for supporting me through out. It's good to see that I have been an inspiration in my sisters decision to return to academia.

CONTENTS

LIST OF FIGURES

LIST OF TABLES

Chapter 1: Introduction

1.1. GEOCHEMICAL BEHAVIOUR OF CHROMIUM

Chromium is the 16th most abundant element in the solar system. It is a slightly volatile element, with a half-mass condensation temperature of 1296 K (Lodders, 2003). Chromium occurs in a range of valence states in natural systems (Cr^{2+}, Cr^{3+} and Cr^{6+}), which have widely different geochemical behaviour. For example, depending on the oxygen fugacity, Cr may be a lithophile, siderophile or chalcophile; under oxidising conditions Cr becomes more volatile (O'Neill, 1991); and the oxidation state of Cr determines its behaviour during melting in silicate systems. This variable behaviour makes chromium a useful tool for investigating the geochemical development of our Solar System.

1.1.1. Chromium in the bulk Earth and core formation

The bulk Earth is thought to have formed from material with chondritic (i.e. solar) relative abundances of refractory and moderately volatile elements. Chondrites are ancient meteorites that never experienced the high temperatures required for melting on their parent body and as a result are undifferentiated. This is either because they did not form early enough to be heated by the decay of short lived radionuclides (such as ^{60}Fe and ^{26}Al) (Hevey and Sanders, 2006), they formed in regions that were deficient in radionuclides (Larsen et al., 2011), or that they did not grow large enough to experience significant gravitational heating (Palme and O'Neill, 2014). As their composition has not been fractionated by metal-silicate differentiation or melting they provide an insight into the early solar system composition. Variations in the abundances of elements in the bulk silicate Earth (BSE) relative to chondrites reflect loss of material to the core and through volatilisation. Chondrites are comprised of three classes, ordinary, carbonaceous and enstatite, which vary in their chemical and isotopic composition (e.g. Wasson and Kallemeyn, 1988; Trinquier et al., 2007; Warren, 2011 etc.). Isotopically the enstatite chondrites are most similar to Earth (e.g. Javoy et al, 2010 and

Warren, 2011), however they have different chemical compositions. The Mg/Si ratio of enstatite chondrites is much lower than that of Earth's upper mantle, which requires an unrealistic amount of Si included in the core (Fitoussi and Bourdon, 2012), or invoking a chemically distinct lower mantle (Javoy et al., 2010). None of the chondrites provide a close approximation of the chemical composition of Earth (Jagoutz et al., 1979). Heterogeneous accretion models for the formation of Earth show that the isotopic composition can be recreated if a small amount of ordinary chondrites are included during the early stage of the formation of Earth (Dauphas, 2017). This reduces the problems associated with using either class of chondrite. While it is unclear if enstatite or ordinary chondrites are the most important constituent, they have similar Cr concentrations which constrains the Cr composition of the bulk Earth to be between 3050-3740 ppm (Wasson and Kallemeyn, 1988). This value is enriched compared to that of the BSE at 2520 ppm (Palme and O'Neill, 2014), therefore Cr has been lost from the BSE during the formation of Earth.

Part of the Cr lost from the BSE may have been through volatilisation. The half condensation temperature of Cr designates it a transitional volatility element, i.e. a slightly volatile element (McDonough and Sun, 1995). The depletion of Cr in the BSE can be compared to other elements with similar volatilities (e.g. Si and Li) (Lodders, 2003)Lo. These elements are less depleted than Cr within the BSE, suggesting that the Cr abundance cannot be explained by volatility alone (McDonough and Sun, 1995). The half condensation temperature used in McDonough and Sun (1995) relates to conditions in the solar nebula and not terrestrial conditions. Under more oxidising conditions the volatility of Cr will not be the same (Lamoreaux et al., 1987; O'Neill, 1991). The numerous oxidised gaseous species that Cr can form (Chase, 1998) become more stable under oxidising conditions making Cr more volatile (O'Neill, 1991; Sossi et al., 2018a, 2019). Depending upon the conditions of Earth's formation,

volatilisation may have had a greater impact on the Cr content of Earth, than suggested by the half condensation temperature of McDonough and Sun (1995).

The depletion in the mantle can also be explained by removal of Cr into the core. Geophysical data suggests that the core is mainly made up of Fe and Ni, with 5 - 10 % lighter elements (Birch, 1964), which could include Cr. Experiments have shown that Cr can act as a siderophile (e.g. Wood et al., 2008). Mass balances used to estimate the amount of Cr within the core range from 7790 and 8000 ppm (Allègre et al., 1995; McDonough and Sun, 1995).

The metal / silicate partitioning of Cr during core formation can help determine the conditions of planetary formation. The behaviour of Cr is controlled by a number of parameters, such as pressure, temperature and fO_2 (Wood et al., 2008; Siebert et al., 2011; Fischer et al., 2015). Increasing pressure and temperature result in a small increase in the Cr solubility within metal, however the largest effect is from fO_2. Changes in the oxygen fugacity from ΔIW -1 to -4 increases the compatibility of Cr by over an order of magnitude (Siebert et al., 2011; Bonnand and Halliday, 2018). The reduced conditions required for Cr to enter the core therefore appear inconsistent with the present oxidised Earth's mantle. Core formation on Earth lasted for an extended period of time, >10 million years (e.g. Kleine et al., 2004), over which the oxygen fugacity of Earth may have changed. Contradictory studies suggest that during this time the Earth became more oxidised (Wade and Wood, 2005; Rubie et al., 2011), and less oxidised (Badro et al., 2015). A period of reduced conditions during core formation, whether early or later, can explain the Cr depletion in the mantle.

1.1.2. Chromium behaviour in the mantle

The BSE is comprised of the mantle and the crust. The crust and mantle system has evolved in composition through billions of years of melting and recycling. The Cr

concentration of the crust is lower than the mantle, as Cr behaves compatibility during melting. The chromium concentration of basalts, melts that form the oceanic crust today, is less than 500 ppm (Basaltic Volcanism Study Project, 1981). This is depleted compared to the mantle value of 2500ppm (McDonough and Sun, 1995), therefore melting of the mantle under normal conditions Cr has a bulk coefficient (K_d = ($[Cr]_{mantle}/[Cr]_{melt}$)) of > 5. Chromium's compatible nature during melting under normal mantle conditions has been reproduced by experiments, that show melts become saturated in Cr at 500 ppm (Li et al., 1995; Hanson and Jones, 1998). A bulk coefficient of 5 is required to explain the composition of the crust, but this value can vary greatly to create an array of Cr concentration in melts. High degree partial melts, such as komatiites, have much higher Cr concentrations (Liang and Elthon, 1990), while low degree partial melts such as carbonatities and nephelinites can have Cr concentrations of less than 100 ppm, which requires a bulk coefficient greater than 20. Different conditions existed in the mantle in the past which may have changed the Cr behaviour of the mantle over time.

Figure 1.1.

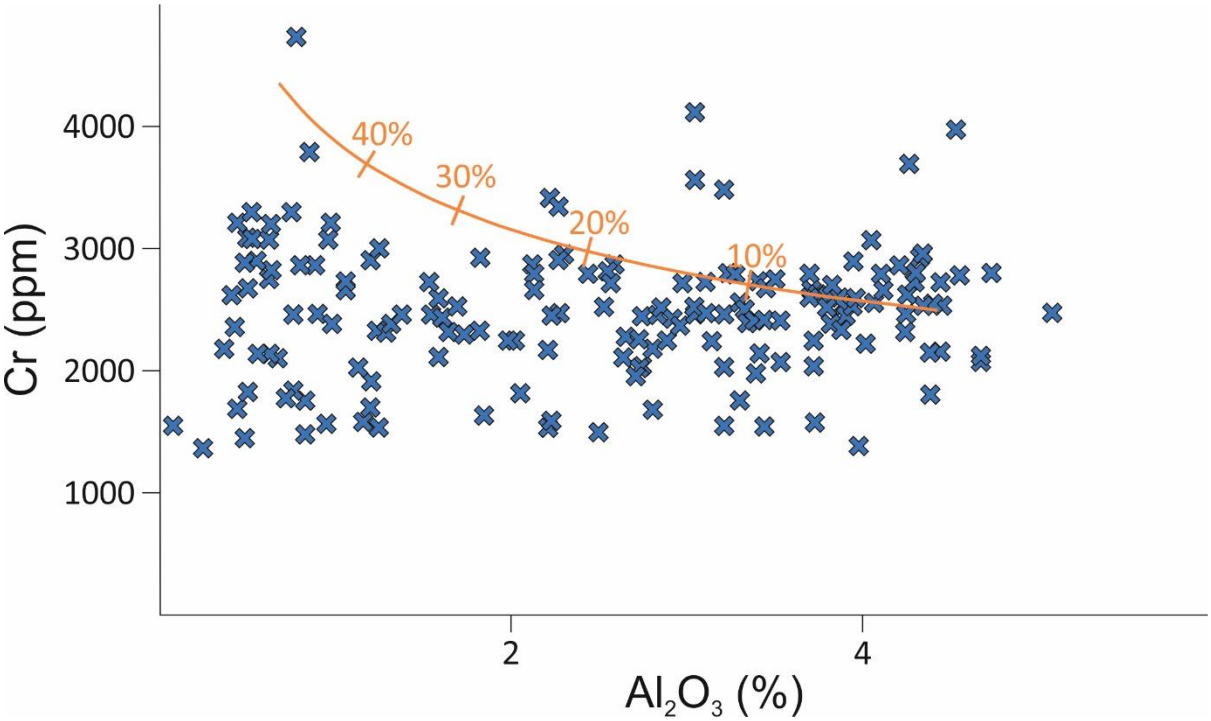

Figure 1.1. Peridotite compilation of Cr concentrations plotted against the Al_2O_3 %, which can be used as a proxy for partial melting. The Cr concentrations show no variation with degree of melting, as indicated by decreasing Al_2O_3 %. The orange line shows the calculated evolution of Cr concentrations within the residue, if the bulk coefficient of Cr is 5, which does not fit with the [Cr] data. Peridotite data from Ionov, (2004); Ionov et al., (2005); Ionov and Hofmann, (2007); Ionov, (2010); Harvey et al., (2012); Xia et al., (2017).

The conditions of partial melting will be recorded within the residues of melting (mantle peridotites), as well as the melt products. Mantle peridotites chemical composition records the cumulative effects of melt extraction of the upper mantle. If Cr has behaved compatibility throughout the history of Earth then there will be an increase in its concentration within the mantle. Peridotites that have undergone 20 % melting, with a bulk coefficient of 5, would have an increase in their Cr concentration by >450 ppm (as modelled

in Figure 1.1.). This increase in Cr is not seen (Figure 1.1.). Instead, Cr concentration within peridotites is best described by a bulk distribution coefficient for Cr of 1, i.e. melts removed from the mantle have the same Cr concentration as the mantle. No melts being created today have the same Cr concentration as the mantle, suggesting that the Cr signature recorded in mantle peridotites is preserved from an earlier epoch. Two types of high Cr melts have been proposed to explain this signature. Liang and Elthan (1993) suggested that melts extracted from peridotites were komatiitic in composition, with Cr concentrations of 1000-3000 ppm. Alternatively, Frey et al (1985) suggested that the high Cr melts fractionated into chromium pyroxenites and basaltic melts, the latter of which were erupted. This explanation can be discounted as the composition of basalts created from this melt would be fractionated and not representative of basalts. The type of melt extracted from the mantle remains unclear, however in order to create high Cr melts different conditions of melting were required compared to those present today.

The compatibility of Cr can be affected by the physical conditions experienced during melting. Chromium in the mantle can occur as either Cr^{3+} or Cr^{2+}, which have very different compatibilities. The presence of Cr^{2+} has been confirmed by XANES (Berry and O'Neill, 2004; Berry et al., 2006), although the amount of Cr^{2+} within the mantle is hard to quantify as it becomes oxidised at low pressures through donation of electrons to Fe ($Cr^{2+} + Fe^{3+} \rightarrow Cr^{3+} + Fe^{2+}$ (Berry and O'Neill, 2004)). The $Cr^{2+}/\Sigma Cr_{TOT}$ of the mantle will alter the behaviour of Cr. During melting Cr^{3+} behaves compatibly, while Cr^{2+} is incompatible (Schreiber and Haskin, 1976; Roeder and Reynolds, 1991). For most mantle minerals Cr^{3+} is preferred to Cr^{2+}, apart from olivine where the larger Cr^{2+} ion is able to substitute more easily with Mg^{2+} (Hanson and Jones, 1998; Papike et al., 2005). The compatibility of Cr is lower when melting a rock with higher $Cr^{2+}/\Sigma Cr_{TOT}$, however within the modern mantle, the Cr^{2+} is low.

The $Cr^{2+}/\Sigma Cr_{TOT}$ is controlled by the oxygen fugacity and the temperature (Li et al., 1995). Studies into the oxidation state of the Earth's mantle show that it has been constant over time (e.g. Canil, 1997; Hibbert et al., 2012) and therefore cannot not have affected the $Cr^{2+}/ \Sigma Cr_{TOT}$. High temperature conditions are likely to have prevailed in the past, as shown by abundant high degree melts created within previous epochs. The higher temperature within the mantle would increase the $Cr^{2+}/ \Sigma Cr_{TOT}$ and so lower the compatibility of Cr (Li et al., 1995).

The mineral assemblage of the mantle being melted will also affect the compatibility of Cr. The upper mantle contains the spinel facies at lower pressures and the garnet facies at higher pressures. Spinel becomes unstable at higher pressures and reacts with orthopyroxene to form garnet and olivine (Spinel + Orthopyroxene -> Garnet + Olivine). The pressure that this reaction occurs at depends upon the temperatures, but will not occur at less than 1.5 GPa (Klemme and O'Neill, 2000). Spinel has the greatest affinity for Cr with a partition coefficient of $Kd_{spinel\text{-}melt}$ = 170, while Cr is still compatible within garnet with a $Kd_{garnet\text{-}melt}$ =5.5 (Liu and O'Neill, 2004). Compared to melting of spinel facies peridotites, melting under the garnet facies conditions will produce melts with higher Cr concentrations. The increase in the Cr content of the melt is not great, low degree melting of the garnet facies is only able to create melts with ≤600 ppm Cr (Bonnand, et. al. in review). Melting within the different facies will not greatly change the Cr compatibility and cannot produce high Cr melts.

Table 1.1.

Mineral	Olivine	Orthopyroxene	Clinopyroxene	Spinel	Garnet
$KdCr_{mineral\text{-}melt}$	0.8	7	9	170	5.5

Table 1.1. Partition coefficients for the major phases within the upper mantle. Chromium will be more compatible within spinel bearing rocks, however even if garnet is present Cr will be compatible. Data taken from Liu and O'Neill, (2004).

The degree of partial melting affects the Cr within the melt. The compatibility of Cr will change during partial melting due to minerals with different KdCr, being fully consumed. Minerals within the mantle melt at different temperatures; spinel/garnet and clinopyroxene are the first to melt and to be fully consumed. These minerals are also the phases that contain the highest concentrations of Cr. After 20 % of melting, these phases will start to be consumed, at which stage the mantle will be able to hold less Cr and an increase in the Cr concentration of melts will occur (Walter, 1998). This explains why the most depleted peridotites in Figure 1.1. do not have a large increase in their Cr concentration. However, mantle peridotites that have undergone smaller degrees of melting (<20 %), would still be expected to have a noticeable increase in the Cr concentration, which is not seen within the mantle compilation (Figure 1.1).

The majority of melting of the mantle today is low degree melting (<20 %) at temperatures with low $Cr^{2+}/\Sigma Cr_{TOT}$ and so Cr behaves compatibly. The Cr signature within peridotites suggests that there have been epochs in the Earth's history when Cr rich melts were removed. The most likely explanation is that this occurred under higher temperatures, increasing the Cr^{2+}/Cr_{TOT} ratio and decreasing compatibility of Cr. More recently Cr has

behaved more compatibly due to the lower temperature, which is reflected in the Cr concentration of the crust and modern melts.

1.1.3. The Cr content of the continental crust

The Cr concentration in the continental crust and on the surface of Earth is altered after its formation by other processes. Over time this material may then be recycled back into the mantle through subduction. Sediments can be used to chart the Cr content of the crust over time, with a decrease identified since the Archean (Shikari, 1997). Chromium may be included in sediments through detrital clasts or precipitation from the water column. The detrital clasts directly sample rocks from the continental crust. During reworking of the continental crust, the Cr concentration decreases as rocks become more evolved. As the crust has evolved from the Archean to the Proterozoic the amount of felsic material has increased (Condie, 1993), which reduced the amount of Cr available (today the Cr concentration of the continental crust is only 92 ppm (Rudnick and Gao, 2003)). Chromium can also be concentrated in sediments by precipitating out of the water column. On the Earth's surface Cr is stable in two oxidation states, Cr^{3+} and Cr^{6+}, with hexavalent Cr being more soluble. Changes in the oxidation state of the environment can lead to sudden increases in the Cr content of sediment, e.g. during the great oxidation event marine sediments showed an increase in their Cr content due to the oxidisation of terrestrial pyrite (Konhauser et al., 2011). Increases in the Cr concentration of sediments due to changes in oxidation state will not be sustained, but return to initial levels after the reduced reservoir has been consumed. The Cr concentration of modern sediments is low, typically less than 100 ppm (Shikari, 1997), hence

a large amount of subducted material would be required to contribute to the Cr mantle abundance.

1.1.4. Chromium in other Solar System bodies

Variations in the oxygen fugacity of planets leads to different distributions of Cr. A clear example of this is the iron meteorites, which have Cr concentrations much lower than that expected to occur within the Earth's core. Iron meteorites are thought to be from bodies that have undergone metal-silicate differentiation. Two types of iron meteorite exist for which different formation processes have been proposed; 1) magmatic iron meteorites which are believed to have differentiated through core formation, initiated by heating from ^{26}Al decay on early formed planetary bodies, (Goldstein et al., 2009); 2) non-magmatic iron meteorites, which were created through impact melting at the surface (e.g. Wasson and Wang, 1984). The magmatic iron meteorites provide the only direct samples of planetary cores. While the Cr concentration of the Earth's core is estimated to be ~8000 ppm, the compositions of iron meteorites are much less, 10-300 ppm (Wasson et al., 1998; Wasson and Richardson, 2001). The difference in Cr concentrations has been shown to be due to metal silicate differentiation under oxidising conditions within iron meteorites (Bonnand and Halliday, 2018), with Cr much less compatible in the metal phase under these conditions. During core crystallisation Cr is further fractionated. A negative correlation with Au suggests that Cr behaves compatibly, however Cr is not entering into the Fe-Ni metal phases but rather into exsolving phases such as daubréelite and chromite (Wasson and Richardson, 2001; Chabot et al., 2009).

The Cr concentrations within stony achondrites are enriched compared to the BSE. The SNC group of meteorites, believed to have originated from Mars, have Cr concentrations

from 1750-5700 ppm, while the HEDs, a group of meteorites linked to the Vesta 4a asteroid, have a range of 1700-3300 ppm (Bonnand et al., 2016b; Schoenberg et al., 2016). The oxygen fugacity on these bodies is higher than conditions at the time of core formation on Earth, but lower than the conditions present within the BSE today. This creates mantles on these planets with enriched Cr concentrations, as Cr behaves as a lithophile during core formation. The more reduced mantles will create melts with higher Cr concentrations, due to the less compatible behaviour of Cr at higher $Cr^{2+}/ \Sigma Cr_{TOT}$. These factors combined create the high Cr concentrations within the igneous meteorites from the stony achondrites.

There is one group of differentiated meteorites which has a deficit in their Cr concentrations compared to the BSE, the aubrties. These meteorites typically contain less than 600 ppm of Cr (Easton, 1985; Shukolyukov and Lugmair, 2004). Aubrites are achondrites that formed from the differentiation of one or more bodies with compositions similar to the enstatite chondrites (Keil, 1969; Keil, 1989). Reducing conditions during enstatite meteorite formation have long been acknowledged, with evidence including unusual minerals that must have formed in low oxygen environments (Andersen et al., 1964; Keil and Andersen, 1965). Measurements of these meteorites show that they have oxygen fugacity of -4 ΔIW log units (Brett and Sato, 1984; Cartier et al., 2014) . Under reducing conditions the amount of Cr that would enter the metallic phase would increase and leave the silicate phase depleted in Cr. This depletion is greater than seen for terrestrial samples, suggesting that unlike on Earth, the aubrite parent body did not become more oxidised during formation.

Chromium concentrations of lunar basalts are much greater than those seen on Earth, (800 to 6000 ppm (Hallis et al., 2014; Sossi et al., 2018a). This is due to the lower oxygen conditions in the lunar mantle, higher $Cr^{2+}/\Sigma Cr_{TOT}$ ratios, and so Cr behaving more

incompatibly and becoming enriched in melts compared to the lunar mantle (Roeder and Reynolds, 1991; Hanson and Jones, 1998). The Cr concentration of the lunar mantle has been calculated to be 2125 ppm (Jones and Palme, 2000; Sossi et al., 2018a), depleted compared to the Earth's mantle. The Moons core is not large enough to contain a significant amount of Cr, instead volatile loss may best explain the variation between the lunar mantle and Earth (Sossi et al., 2018a).

As can be seen the Cr concentration behaviour throughout Earth's history and in the solar system varies greatly. The behaviour is dependent upon the oxidation state of Cr. The different concentrations of Cr reflects changing conditions and so can be used as a marker for the evolution of the solar system.

1.2. BACKGROUND TO CR ISOTOPES

1.2.1. Isotopes of chromium

Chromium has 4 stable isotopes, 50 (4.35 %), 52 (83.79 %), 53 (9.50 %) and 54 (2.36 %) (Shields et al., 1966). The abundances of these isotopes vary within natural samples. Differences in Cr isotope composition can be inherited from pre-solar material, altered by the creation of new isotopes, and fractionated by processes after their creation. These variations are described using either the epsilon notation for mass independent variations, or the delta notation if the variations are mass dependent, both of which are shown below.

Equation 1. Epsilon Notation $$\varepsilon^{5x}Cr = \left(\frac{\left({}^{5x}Cr/_{52}Cr\right)_{Sample}}{\left({}^{5x}Cr/_{52}Cr\right)_{Standard}} - 1 \right) * 10{,}000$$

Equation 2. Delta Notation $$\delta^{53}Cr = \left(\frac{\left({}^{53}Cr/_{52}Cr\right)_{Sample}}{\left({}^{53}Cr/_{52}Cr\right)_{Standard}} - 1 \right) * 1{,}000$$

The isotopes of Cr are created within different stellar environments. Oxygen and silicon burning in supernovae produce the lightest three Cr isotopes, while ^{54}Cr is created in rare supernovae with neutron rich environments (Hartmann et al., 1985; Woosley et al., 2002; Clayton, 2003). As ^{50}Cr, ^{52}Cr and ^{53}Cr are created within the same environment, their initial ratio within the solar system should be the same throughout. Anomalies in ^{54}Cr were predicted following the identification of ^{50}Ti excesses (Niederer et al., 1981), a neutron rich isotope created in the same environment (Birck et al., 1980). Nucleosynthetic excesses of ^{54}Cr were first identified in refractory inclusions (e.g. Birck and Allègre, 1984), however limitations on the precision of measurements prevented variations between bulk meteorites from being identified. The ^{54}Cr variations in bulk meteorites only became apparent with the advent of improved mass spectrometer measurements (Trinquier et al., 2006) which have identified widespread ^{54}Cr variations within solar system bodies. Variations in ε^{54}Cr have been related to the heliocentric distance (Yamakawa et al., 2010) and age (Sugiura and Fujiya, 2014). These two variables may represent the same event, a late injection of a ^{54}Cr rich phase, which was preferentially included in younger planetary bodies further from the Sun, due to lower surface area / volume ratio of bodies that had not grown so large at greater heliocentric distance. A close similarity in composition of the Earth and enstatite chondrites (Warren, 2011) suggest that they formed in a similar region at the same time. The ^{54}Cr can also be used as a tracer to identify the class of meteorite responsible for ancient meteorite impacts e.g. (Trinquier et al., 2006; Mougel et al., 2017)).

The chromium isotopic composition can be altered within the solar system by the creation of new isotopes by spallation and radioactive decay. Spallation can greatly alter the Cr isotope composition if meteorites have high exposure ages and iron contents (Leya et al., 2003). Spallation produces Cr by bombarding iron nuclei with cosmic rays. The Cr isotopes produced have a ratio of 0.2:1:1:1 (Birck and Allègre, 1985) , which is very different to the abundance of the solar system. This effect is seen within iron meteorites where $\varepsilon^{53}Cr$ and $\varepsilon^{54}Cr$ anomalies in excess of 100 ε-units are seen (Bonnand and Halliday, 2018, Liu et al, 2019).

Radioactive decay is also a source of Cr. The short-lived isotope ^{53}Mn, has a half-life of $t_{1/2}$ = 3.7 Ma (Honda and Imamura, 1971), and decays through beta decay to ^{53}Cr. Variations in the Mn / Cr ratio prior to ^{53}Mn becoming extinct (within 5 half-lives) will lead to different $\varepsilon^{53}Cr$ compositions. This allows early solar system processes to be investigated such as formation of chondrules (Yin et al., 2007), crust-mantle differentiation of other planets (Trinquier et al., 2008b) and volatilisation (Moynier et al., 2007). The Mn-Cr system requires a homogeneous distribution of ^{53}Mn and $^{53}Cr_{initial}$, whether this was the case has been debated (e.g. (Yamashita et al., 2010; Larsen et al., 2011).

1.2.2. Types of Cr isotope fractionations

Chromium isotopes ratios can be further altered through fractionation due to the different physical properties of the isotopes. Nuclear field effects can lead to fractionations between the odd and even masses. These effects have been recorded in Tl and Hg (Blum and Bergquist, 2007; Fujii et al., 2013). However, these effects become important only in heavier elements (+200 amu) and are not observed in chromium isotopes.

Mass dependent fractionations can be split into non-equilibrium (kinetic fractionations) and equilibrium fractionations. Kinetic fractionation may occur during non-

equilibrium processes, including diffusion (e.g. Pogge von Strandmann et al., 2011) and evaporation (Richter et al., 2002). During kinetic fractionation processes, light isotopes are preferentially removed and re-equilibration between the separate phases does not occur. The removal of lighter isotopes occurs due to their higher velocities at the same kinetic energy. Kinetic energy of a particle is described by K.E. = $1/2mv^2$, so for a given K.E., light isotopes will move faster, and travel further.

Equilibrium isotope fractionations occur due to the difference in the bonding strengths of the site that the isotopes inhabit. Mineral sites will preferentially include isotopes that provide the lowest potential energy within the system. Higher energy sites, those with stiffer bonds, will more efficiently decrease their potential energy if they incorporate heavier isotopes. Schauble (2004) described six factors that control the energy levels of sites (derived from Bigeleisen and Mayer 1947), which can be used to approximate which phases contain heavier or lighter isotopes.

Figure 1.2.

Rules for the energy levels of sites

Sites will form stronger bonds if they meet these conditions

a) *High oxidation state in the element of interest*
b) *For anions like Cl^- and Se^{2-} and (O^{2-}), high oxidation state in the atoms to which the* element of interest is bonded
c) *Bonds involving elements near the top of the periodic table*
d) *The presence of highly covalent bonds between atoms with similar electronegativities*
e) *For transitition elements, low-spin electronic configurations, also d^3 or d^8* electronic structure for octahedrally coordinated atoms
f) *Low coordination numbers* *(Schauble, 2004)*

Figure 1.2. Rules for estimating mass dependent fractionations taken from Schauble (2004). The two most important factors for Cr isotope equilibrium fractionations in rock forming minerals are the oxidation state and the coordination number.

Not all of these factors will affect high temperature Cr stable isotope composition. The two most important factors considered in this work are the coordination number and the oxidation state. As higher oxidation states prefer heavier isotopes, Cr^{6+} phases will be isotopically heavier than Cr^{3+}, which will be heavier than phases containing Cr^{2+}. The coordination number refers to the number of nearest neighbours within minerals. Chromium is commonly found within in tetrahedral and octahedral sites, which have coordination numbers of 4 and 6, respectively. The lengths of bonds are shorter and so stronger if the coordination number is lower, which means the low coordination number sites will preferentially include heavy isotopes. Minerals where Cr inhabits tetrahedral sites, such as garnets and spinel are expected to be isotopically heavier than minerals with octahedral sites in the mantle, such as olivines and pyroxenes.

A final consideration for estimating the magnitude of equilibrium fractionation is the temperature. The higher the temperature the smaller the equilibrium fractionation. The magnitude of the fractionation is proportional to $1/T^2$. Fractionation factors between phases at temperatures >1500°C becomes very small.

1.2.3 Theoretical calculations

Theoretical calculations can be used to predict the fractionation factors ($\ln \alpha_{A\text{-}B}$) between phases at equilibrium. The preference for heavy or light isotopes is dictated by the vibrational energies acting on mineral bonding sites (Bigeleisen and Mayer, 1947; Urey, 1947). The average energies acting on these sites is described as the force constant (K_f). The differences between the force constants of Cr within different sites (A and B) is used to calculate the fractionation factors using Equation 3.

Equation 3. $$\ln \alpha_{A-B} = \frac{1}{24}\left(\frac{h}{k_b T}\right)^2 \left(\frac{1}{m_1} - \frac{1}{m_2}\right)\left[\frac{K_{fA}}{4\pi^2} - \frac{K_{fB}}{4\pi^2}\right]$$

Equation 3. includes the term $1/T^2$, showing that the differences in energy of the sites becomes less important in fractionating stable isotopes at higher temperatures. The term for the mass difference between the isotopes of interest, ($1/m_1$-$1/m_2$), shows how the fractionation factor scales with the mass difference. Other terms in the equation are the Boltzmann constant (k_b) and the Planck constant (h).

Force constants can be calculated for stable isotope fractionations using two methods, density functional theory (DFT) (Schauble et al., 2006) and ionic models (Young et al., 2015). Density functional theory uses the electron density to determine the energy of sites, while the ionic models uses the valence state and the interionic species to estimate the force

constants (Young et al., 2015). DFT provides a more robust analysis of the forces involved, however it has been noted that for Fe isotopes, ionic models provide a closer approximation to natural samples than other methods (Macris et al., 2015). Ionic model calculations of isotope fractionations can only be applied to higher temperature (>500°C) fractionations when quantum effects are negligible (Young et al., 2015).

Chromium isotope fractionation factors have been calculated for phases important during core formation, including silicates, metals and sulphides, by DFT (Moynier et al., 2011b). Theoretical calculations using ionic models have been calculated for common mantle minerals (Shen et al., 2018). Comparisons of the force constants for these methods are shown in Table 1.2.

Table 1.2.

Phase	K_f	Method	Study
Cr Metal	624	DFT	Moynier
$Fe_{15}Cr$	416	DFT	Moynier
Olivine M1	643	DFT	Moynier
Olivine M2	492	DFT	Moynier
CrS	322	DFT	Moynier
$MgCr_2O_4$ (Chromite)	1229	DFT	Moynier
$FeCr_2S_4$ (Daubréelite)	511	DFT	Moynier
Olivine (Cr^{2+})	980	Ionic	Shen
Olivine (Cr^{3+})	1918	Ionic	Shen
Pyroxene (Cr^{2+})	829	Ionic	Shen
Pyroxene (Cr^{3+})	1937	Ionic	Shen
Spinel (Cr^{2+})	1917	Ionic	Shen

Table 1.2. Force constants for Cr collected from the literature. Differences are seen between the methods used for calculating the force constants. Values taken from (Moynier et al., 2011b; Shen et al., 2018).

Variations in the force constants for specific phases are seen between different studies. The force constants calculated using DFT calculations are smaller than those returned from the ionic models. This is due to the different methods used, only able to reproduce results within a factor of 2-3 (Young et al., 2015). Similarities are seen in the relative K_f energies of the studies; chromite/spinel has a K_f twice that of Cr^{2+} within olivine, when calculated by either method.

The calculated compositions from Moynier et al., (2011b), suggest that core forming phases (Cr sulphides and Cr within metal) would be lighter than Cr within the mantle (olivine and chromites). The magnitude of fractionation will depend upon the Cr bearing phases within the core and the oxidation conditions. The timing and conditions of metal-silicate segregation will also affect any fractionation, as the temperatures of terrestrial core formation may have been too great to allow measurable fractionations to occur (Moynier et al., 2011b). The mineral within the mantle containing the isotopically heaviest Cr, depends on the oxidation state. Shen et al., (2018) suggests that pyroxenes have a higher force constant than spinel, if only Cr^{3+} is included. Under mantle condition Cr^{2+} may also be present in pyroxene, which makes spinel the heaviest phase (Shen et al., 2018). Depending upon the compatibility and melting point of these minerals in the mantle, variations in the Cr isotope composition could arise.

1.3. CHROMIUM MASS DEPENDENT VARIATIONS

Chromium mass dependent isotope measurements were first carried out nearly 20 years ago, with significant improvements made to the precision of measurements since. Initial studies focussed on low temperature samples, which exhibit large easily identifiable

variations. Low temperature studies showed that Cr isotopes were fractionated during the reduction of Cr^{6+} to Cr^{3+} (Ellis et al., 2002; Ellis et al., 2004). These fractionations have been used for tracing toxic Cr^{6+} (Ellis et al., 2002; Ellis et al., 2004; Izbicki et al., 2008) and as a proxy for past oxygen levels; in the atmosphere (Frei et al., 2009) and in past oceans (Frei et al., 2011; Bonnand et al., 2013; Frei et al., 2013).

1.3.1. High temperature $\delta^{53}Cr$ variations on Earth

Improved techniques (discussed in greater detail in Chapter 2) for measuring Cr isotopes unlocked research into high temperature samples. Variations within high temperature rocks were first reported by Schoenberg et al. (2008), who studied a range of crustal and mantle rocks, and found that $\delta^{53}Cr$ variations exist in the mantle. The average composition of mantle peridotites from this study has been used to define the BSE (-0.12 ± 0.10 ‰). Partial melting can lead to changes in the stable isotope composition in other transition metal isotope systems such as Fe and V (Williams et al., 2005; Weyer and Ionov, 2007; Prytulak et al., 2013). These variations arise from the preferential melting of light / heavy minerals and the different compatibilities of oxidation states. Similar effects may be expected for Cr, as theoretical calculations suggest that spinel and Cr^{3+} contain heavier Cr than silicates and Cr^{2+} (Moynier et al., 2011b; Shen et al., 2018). However, Schoenberg et al (2008) showed that the Cr isotope composition of melt products (basalts) was within error of their source rock (peridotites). Therefore, only a small isotopic fractionation between the mantle and melt can occur.

Figure 1.3.

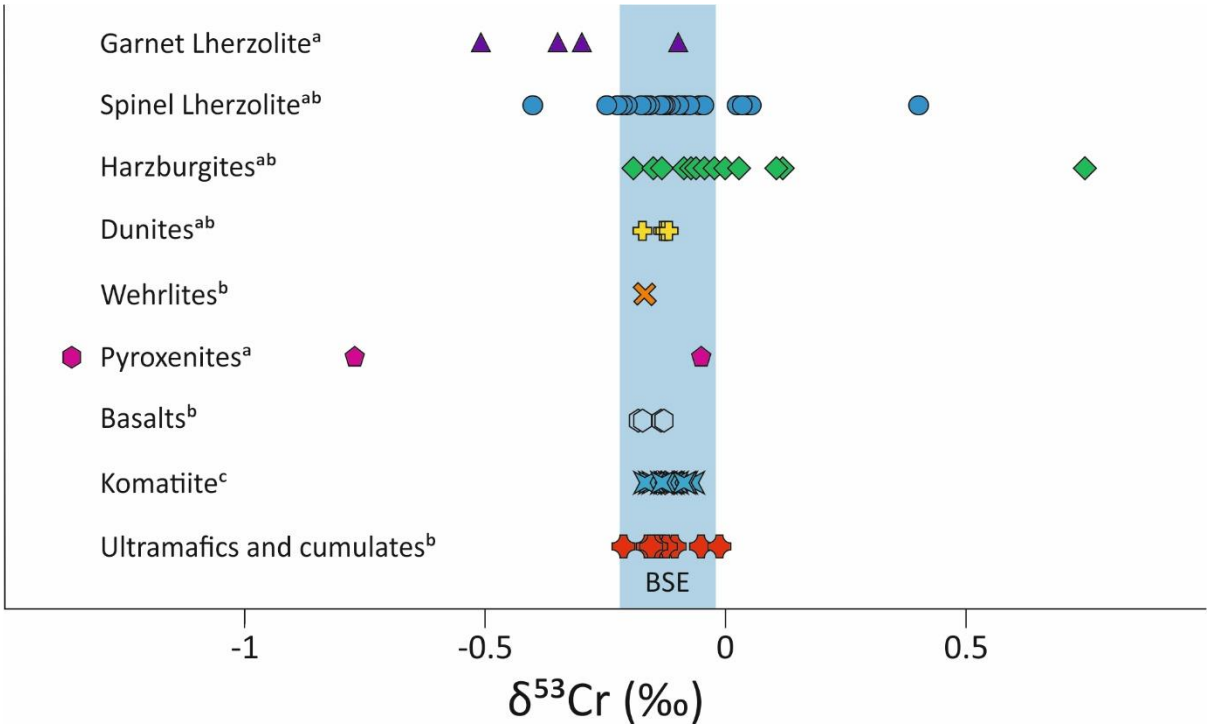

Figure 1.3. Caltech diagram of Cr stable isotopic compositions of terrestrial samples. All melts lie within the range of the BSE (Schoenberg et al., 2008)*, while mantle samples show greater variability.* δ^{53}Cr measurements from *a) Xia et al. (2017), b) Schoenberg et al. (2008), c) Sossi et al (2018a).*

Later work has further investigated δ^{53}Cr variations within the mantle. Using a large data set of mantle peridotites Xia et al., (2017) observed that δ^{53}Cr became heavier with increasing degree of melting. Further evidence for fractionation during partial melting has been provided through the composition of mantle minerals. Shen et al (2018) measured mineral separates from fertile and metasomatised peridotites. The inter-mineral isotopic variations identified by Shen et al. (2018) agreed with theoretical calculations (δ^{53}Cr= Spinel > Pyroxenes > Olivine (Shen et al., 2016; Shen et al., 2018)). These inter-mineral isotope fractionations were used in melting models, to show that the mantle residue would become

heavier, during partial melting, in agreement with the observations of Xia et al., (2017). The $\delta^{53}Cr$ composition of the minerals was affected by the $Cr^{2+}/\Sigma Cr_{TOT}$ of the mantle (Shen et al., 2018).

These studies are unable to explain the $\delta^{53}Cr$ composition of primary mantle melts. The $\delta^{53}Cr$ of melts are consistently similar to the mantle (Figure 1.3.), suggesting that any fractionation that occurs must be small (e.g. Schoenberg et al., 2008; Sossi et al., 2018a and Bonnand et al., in review).

Variations are seen within mantle samples, that cannot be explained by partial melting alone (Xia et al., 2017). Metasomatism has been invoked to explain some of the most heaviest $\delta^{53}Cr$ values measured (Xia et al., 2017; Shen et al., 2018). Xia et al (2017) suggested that the highest $\delta^{53}Cr$ compositions of peridotites were due to loss of light Cr isotopes to basaltic melts. A similar process was used to explain isotopically heavy Cr in mantle olivines (Shen et al., 2018), although the metasomatic agent in this case was identified as a carbonatitic melt.

The impacts of other processes on the $\delta^{53}Cr$ composition of rocks has also been investigated to see if these can also affect the $\delta^{53}Cr$ composition of rocks. Farkaš et al (2013) showed a positive correlation between the LOI and $\delta^{53}Cr$ of altered rocks, to show that serpentinisation led to an increase in the $\delta^{53}Cr$ composition. Rocks of different metamorphic grades were found to have no variations in their $\delta^{53}Cr$ (Shen et al., 2015). While the bulk $\delta^{53}Cr$ composition does not change with metamorphism, Cr-rich metamorphic minerals may have compositions different to their host rocks (Schoenberg et al., 2008; Farkaš et al., 2013). Weathering can alter the chemical composition of rocks at Earth's surface, and has also been shown to affect the Cr isotope composition (Frei et al., 2014).

Obtaining a precise value of the BSE is important for understanding Cr istope fractionations. The commonly used value, taken from Schoenberg of -0.12 ± 0.10 ‰ is poorly constrained due to the heterogeneous nature of δ^{53}Cr within ultramafic rocks. Attempts to refine the BSE have met with mixed success. Farkas et al., (2013) measured a large suite of mantle derived chromites, arguing that they were representative of the mantle, and gave a value of -0.08 ± 0.13 ‰. Xia et al., (2017) used fertile peridotites, so that δ^{53}Cr variations due to partial melting would not be included. An average of these peridotites was used to calculate a BSE value of (-0.14 ± 0.12 ‰). While these reproduced the same BSE value as Schoenberg et al (2008), they have been unable to improve on the precision. Difficulties in obtaining a precise BSE value are due to the widespread variations seen within mantle samples (-1.36 ‰ to 0.75 ‰ Xia et al., 2017). A different approach was taken by Sossi et al., (2018a), who used komatiites to calculate an average composition. Komatiite melts sample a larger volume of mantle than xenoliths, and so any small-scale heterogeneities will be homogenised. Komatiites are created through high temperature, high degree partial melts, which reduces any fractionation during melting, making them more representative of the mantle. These komatiites were combined with a filtered set of peridotites to give a composition for the BSE of δ^{53}Cr =-0.11 ± 0.06 ‰, which agrees with previous estimates while improving on the precision.

During fractional crystallisation, of terrestrial and extra-terrestrial samples, variations in the δ^{53}Cr can occur. Variations during crystallisation were first presented by Bonnand et al (2016a), who showed that δ^{53}Cr decreases in more evolved lunar basalts. These variations were shown to be due to the crystallisation of isotopically heavy spinel, although whether this was due to the preference of spinel for heavy Cr^{3+} or the energetically favourable spinel mineral sites, is unclear. The effect of fractional crystallisation on Cr isotopic composition

within terrestrial magmatic systems was studied by Bonnand et al. (in review), who investigated suite of ocean island basalts (OIBs). The $\delta^{53}Cr$ composition in these basalts became lighter as crystallisation proceeded. Although both OIBs and lunar basalts evolve to lighter $\delta^{53}Cr$ compositions, the magnitude of the variations is smaller for the OIBs. This smaller variation is best explained by clinopyroxene co-crystallising with spinel. As clinopyroxene has a lighter $\delta^{53}Cr$ composition than spinel, the magnitude of $\delta^{53}Cr$ fractionation is smaller.

1.3.2. Solar System variation in $\delta^{53}Cr$

The $\delta^{53}Cr$ composition of bodies from other parts of the solar system have been used to investigate the effects of planetary formation on $\delta^{53}Cr$ and to determine whether there were variations within the solar nebula. Chromium is included in the core during terrestrial core formation, which may lead to variations in Cr isotopes, as seen for other elements, such as Si (Shahar et al., 2009; Armytage et al., 2011). Theoretical calculations (Moynier et al., 2011b) suggest that fractionations would be expected between Cr phases in the core, (e.g. Cr metal, Cr-Fe metal, daubréelite and CrS,) and silicate and oxide phases in the mantle, (e.g. olivine and chromites). However experiments carried out into Cr fractionation between metal phases and silicates show no fractionation (Bonnand et al., 2016b). This may be due to the high temperatures experienced during core formation reducing the magnitude of fractionation (Moynier et al., 2011b).

Figure 1.4.

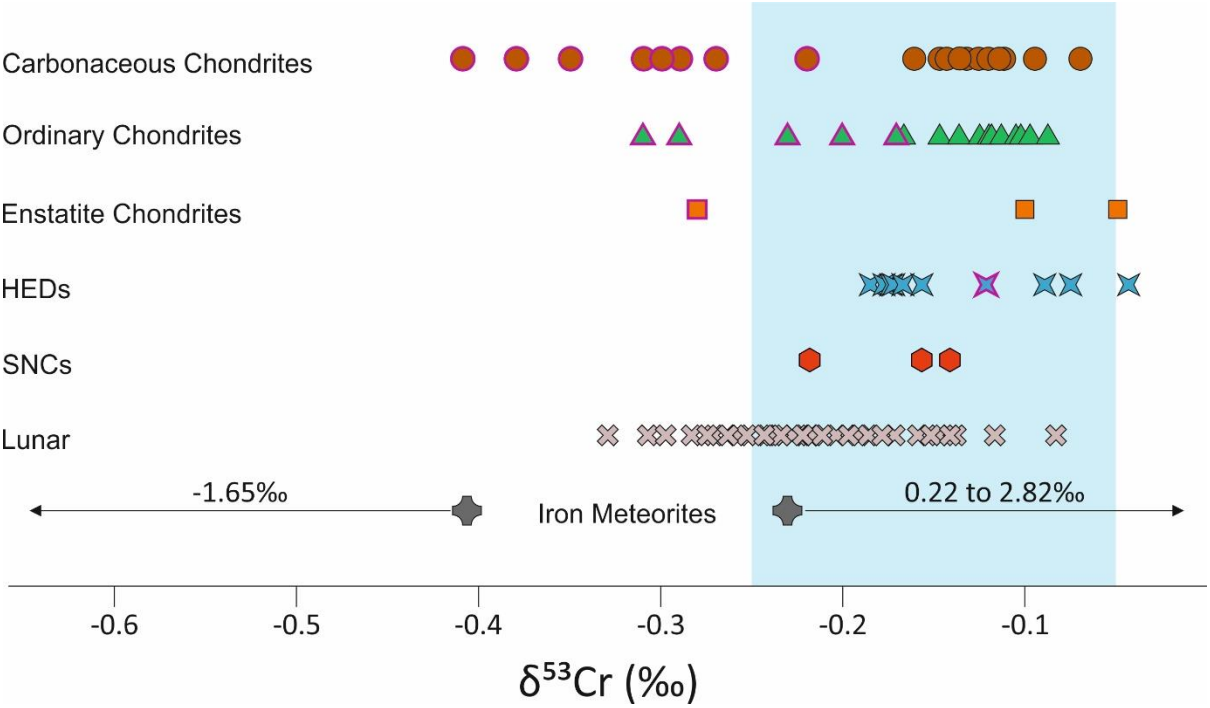

Composition of extra-terrestrial samples. Dark borders shows measurements made using the double spike technique, while those with purple borders were obtained using sample standard bracketing only. Iron meteorite compositions cover a large range, with one sample at -1.65 ‰ and all others within the range from 0.22 to 2.82 ‰. Data compiled from Moynier et al. (2011b), Schiller et al. (2014), Bonnand et al. (2016a, 2016b), Bonnand and Halliday (2018), Schoenberg et al. (2016), and Sossi et al. (2018a). The composition of the BSE from Schoenberg et al. (2008) is represented by the light blue bar.

Comparisons between chondrites and the BSE is commonly used to study the extent of fractionation during core formation. Initial $\delta^{53}Cr$ measurements on chondrites showed a $\delta^{53}Cr$ value 0.2 ‰ lighter than the BSE (Moynier et al., 2011b), as shown in Figure 1.4., suggesting that there had been fractionation during metal-silicate differentiation. This result was replicated by Schiller et al (2014). A difference between the Earth and chondrites has not been seen in later studies (Bonnand et al., 2016b; Schoenberg et al., 2016). The discrepancy

is explained by the measurement techniques. The two earlier studies did not use a double spike, but instead relied on sample-standard bracketing to correct for instrumental fractionation. It is possible that complete yields were not obtained on the extra-terrestrial samples of these studies (Bonnand et al., 2016b). The consensus is that the double spiking measurements are more reliable and therefore that metal-silicate differentiation did not fractionate $\delta^{53}Cr$ during the formation of Earth.

The chondrites are within error of the BSE, but Figure 1.4. shows that the enstatite chondrites are slightly heavier than the others (-0.10 to -0.05‰) compared to (-0.16 to -0.07‰) for the ordinary and carbonaceous chondrites. All of the chondrite classes have $\delta^{53}Cr$ compositions within error of the BSE.

The conditions of metal - silicate segregation on iron meteorite parent bodies were very different to those on Earth. Iron meteorites contain very little Cr, due to the more oxidised conditions that they formed under. Measurements of the Cr isotopic composition of iron meteorites show significant variations compared to other meteorites. In these samples, the $\delta^{53}Cr$ composition reached heavy values, up to 2.85 ± 0.1 ‰, with the isotopically heaviest samples having the lowest Cr concentrations. The variation is due to the crystallisation of a $\delta^{53}Cr$ light phase, such as a Cr rich sulphide, leading to an increasingly isotopically heavy and Cr depleted residue (Bonnand and Halliday, 2018).

Volatility has been linked to Cr variations within bodies in the solar system. The lower Cr concentrations of the lunar mantle, compared to the BSE, are accompanied by Cr isotope compositions of the Moon that are lighter than Earth (Bonnand et al., 2016; Sossi et al., 2018a). If evaporative loss of Cr occurs as a disequilibrium process, then the isotope composition of the solid will become heavier. However, theoretical calculations of

fractionation between CrO_2 and Cr^{2+} in minerals shows that the higher oxidation state of the gas means that it will preferentially include heavier Cr (Sossi et al., 2018a). Loss of heavy Cr from the Moon to a gaseous phase may have occurred during cooling of the post giant impactor cloud (Deng et al., 2018). Volatility has also been used to explain the correlation between Cr concentrations and Cr isotope composition within the HED parent body (Bonnand et al., 2016b; Schoenberg et al., 2016; Zhu et al., 2018), with the loss of heavy Cr during impacts. Experiments have also been performed to show that Cr isotope variations due to volatilisation may also occur within silicate melts (Klemme et al., 2018).

1.4. OBJECTIVES OF THIS WORK

Research into the variations of stable chromium isotope ratios has expanded in the last ten years, however there are some major areas that need to be further investigated in order for a better understanding of the processes behind Cr isotope fractionation.

Chromium isotope fractionation during melting: Contradicting studies disagree on the degree of fractionation that occurs during melting. Initial work showed no fractionation between mantle and basaltic samples, however later studies suggested that partial melting was able to alter the $\delta^{53}Cr$ composition of the mantle, which should also create resolvable differences in the composition of the crust. Understanding Cr's behaviour during melting is important for calculations of the BSE. If fractionation does not occur during partial melting this requires a different set of constraints when calculating the composition of the BSE.

Composition of the BSE: The BSE has been poorly constrained. Providing a better understanding of the behaviour of Cr will allow a selection of samples that will best represent the BSE. This requires a knowledge of how Cr behaves in the mantle, the composition will be

calculated using mantle peridotites. The approach by Sossi et al. (2018a) using komatiites, has helped to better constrain the value of the BSE. Further improvements may be possible by developing an understanding of the isotopic variation during fractional crystallisation of komatiites.

The composition of enstatite chondrites: Limited measurements of enstatite chondrites show that they are heavier than other groups of chondrites, which may prevent them from contributing a significant amount of material to the formation of the Earth. Too few measurements have been made so far to ascertain if there is a resolvable difference in the composition. Enstatites chondrites show similar isotopic compositions to Earth, suggesting a similarity in their parent material. Investigating whether the BSE of Earth is similar to the enstatite chondrites will help to resolve this discussion.

Chapter 2: Methods and techniques for stable chromium isotopes analysis

2.1. INTRODUCTION

This chapter describes the methods used in this research project to make Cr isotope measurements, including the sample dissolution, chemical purification and the mass spectrometry. As well as a detailed description of the methods, the theoretical aspects and practical steps taken to ensure that the highest quality data are acquired, is also discussed. Comparisons with other methods of measuring Cr isotopes, highlights the benefits of our approach. The method used within this study is based on the column chemistry techniques and the mass spectrometry set up described in Bonnand et al (2016b). These methods yield Cr isotope data that, in terms of precision and reproducibility, are comparable to or better than any previously reported.

2.2. METHODS AVAILABLE FOR THE DETERMINATION OF CHROMIUM STABLE ISOTOPE COMPOSITIONS

Measurements of Cr isotopic compositions were first made over 30 years ago using single collector thermal ionisation mass spectrometers (TIMS) (Birck and Allègre, 1984). Initially work was carried out to investigate mass independent Cr isotope variations; nucleosynthetic $^{54}Cr/^{52}Cr$ variations within presolar grains, (Birck and Allègre, 1984) and mass independent radiogenic $^{53}Cr/^{52}Cr$ variations within a CV chondrite (Birck and Allègre, 1985). Mass independent variations are presented using the epsilon notation ($\varepsilon^{5x}Cr = (((^{5x}Cr/^{52}Cr)_{sample} /(^{5x}Cr/^{52}Cr)_{standard} -1) * 10{,}000$). Single collector mass spectrometry was limited by non-ideal machine fractionation effects, which were large due to the mass range of Cr isotopes (Trinquier et al., 2008a).

Improvements in mass spectrometers since the early studies have helped to increase the precision of measurements, with the development of multi-collector mass spectrometers

providing significant improvements. Simultaneous isotope measurements using multiple collectors negate fluctuations within the ion beam strength. Other improvements to mass spectrometers included an increase in the dynamic range up to 50 V, which provides benefits for large isotope ratios, and improved optics to facilitate peak jumping in multi-dynamic measurement protocols.

In order to make high precision measurements improvements to the chemical separation were also required (Trinquier et al., 2008a). Incomplete yield of Cr during column chemistry's can lead to fractionations, the presence of isobaric interferences can cause to inaccurate beam measurements, and other impurities can affect the strength and behaviour of the ion beams. These effects can be reduced by producing a cleaner Cr sample.

Higher precision measurements identified previously unresolvable variations of $\varepsilon^{54}Cr$ (Trinquier et al. 2007). Anomalies in presolar material were identified within the first mass independent studies (Birck and Allègre, 1984), however it was assumed that no variations were present on the planetary scale. Trinquier et al., (2007) were able to resolve variations between the compositions of bulk meteorites to show that $\varepsilon^{54}Cr$ was heterogeneously distributed. This study showed that using a double normalisation, including the terrestrial $^{54}Cr/^{52}Cr$ ratio, yielded incorrect $\varepsilon^{53}Cr$ measurements (e.g. (Lugmair and Shukolyukov, 1998)).

Mass independent measurements have also been carried out using secondary ionisation mass spectrometry (SIMS). This is an *in situ* method that bombards the sample surface with an ion beam, and ionises the element of interest by knocking off electrons. The beam area is small (20 x 20 µm). The secondary ions are then extracted by applying a field at the front end of the extraction optics. The most advanced SIMS method is highly sensitive and is branded by Cameca as the "NanoSIMS". As the ions are being removed in very small

amounts from the surface, they have a wide range of energies and need to be focused down to a very small beam width to resolve the many spectral interferences. Therefore, the method does not have anything like the precision of samples that have been processed through chemistry to remove spectral interferences and measured on more conventional mass spectrometers. It does allow smaller sample sizes to be measured than would be possible in other ways and is particularly useful for measuring presolar grains, as the target material is very small, but has extremely large anomalies that do not require high precision measurements in able to resolve them from Earth (e.g. $\varepsilon^{54}Cr$= +100 Qin et al., 2011). The method may lead to the identification of presolar grains but not always the absolute isotopic values, if the ionized surface includes a mixture of material within the beam area.

Mass dependent measurements of Cr isotope compositions were first explored in low temperature studies to trace pollutants (Ellis et al., 2002; Ellis et al., 2004). These early studies used multi-collector thermal ionization mass spectrometry (TIMS), and a double spike to correct for machine fractionation. Double spiking has the advantage that laboratory induced mass dependent fractionation is corrected. Mass dependent measurements cannot be corrected by using an internal normalisation. In order to prevent fractionations during chromium purifications, a complete yield of sample is required, which can be difficult (e.g. (Schoenberg et al., 2008)). If a double spike is used a complete yield of Cr is not required, as any mass dependent fractionations during separation can be corrected for. This, more reliable, method has been used in both low temperature Cr measurements, as well as for studying the smaller fractionations arising from high temperature processes. In nature, the magnitude of fractionation varies with a $1/T(K)^2$ relation, so high temperature fractionations can be over an order of magnitude smaller. Therefore, the small effects of high temperature

fractionation necessitate greater precision before they can be clearly resolved (Schoenberg et al., 2008).

Chromium mass dependent measurements on high temperature samples have been carried out using both multiple collector inductively coupled plasma mass spectrometry (MC-ICPMS) (e.g. Schoenberg et al., 2008; Moynier et al., 2011b; Schiller et al., 2014; Bonnand et al., 2016a; Sossi et al., 2018a) and TIMS (e.g. Xia et al., 2015; Bonnand et al., 2016b; Schoenberg et al., 2016; Bonnand and Halliday, 2018). Different ionisation sources are used for TIMS and MC-ICPMS. Heating filaments loaded with Cr samples facilitates ionisation in TIMS, whereas ionisation in MC-ICPMS utilises an argon plasma to strip electrons from the injected Cr atoms. The high energy of the argon plasma is able to efficiently ionise nearly all elements, facilitating precise isotopic measurements on much smaller amounts of material (100s of ng), than needed for precise measurements using TIMS, where overall sensitivity is lower.

The main advantage of TIMS is that the mass fractionation associated with ionization and ion extraction from the source is an order of magnitude lower than with MC-ICPMS. In both cases the instrument fractionation is corrected, but the smaller fractionation of TIMS allows better reproducibility and more accurate measurements through this correction. MC-ICPMS, while unable to achieve the same precision as TIMS, has other benefits. Measurements can be made using smaller sample sizes because the overall sensitivity (ions detected per atoms used) is higher. MC-ICPMS is also faster, allowing multiple measurements to be collected for one sample. The ions being extracted from an MC-ICPMS source are strongly fractionated by space charge in the extraction optics, leading to a distortion (“mass bias”) of the isotopic ratio of the order of about 1 % per amu. However, this can remain stable

throughout a sample run and be measured with limited reliability using a bracketing standard (e.g. for Si samples) or in some cases another element of similar mass (e.g. Tl doping of Pb samples). This is not the case with TIMS, where the fractionation changes as the sample is evaporated from the filament. Therefore, MC-ICPMS is invaluable for elements such as Si, V and Rb, for which less than four isotopes are available for correcting mass fractionation using double spiking. Despite the disadvantage in terms of reproducibility, some studies have measured Cr using sample-standard bracketing MC-ICPMS without double spiking (Moynier et al., 2011b; Schiller et al., 2014).

Measurements of the mass independent and mass dependent chromium isotope composition are required for stable isotope measurements of some extra-terrestrial samples. Mass dependent measurements using a double spike assume an unfractionated composition that is terrestrial, i.e. there is no mass independent fractionation. Measurements of extra-terrestrial samples may have mass independent effects as well, such as nucleosynthetic, radiogenic and cosmogenic anomalies. To correct for these effects, an iterative correction of coupled unspiked and spiked measurements is used, (e.g. Bonnand et al., 2016b; Schoenberg et al., 2016; Bonnand and Halliday, 2018).

2.3. SAMPLE PROCESSING

2.3.1. Lab materials

Laboratory work was carried out in the Metal Free Laboratories of the Department of Earth Sciences Oxford. The Metal Free Labs use HEPA filtered air (specified to Class 10,000). Samples were only exposed for dissolution and column chemistry in Class 100 laminar flow exhaust hoods.

In-house purification of HCl, HNO_3 and HF was achieved through sub-boiling distillation. Romil Ultra Pure hydrogen peroxide was used. All water used was of high purity with a resistivity of 18.2 MΩ•cm, which was deionised using a Millipore Milli-Q element.

Table 2.1.

Regent	HNO_3	HCl	HF	MQ H_2O	H_2O_2
Cr (pg/ml)	9	6	18	1	<100
Total reagent blank (pg)	28	46	18	31	5

Table 2.1. Typical Cr blanks for reagents and water used in this study (pg/ml). The total blank contributed from the different acids used, from the dissolution and chemistry, are also calculated (pg).

The blanks for the different reagents used within this study and the total blank that they add to the sample are shown in Table 2.1. The blanks for reagents prepared in-house were calculated by drying down large volumes of acid, to concentrate a measurable amount of residue. The residue was taken up in 2% HNO_3, for introduction into the Department of Earth Sciences, University of Oxford's Thermo Element 2 ICP-MS. The blank for the 2 % HNO_3 was also measured and removed from the final calculation of the reagents blank.

Full procedural blanks were calculated by running a blank sample through both columns. The Cr blank was insignificant <4 ng compared to the amount of Cr processed (2 µg). The full procedural blank was similar to the reagent blank, which suggests that Cr is efficiently removed from the resin columns in between the runs. That is, there is no memory. As the resin was efficiently cleaned, it was reused multiple times.

2.3.2. Sample preparation

Samples were provided for this study in a range of states of preparedness, requiring some to be sampled and powdered. Care must be taken during preparation to ensure that the sample is representative, which is more problematic with grossly heterogeneous, coarser grained material. The aim of sampling is to try to ensure that measured material has the same composition as the bulk rock, and that measurements of different samples from the same rock will be reproducible. If an element is concentrated in only one phase, then it will be easy to over or under sample. However, if the element is ubiquitously distributed then sampling becomes less important.

Peridotites and komatiites have coarse grains. Greater amounts of these rocks were required to provide representative samples. These samples were amply available and 10's of grams could be used. Extra-terrestrial samples were limited by the availability of sample to 50 to 500 mg. While amounts were limited, the grain size of many of the extra-terrestrial samples was small and so lesser quantities were required in order to be representative. To ensure that representative geochemical data for these small extra-terrestrial samples was available, the major and trace element composition was obtained on the same dissolution as used for the isotopic analyses.

Bulk rock samples were reduced to a fine powder, from a ~10 g sample. Powdering rocks provides a homogenised sample, from which a small amount can be taken, that will be representative of the larger rock. Powdering has the additional benefit that surface to volume ratios are increased allowing more effective acid dissolution.

Large samples that could not fit within a mortar, were first broken up using a field hammer. To prevent contamination of the rock, layers of paper and plastic bags, were

wrapped around the sample. Samples were broken down to fragments of less than 1 cm in size. A pestle and mortar was then used to grind this material to a fine powder. A dedicated ceramic pestle and mortar was used for extra-terrestrial samples to avoid contamination. To prevent loss of sample during powdering, the pestle and mortar were covered in a parafilm wrap, which stopped material from scattering out of the mortar. Native metal was problematic, as it could be lost by being streaked over the surfaces of the pestle and mortar. This was avoided by only very gently tapping these samples. Blanks for the mortar and pestle were small <5 ng, which was much smaller than the 10s μg of Cr that were processed for each sample.

Mineral separates were measured for selected samples, requiring careful preparation. Inclusions and dirty grain boundaries are present in mantle rocks due to extended interactions with fluids. This can affect the composition of mineral separates, and may give incorrect results when investigating equilibrium between minerals. Care was taken when preparing mineral separates to select clean grains. Mineral separates were picked under a microscope to ensure that only clean grains were chosen. Picking was aided by washing crushed samples to remove fine material, which can be difficult to identify and often sticks to grains. Crushed material was then sieved to produce a range of size fractions. Choosing the right size fraction to pick from is helpful; too large will increase the amount of dirty grains and too small will take a long time to collect sufficient material.

Samples were weighed using a Sartorius 5 decimal place balance. The error of the measured weight was reduced where possible by weighing out 20 mg of a sample. Each sample was weighed three times. The Savillex beakers were weighed three times empty and

three times after sample was added. The benchmark of the acceptable error when weighing samples was 500 µg.

Repeated weighing also allowed the static conditions to be assessed. Static is a common problem when making low mass measurements, as it causes instability to the balance and greatly increases the error. Steps were taken to reduce the static such as the wearing of antistatic bracelets and deployment of antistatic guns. Static instability changes with humidity, which varies daily. If static instability was too great, weighing samples would be delayed until measurements could be made under more desirable conditions.

2.3.3. Sample dissolution

The mass of samples dissolved was typically 20 mg, although this varied depending upon sample availability, e.g. Cr rich oxides were low in abundance within samples, and as they were high in Cr, 10 mg would be sufficient. Different acid stage were used for dissolving rocks, with the first dissolution stage using an HF-HNO_3 mix to break down silicates. This is followed by an HCl stage which attacks oxides. High-pressure digestion vessels, Parr bombs and a high pressure Asher, were used to dissolve resistant grains.

1) Hotplate

The first digestion step for all samples was on a hotplate. Samples were dissolved inside 5 ml square-body Savillex beakers. The first digestion step used for silicate samples, was an HF/HNO_3 mixture. A ratio of six moles of HF for every mole of Si was sufficient to dissolve the silicate portion of samples. One millilitre or more of concentrated HNO_3 was used, which was always a greater volume than HF (~100 µl). The small volume of HF used, was to prevent fluorides forming. Fluorides may form when carrying out HF dissolutions, and can be difficult to re-dissolve. Other steps were taken to prevent the formation of fluorides by

keeping the temperature during dissolution low. Hotplates were heated to 110°C and maintained at that temperature for 2-3 days. After drying down the sample, 2-3ml of 6M HCl was added, which is effective at dissolving oxide phases. The samples were kept on hotplates at 120-140°C for 2-3 days. When samples did not fully dissolve, the 6M HCl step was repeated.

Oxides such as spinels do not require HF and HNO_3 to digest, as they do not contain Si-O bonds. For these samples, only the 6M HCl step was used. Some minerals, (e.g. spinels and garnets) were resistant to dissolution. If dissolutions using the hotplates were ineffective, high-pressure methods were used instead.

2) Parr bombs

Parr bombs provide higher pressure and temperature conditions than hotplates and are able to break down minerals more effectively. The sample beaker is placed inside a PTFE liner, along with a small amount of acid. The amount of acid within the sample beaker and plastic liner was balanced to maintain a constant pressure within the vessel, and so reduce the exchange of acid vapour between the two. The PTFE liner was enclosed within a metal jacket, which kept the lid firmly in place. The HF-HNO_3 dissolution step effectively dissolved silicates on hotplates, so only 6M HCl digestions required the use of Parr bombs. The bombs were heated in an oven to 200°C, and held at the same temperature for 3-4 days. This digestion step was repeated until there no visible residue remained. Acid was replaced after every run. The blank for one dissolution step was small (0.4 ng). Parr bombs may require repeated dissolutions, which can be time consuming and increase the blank. However, complete dissolution of all samples within this study was possible using Parr bombs.

3) High pressure Asher

Anton Parr HPA-S High Pressure Asher digestions were an alternative method to dissolve resistant materials. The high-pressure conditions were obtained by pressurising a chamber with an inert gas. The vessels loaded with samples were placed in a metal carousel which can be rapidly heated through a heating element. The pressure is maintained within the vessels by the over pressure within the chamber. For one dissolution run a sample was loaded with 3 ml of 6M HCl. The chamber was pressurised to 100 bars and the sample carousel heated to temperatures over 200°C. A digestion sequence lasted 5 hours. Repeated dissolution runs were used for resistant grains, with the overall time to dissolve samples shorter than when using Parr bombs. The blank for one stage of dissolution in the Asher was <3 ng.

2.3.4. Double spike

Stable isotope fractionations of Cr may occur at many stages throughout sample processing. Column chemistry can fractionate the stable isotope composition if there is not a 100 % yield. Machine fractionation can also change the composition. Measurements using TIMS, evaporate the sample off the filament, which will preferentially release lower mass isotopes, at the start of a run. Ionisation is also a mass dependent process. Naturally-, and experimentally-induced mass dependent fractionation can be corrected with internal normalisation, when making mass independent measurements. However, this correction cannot be used to evaluate natural mass dependent fractionation, as the normalisation will also cancel out all natural mass dependent fractionation. Three methods have been used to correct for experimentally-induced mass dependent fractionations, while allowing measurements of natural mass dependent fractionation, elemental doping, sample standard

bracketing and double spiking. The different methods are not suitable for all elements and mass spectrometers.

Elemental doping adds a second element that is measured simultaneously with the one of interest. The element that is added has a known composition. Elemental doping is not feasible for TIMS, but is used for ICP ion sources. The machine fractionation will be recorded in the measured isotopic ratio of the second element. Elemental doping is limited in two ways. First, the elements need to have similar ionisation energies, which will make them behave in a similar manner during ionisation. Second, the range of isotopes have to fit the collector array of the mass spectrometer. This method has been used, with varying success, in Zn normalisation of Cu and vice versa, and Pb normalisation of Tl, and vice versa. Elemental doping is not an appropriate method for Cr measurements. Elements that could fit in the same collector array as Cr have isobaric interferences and so cannot be used.

Sample-standard bracketing is widely used for MC-ICPMS, and has the benefit that it can be used in tandem with element doping and double spikes method to further improve the accuracy of measurements. Sample-standard bracketing monitors the fractionation using the same element, in a standard of known composition, measured before and after each sample. The instrumental fractionation for the sample is calculated by taking the average fractionation of these two standards. Because the standard is the same element as the sample, the fractionation should be applicable to the samples. The sample-standard bracketing method requires that the variation of the instrumental fractionation is linear. Sample-standard bracketing is most effective if measurements are short, so that machine fractionation will not vary greatly between standards. This is possible when making measurements using MC-ICPMS, where it is possible to change between samples and

standards quickly. It is not an appropriate technique for TIMS, where one measurement will last for many hours, during which time the machine fractionation will vary. Each filament will ionise the element of interest under different conditions, which will vary the instrumental fractionation. The activator and sample will not be loaded identically on every filament, and samples will be run at different temperatures. The fractionation that every sample experiences is affected by these variations, and correlations between different filaments cannot be made. Sample standard bracketing has been used for stable Cr isotope measurements on ICPMS, with or without a double spike (Schoenberg et al., 2008; Moynier et al., 2011b; Schiller et al., 2014; Sossi et al., 2018a). There were differences between the stable chromium isotope composition of meteorites reported in studies not using a double spike and those that used a double spike (Bonnand et al., 2016b; Schoenberg et al., 2016). As sample-standard bracketing will only correct for machine fractionations and not fractionations that occur beforehand, the difference between the studies has been explained by fractionations from incomplete yields of Cr during chemical purification (Bonnand et al., 2016b).

The double spike method is a well-established technique (Dodson, 1963), which can be used on isotope systems with four or more isotopes, although recent studies has shown it is possible to use a double spike on a three isotope system (Coath et al., 2017). This method will correct for all fractionations that occur during processing of the sample. A full description of how double spikes operate are provided in Albaréde and Beard, (2004) and Rudge et al., (2009). Double spikes are made of two isotopes of the element that will be measured. The ratio of the two isotopes comprising the double spike is accurately measured when it is calibration. Fractionations that occur during the processing of the sample will be recorded in this ratio as well. The fractionation recorded in the double spike can be used to correct the

natural sample, however the double spike isotopes needs to be mathematically deconvolved from the sample isotopes. The measured isotopes are described by Equation (1). Solving this equation requires solving three simultaneous equations for three unknowns, the natural fractionation, the combined processing and instrument fractionation and the ratio of spike to sample. Three isotope ratios are required to solve the three simultaneous equations.

There are two main laws that are used to describe the fractionation - power or exponential. The exponential law is used in this study as this provides the best fit to the Cr data collected (Bonnand et al., 2011). Equation 1. uses the exponential fractionation law.

Equation (1):

$$F_i\left(\varphi_{ref}^{sp}, \beta_{sample}, \beta_{mix}\right) = \varphi_{ref}^{sp} R_i^{sp} + \left(1 - \varphi_{ref}^{sp}\right) r_i^{sample} \left(\frac{M_{ref}}{M_i}\right)^{\beta_{sample}} - r_i^{mix} \left(\frac{M_{ref}}{M_i}\right)^{\beta_{mix}} = 0$$

Taken from (Albaréde and Beard, 2004), where φ_{ref}^{sp} is the ratio of spike to sample, β_{sample} and β_{mix} are the natural fractionations and the fractionation from processing, $R_i^{sp} r_i^{sample}$ and r_i^{mix} are respectively the initial isotope ratios of the spike, sample and the mixture. The mass of the reference isotope and the normalising isotope are donated by M_{ref} and M_i.

The double spike used must be carefully chosen to reduce the error magnification. The sample to spike ratio, the composition of the spike, and the ratio of spike to sample must all be considered. The double spike used in this study is a ^{50}Cr-^{54}Cr spike which was calibrated by (Bonnand et al., 2011). Other work suggests different spike compositions (Rudge et al., 2009), however the ^{50}Cr-^{54}Cr spike provides the smallest error for the isotope ratios $^{50}Cr/^{52}Cr$,

$^{53}Cr/^{52}Cr$ and $^{54}Cr/^{52}Cr$ (Bonnand et al., 2011), which are all used within the deconvolution procedure.

2.3.5. Column Chemistry

The Cr purification method used, follows that described in Bonnand et al., (2016b). The first column in this study is described in detail within Bonnand et al., (2011). This method deployed two cation exchange columns. The cation exchange resin (AGW50-X8 200-400 mesh) was packed in BioRad columns with a 10 ml reservoir. The first column separated Cr from major matrix elements, while the second column was designed to further clean isobaric interferences, such as ^{50}V, ^{50}Ti and ^{54}Fe.

Cation exchange resin was extensively cleaned in batches of 200 ml in order to remove fine material. Cleaning was carried out with alternating stages of water and acid. The acid molarity used in each stage was varied from 2M up to 6M HCl, followed by weak HNO_3. The acid molarity was changed to remove material that would stick under different conditions. During each stage of cleaning the bottle was shaken and allowed to settle. The resin was agitated to suspend the fine material, which was then removed as it was drained.

After the resin had been cleaned, 1.2 ml of the resin was loaded into each biorad column. The excess resin was stored in weak HCl. The resin was checked by eye to ensure that no bubbles were present. Additional cleaning was carried out within the columns using 6M HCl and MQ H_2O. The low blanks of the method demonstrated that all Cr from previous usage was effectively removed, allowing the resin to be used for multiple samples. Columns were stored with a full reservoir of H_2O to prevent the resin from drying.

2.3.5.1. Column 1

To ensure that Cr was loaded in the correct oxidation state, samples were dissolved in 6M HCl and heated to 120°C on the hotplate. The 6M HCl solution was then diluted to 1M HCl, immediately prior to loading on the columns, to ensure that Cr remained in the divalent form. In weak HCl, divalent Cr passes straight through the resin, while other cations remain attached. This allows a thorough cleaning of the sample for major elements (Figure 2.1.). It was not possible to obtain a 100 % yield of Cr, as weak HCl will also elute Na from the column (Bonnand et al., 2011). To avoid this, only 10 ml of weak HCl was used to collect the chromium, the initial 4ml that the sample was loaded in, along with 6 ml of 0.5M HCl. The Cr yield for this column chemistry is approximately 80 %.

Table 2.2.

Column 1	
Preconditioning	8ml 0.5M HCl
Sample Loading	4ml 1M HCl
Chromium Elution	6ml 0.5M HCl

Table 2.2. Recipe of Cr separation column 1.

Figure 2.1.

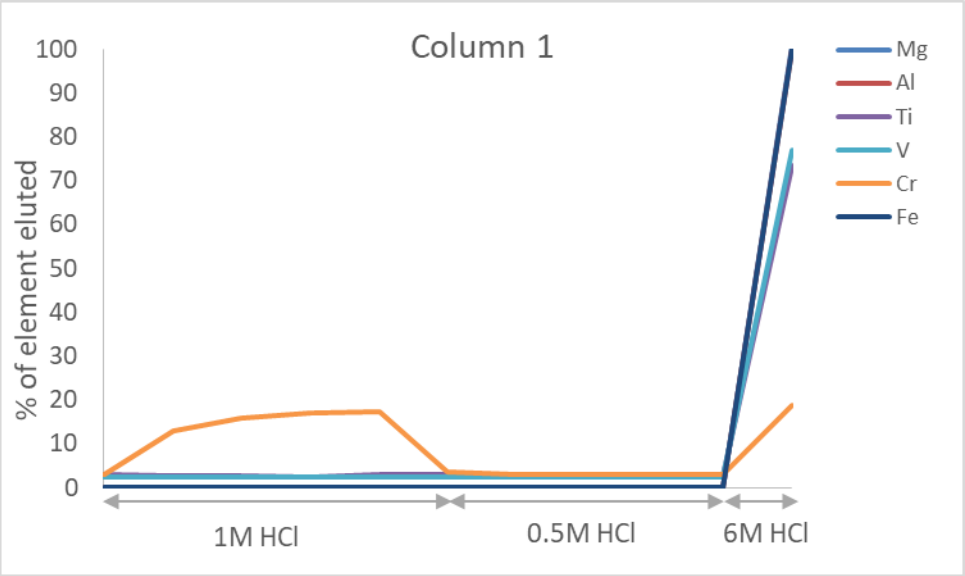

Figure 2.1. Elution curve for geological standard JP1, for column 1, using 1.2 ml of AGW50-X8 200-400 mesh in biorad columns. Not all of the Cr is eluted with weak HCl as past 10ml Na is also eluted. The elution curve is created from analysis of 1 ml cuts and represented as a percent of the total of that element loaded.

2.3.5.2. Column 2

Although only a few percent of V and Fe make it through the first column with the Cr cut, the impact that they have on the measurements necessitates that further steps are taken to reduce their concentrations. This is carried out using a second column designed to further clean the isobaric interferences on Cr. The sample is loaded onto column 2 in a 0.5M HNO_3 solution. Under these conditions Cr will stick to the cation resin. Iron is eluted using 0.5M HNO_3, and V using 0.2M HCl. The Cr is then eluted using 3M HCl. As well as V and Fe, the other element which can produce isobaric interferences is Ti. As Ti is efficiently removed by the first column no additional cleaning is required. The total Cr yield of the 2nd column is close to 100%.

Table 2.3.

Column 2	
Preconditioning	8 ml 0.5M HNO_3
Sample Loading	4 ml 0.5M HNO_3
Iron Elution	4 ml 0.5 HNO_3
Vanadium Elution	7 ml 0.2M HCl
Chromium Elution	6 ml 3M HCl

Table 2.3. Method used in the secondary column. Acid was added into the biorad columns 1ml at a time.

Figure 2.2.

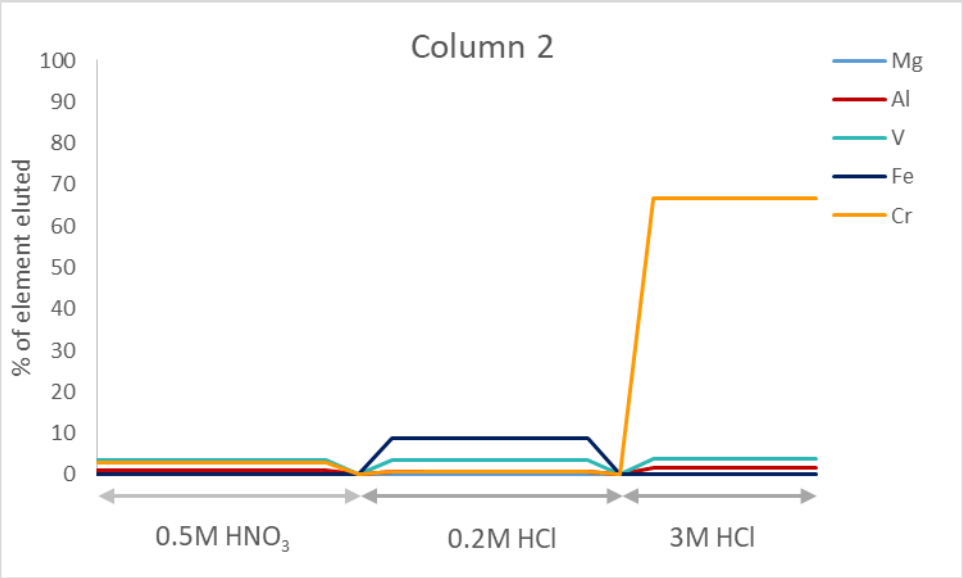

Figure 2.2. Elution curve for geological standard JP1, for column 2, using 1.2 ml of AGW50-X8 200-400 mesh in biorad columns. Each step in the column chemistry was collected in one aliquot for measurements. The % of element eluted, is the percent compared to the starting composition of JP1, (prior to column 1). Vanadium is removed in the 0.5M HNO_3, and 0.2M HCl stages, while Fe is removed using 0.2M HCl. The yield of Cr is close to 100 %.

Samples with low Cr concentrations required a greater mass of starting material, which could lead to overloading of the columns. If a column had been overloaded it was apparent after drying down the eluent. For samples that were effectively cleaned the residue was dark green, however if samples had overloaded a column, the residue would be larger and white or grey in colour. In an attempt to avoid this, a greater volume of resin was used within column 1. However, this was not always successful. Instead, these samples were run through column 1 a second time to remove any remaining matrix material, which was successful.

Cation exchange resin releases some organic material when eluting Cr. This suppresses ionisation of Cr as organic matter can ionise at a lower energy. Organic matter can be effectively removed through oxidation, using H_2O_2. Small volumes of H_2O_2 are therefore added to the samples and heated at low temperatures (<60°C). Hydrogen peroxide is very volatile; if heated to high temperature it will vigorously bubble and disturb the Cr sample. If HCl remains in the sample when H_2O_2 is added Cr can be volatilized. These issues can be alleviated by adding HNO_3 while drying down to dilute the H_2O_2.

2.4. MASS SPECTROMETRY

All Cr isotopic measurements in this study were made using a Thermo Scientific Triton TIMS at the Department of Earth Sciences, University of Oxford, and at Laboratoire Magmas et Volcans, Université Clermont Auvergne. All measurements of chromium stable isotope compositions were made using TIMS, as high precision measurements were required to differentiate between the small $\delta^{53}Cr$ variations in high temperature rocks. Within this section, a brief description of the working of a TIMS is given, with descriptions expanded from de Hoffmann and Stroobant, (2007). Following this, the specific mass spectrometer method used within this study is described.

2.4.1. Mass spectrometry theory

Mass spectrometers measure the isotopic composition of elements by distinguishing the mass to charge ratio of accelerated ions. Powerful magnets are used to separate the ion beam based on the momentum to charge ratio. Mass discrimination will only be effective if the incoming ions have a narrow range of velocities. The separated ion beams are directed

into collectors that are able to detect a very small ion current. This current is then converted into a large voltage (10s of volts) using very high ohmic resistors.

The TIMS used within this study, can be considered to consist of three sections. The sample introduction, which ionises and accelerates the sample atoms; the mass analyser, that resolves the ion beam into separate masses; and the detector, which measures the amplitude of the incoming beams (or ion current).

2.4.1.1. Sample introduction

Accurate measurements require a steady stream of ions to be supplied into the mass spectrometer. TIMS instruments provide ions by heating a sample under a high vacuum (10^{-7} millibars) until it evaporates. During evaporation, chromium is ionised. Following evaporation and ionisation, the ions enter the mass spectrometer by being accelerated and focused with electrostatic fields.

Ion beams from TIMS need to be maintained for long periods of time to acquire sufficient statistical precision for resolving small isotopic differences. The ionisation can be controlled by the use of activators and the material used to make the filament, with the selection of these materials able to control the rate of ionisation, and improve the ionisation efficiency. Common filament materials used in TIMS are tungsten or rhenium wire. Both elements have high melting points, and will not be deformed by heating to temperatures well over 1000°C. The filament wire acts not just as a heat source but also as a catalyst for the ionisation of the element. Ensuring that the right material is chosen can improve beam stability. An activator also acts as a catalyst to ionise the element being studied. Unlike with MC-ICPMS, ion beams are not simply proportional to the amount of sample; a larger sample may decrease ionisation efficiency.

Ionisation efficiency in the TIMS varies depending upon the element but generally is higher in elements with lower first ionisation potential like the alkalis. Ionisation efficiency of elements within TIMS can vary from <0.1 to 100%. The ionisation efficiency of Cr was <0.1%.

The ions are accelerated at a voltage of 10 kV and focussed using a lens stack. A focussed ion beam facilitates better separation of masses, as described below.

2.4.1.2. Mass analyser

The isotopic composition of an element is determined by separating the ions, based on their mass to charge ratio. The mass analyser used in the Triton TIMS has a Gauss 23 cm laminated magnet with high speed and low hysteresis, allowing fast peak jumping, which can allow multidynamic measurements to be made. The magnet deflects the ions through a 90° angle within the TIMS, with different masses deflecting at different angles. The incoming ions have similar kinetic energies, with a range of just 0.5 keV. Therefore, the separation of the ions in the magnetic field is entirely dominated by the differences in mass / charge ratio. Ions with higher mass have a greater momentum, and will not be deflected to the same extent, leading to a wider path. An explanation of the mechanics of splitting the ion beam is described below.

The kinetic energy of an ion entering the mass analyser is determined by the accelerating voltage (V_s). Equation 2 shows that the kinetic energy (E_k) gained by accelerating an ion using a voltage (V_s) is dependent upon the charge of the particle (q). During thermal ionisation the majority of the ions are singly charged. The kinetic energy produced during evaporation and ionisation is small, so the kinetic energy will nearly all derive from the acceleration.

Equation (2): $E_k = \frac{mv^2}{2} = qV_s$

Charged particles that move through a magnetic field are subjected to a magnetic force. The Lorentz force law describes how the direction of that magnetic force is applied (as shown in Figure 2.3). The force is perpendicular to the direction of travel and the magnetic field (B). The force on the ion (F_M) is related to the strength of the magnetic field, charge and velocity.

Equation (3): $F_M = qvB$

Figure 2.3.

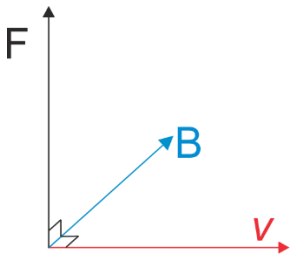

Table 2.3. Diagram illustrating the Lorentz right hand rule. The force applied on a charged particle will be perpendicular to the velocity and the magnetic force.

The magnetic force displaces ions perpendicular to the direction of travel. The displaced ions are balanced by centrifugal forces. The path that the ions take are described by balancing the Lorentz force and the centrifugal force, shown below

Equation (4): $qvB = \frac{mv^2}{r}$ or $r = \frac{mv}{qB}$

The momentum, supplied by the voltage, can be put into equation (4) to show the effect on the radius.

Equation (5): $r = \sqrt{\frac{2V_s m}{qB^2}}$

The kinetic energy can be substituted into the equation using $E_k = qV_s$

Equation (6): $r = \frac{\sqrt{2mE_k}}{qB}$

This shows that ions with a higher mass, but the same kinetic energy, will be deflected to a smaller extent.

Equation (6) shows that ions that have the same mass travelling through the magnetic field will have the same curvature (given by *r* where the larger the radius the greater the curvature, and the smaller the deflection), if the charge and kinetic energy are the same. The same trajectory will be traced for an ion that is double charged, and with twice the mass. The effect of these particles is not significant for measurements of Cr using TIMS, as elements with twice the mass of Cr isotopes are not abundant. The doubly charged ions require higher energy levels and so are much less likely to exist compared to singly charged particles. The combination of these factors makes the contribution to the signal from doubly charged ions insignificant.

Ions exiting the magnet will not form perfectly constrained beams. The simplified derivation given above, assumes that the magnetic field is perpendicular to the velocity of the ions. Ions are not emitted from a point source, so they will not necessarily be travelling parallel to each other, or reach the magnetic field at the same point. The magnets will deflect the ions entering the field in different directions, creating slightly dispersed beam. The small differences in the kinetic energy of the particles lead to slightly different trajectories for ions with the same mass / charge ratio. Poorly constrained beams will have a tail, which can interfere with other ion beams.

The dimensions of the mass spectrometer affect the resolving power, which is the ability of a mass spectrometer to differentiate between masses. The TIMS set up has twice the distance from the mass analyser to the collectors, as the distance to the front end. Greater magnifications allow greater resolution, the peaks will be spread further apart, as there has been a greater distance travelled during which time the different beams will be more horizontally dispersed.

2.4.1.3. Collectors

The Triton TIMS has an array of 9 collectors, which cover a mass range of ± 8.5 %. The central cup is fixed, with the ion beam directed into the cup by varying the magnet strength. The remaining 8 cups are movable which makes it easy to set up isotope systems with a range of mass differences. The Triton collectors have interchangeable Faraday cups and secondary electron multipliers. Faraday cups on the Triton can be paired with 10^{10} up to 10^{12} ohm resistors which allows a large range of currents to be measured. Faraday cups have an upper limit of 50 V, with an effective lower limit of 0.1 V. This allows currents from $1x10^{-13}$ A to 5 $x10^{-9}$ A to be measured. SEMs extend the detection range to very small currents ($<10^{-15}$ A).

Faraday cups are a widely used detector in mass spectrometry. Figure 2.4. shows a schematic of a Faraday cup. The base of the cup has an electrode held at ground potential, and a low noise resistor. When a positive Cr ion beam hits the cup, a flow of electrons is generated to neutralize the positive charge. This electric current varies linearly with the size of the positive ion beam. The signal is then amplified using the high value resistor and the different detectors calibrated to convert the incoming signals into the accurate isotope ratios. Faraday cups can yield incorrect values because of the creation of secondary ions, or because

electrons escape from the cups. To reduce this, the Triton TIMS cups are covered in machined carbon, which makes the behaviour of the cup uniform, as well as suppressing the formation of secondary ions. The deeper cups prevent the loss of secondary charged particles.

Figure 2.4.

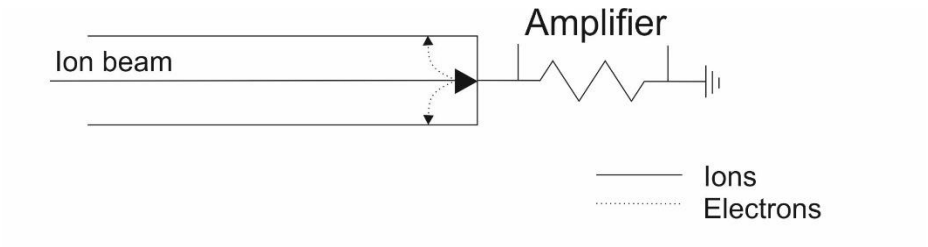

Figure 2.4. Schematic of a Faraday cup, showing an ion colliding with the cup and producing electrons. The deep configurations of the cup prevents loss of the secondary charge particles (de Hoffmann and Stroobant, 2007).

The dominant source of noise in the Faraday cups is Johnson noise, which is generated by the high ohmic resistors in the feedback loop (Wieser and Schwieters, 2005). Steps can be taken when designing the protocol to decrease the noise. The cups and amplifiers are sensitive to changes in temperature (200 ppm/°C), therefore it is important that they are maintained within a very narrow temperature range.

Amplifiers are used to convert the incoming ion current into a measurable voltage. For high fidelity and reproducible isotopic measurements amplifiers have to be able to scale the voltage in an extremely consistent linear fashion in direct proportion to the incoming current. Given that the required precision of isotopic measurements is often at the ppm level, the amplifier has to be able to achieve that same level of consistency. In reality amplifiers show different response from one to another in terms of gain, noise and signal response and decay. Therefore, in a multi-collector instrument they need to be calibrated against each other and

require hardware or software correction protocols to eliminate the effects of differential response times. Furthermore, the gain can change from day to day, requiring regular recalibration between each amplifier. The gains have a typical uncertainty of 5 ppm. The difference in the real behaviour of the amplifier to the shown behaviour is expected to be the same, which allows the uncertainty to be cancelled in certain situations.

When using single collector mass spectrometers, with only one amplifier, the uncertainty in the amplifier behaviour is cancelled out when constructing isotope ratios, as every signal has the same offset. Multi-collector mass spectrometers use multiple amplifier and so the uncertainty cannot be cancelled the same way as single collector measurements. The gain error is propagated when producing isotope ratios, using multiple amplifiers. The error resulting from the amplifiers is given by $\sqrt{n} \times 5$ ppm where n is the number of isotopes or amplifiers involved in the calculation. For Cr isotope measurements this worsens the limit of precision to 8.6 ppm for mass independent measurements (requiring simultaneous measurements of three isotopes) and 10 ppm for mass dependent measurements (requiring simultaneous measurements of four isotopes).

Thermo Scientific mass spectrometers use a virtual amplifier to overcome the limits of precision from amplifier uncertainty. The virtual amplifier rotates which amplifier is paired with a cup. During a run the amplifiers will be rotated between collectors in use. For an element like Cr which has 4 isotopes, the virtual amplifier will rotate 4 amplifiers equally between the collectors used. Assuming that the absolute value of the amplifier gains does not vary during the measurements, the uncertainty of each amplifier can be cancelled out. The following derivations from Wieser and Schwieters, (2005) demonstrate how the amplifier gains cancel out.

Assuming Gain A is 5ppm too high and Gain B is 5 ppm to low.

- Iso1 measured/ Iso2 measured = Iso1true*Gain(A)/Iso2true*Gain(B) = Iso1true/Iso2true x1.00001
- Iso1 measured/ Iso2 measured = Iso1true*Gain(B)/Iso2true*Gain(A) = Iso1true/Iso2true x0.99999
- Average of Iso1truexGain(A)/Iso2truexGain(B) and Iso1truexGain(B)/Iso2truexGain(A) = Iso1true/Iso2true

While the measurements of the isotope ratios for each of the two amplifier set-ups are offset, the average of the ratios cancels out the uncertainties.

2.4.2. Limits of precision

High quality mass spectrometer measurements can be obtained by ensuring that stable conditions are maintained within the instrument, as well as the ion beam itself. Reducing the magnitude of corrections applied to the measured isotopes, for both isobaric interferences and the fractionation corrections provide better measurements. For TIMS measurements the usual limits of precision are the background noise and counting statistics. The main source of background noise during TIMS measurements using Faraday cups comes from the Johnson-Nyquist noise. The Johnson noise is the thermal agitation within high ohmic resistors that are attached to the Faraday cups. The background noise is monitored by taking baselines before and throughout runs to determine the offset. The uncertainty of the background noise measurement (ΔV) depends upon the resistor, temperature and time that the background measurement lasts. High ohmic resistors (R) are more unstable and lead to higher variations in the noise, as do higher temperatures (T), while integration time decreases

the uncertainty of background noise (t_m). The uncertainty of calculating the background is shown in the below equation:

Equation (7): $\Delta V = \sqrt{\frac{4k_B RT}{t_m}}$

The effect of the background noise can be reduced by increasing the signal to noise ratio. As the variability in the background voltage is not affected by the strength of the signal, increasing the voltage measured reduces the noise to signal ratio. A longer integration provides a more accurate value of the background noise. However, as the background noise uncertainty decreases at a rate of $1/t^{-1/2}$, the time that the background integration takes becomes a limiting factor.

There is uncertainty inherent in approximating a continuous quantity such as signal intensity. This is from natural random scatter that will occur in the measurement. The amount of random scatter is calculated using a Poisson distribution. Increasing the number of atoms counted will reduce the uncertainty. Increasing the number of atoms can be achieved through a higher signal or the same strength signal over a longer run. If sample is limited, it is better to use a shorter, higher voltage run rather than spreading out the same number of ions over a longer run. This is because the same uncertainty from counting statistics will be returned, while also decreasing the signal to noise ratio.

The counting statistics uses a theoretically calculated limit of the number of measurements collected using the standard deviation of a Poisson distribution (n).

Equation (8): $\sigma = \sqrt{n}$

The error associated with isotope ratios is then calculated by propagating the standard deviation.

Equation (9): $\sigma_R = \sqrt{\frac{\sigma_a^2}{a^2} + \frac{\sigma_b^2}{b^2}}$

Where a and b are signal intensities. This can be expressed in the total number of ions counted.

Equation (10): $\sigma_{Counting\ Statistics} = \sqrt{\frac{n_a + n_b}{n_a . n_b}}$

The total error of measurements is usually limited by the combined counting statistics and Johnson noise. The combination of the two uses an error propagation (equation 11.).

Equation (11): $E_c = \sqrt{E_1^2 + E_2^2}$

Reducing the error associated with measurements is a play-off between the two sources. Increasing run time and background measurements are the simplest ways to improve the error of measurements. However, these both become time consuming with diminishing returns.

2.4.3. TIMS Methodology

The set up for the TIMS used within this study follows that of previous studies (e.g. (Bonnand et al., 2016b; Bonnand and Halliday, 2018)). Table 2.4. show an overview of the setup of the TIMS.

Table 2.4.

TIMS set up	
TIMS configuration	
Collectors	Faraday Cups
Resistors	10^{11} ohm
Masses	^{49}Ti, ^{50}Cr, ^{51}V, ^{52}Cr, ^{53}Cr, ^{54}Cr, ^{56}Fe
Filament set up	
Activator	Silicon - boron mix
Sample mass	2 µg of chromium
Filament	Single Re-filament
Run conditions	
Filament temperature	1275-1300°C
Pressure	$<10^{-7}$ bars
Run	54 blocks of 10 measurements
Amplifier rotation	After every block
Base Line	50 second log baseline after every block

Table 2.4. The mass spectrometer set-up in this study is given in this table.

The loading procedure for Cr followed that of previous studies (Bonnand et al., 2016b; Bonnand and Halliday, 2018). Zone refined rhenium filaments were welded onto Thermo Scientific filament posts. The filaments were outgassed using a Thermo electronic filament bake out device. Filaments were outgassed under a vacuum of 10^{-7} mbars. An electric current was passed through the filaments, and increased to 4.5 A over 45 minutes. Chromium samples were loaded using small volumes (0.6-0.8 µl) of 6M HCl on to the centre of the filaments. Parafilm dams were placed 5 mm apart to ensure that the Cr solution was concentrated on the filament. A low current was used to dry the Cr solution. On top of the Cr salt, 2.5 µl of activator, made of Si gel and H_3BO_3, was added. The filament was flashed, by gradually heating

until a dull red glow was achieved. Flashing the sample ensures that the activator and sample are homogenised, which allows a consistent emission of material.

Heating of the filaments occurred at a pressure of 10^{-8} mbars. Filaments were heated slowly to 1275°C at which stage a strong Cr beam would be emitted (5-10 x 10^{-11} A). If the beam strength was lower than required, then the sample would be heated up to a maximum of temperature of 1290°C in order to reach these conditions.

The detectors used for this study, were all Faraday cups with 10^{11} ohm resistors. Only one resistor variety was required, as the difference in the abundance of isotopes is a factor of 50, or less, if a double spike was used. The collector configuration was set to measure all isotopes of Cr (^{50}Cr, ^{52}Cr, ^{53}Cr and ^{54}Cr), as well as to monitor elements that produce isobaric interferences (^{49}Ti, ^{51}V and ^{56}Fe). Measurements were made using in static mode.

Prior to each day of measurements, a gain was run for each amplifier. Background noise was measured by taking a 50 second base line between every block. Amplifier rotations were carried out after every block. One measurement consisted of 54 blocks of 10 cycles, with each cycle lasting 8.4 seconds.

Measurements were de-convolved offline using a Newton Raphson iterative process to solve equation 1. Each cycle was calculated separately. The measurement value is then calculated using the average of the cycles. A 6 standard error (s.e.) filter is used to remove outliers. The uncertainty of a measurement is given by the 2 s.e. of the remaining measurements.

Chapter 3: Metasomatism and the chromium isotopic composition of mantle xenoliths and the bulk silicate Earth

3.1. INTRODUCTION

The bulk composition of Earth, and how it evolved through accretion, has been estimated from nucleosynthetic anomalies and is best represented by ordinary and enstatite chondrites (Dauphas, 2017). The chromium (Cr) concentrations of these chondrites lie in the range 3050–3740 ppm (Wasson and Kallemeyn, 1988). The Cr concentration of the bulk silicate Earth (BSE) is significantly lower, estimated at 2520 ppm (Palme & O'Neill, 2014). Therefore, it is most likely that Cr has been partially removed from the BSE by sequestration into core forming metallic liquids. The degree of the BSE depletion constrains the fugacity during core formation as chromium is increasingly siderophile under more reducing conditions and at higher temperatures (Wood et al., 2008; Siebert et al., 2011).

Chromium has multiple oxidation states in the mantle (Berry and O'Neill, 2004; Berry et al., 2006), which are controlled by oxygen fugacity and temperature (Schreiber and Haskin, 1976; Li et al., 1995; Berry et al., 2003). The compatibility of Cr is dependent on the Cr^{3+}/Cr^{2+} (Roeder and Reynolds, 1991). Therefore, the estimated Cr concentration of the mantles of planets and the measured values for basaltic crustal material provide evidence for the level of oxidation during core formation and silicate melting, respectively.

The Cr stable isotope composition of the mantle may initially have been controlled by core formation and melting, but was later further altered through recycling, re-fertilization and metasomatism. These processes could fractionate Cr isotopes through kinetic fractionation and changes in oxidation state. The net result of these Cr isotope fractionating mechanisms is that the isotopic composition currently is not precisely

defined for the BSE. By measuring mantle samples the processes can be better understood and the BSE composition may be more precisely calculated.

Improvements in mass spectrometry have facilitated very precise stable Cr isotope measurements. Chromium stable isotopes are presented here using the delta notation, $\delta^{53}Cr = [(^{53}Cr/^{52}Cr)_{sample} / (^{53}Cr/^{52}Cr)_{std}-1]*1{,}000$. The first results for high temperature terrestrial rocks (Schoenberg et al., 2008) produced an average Cr isotope composition of ultramafic samples of $\delta^{53}Cr = -0.12 \pm 0.10$ ‰, which has since been used as the value for the BSE. Xia et al. (2017) used a filtered compilation of ultramafic rock to calculate the BSE value of -0.14 ± 0.12 ‰. Another method was used by Sossi et al. (2018a), who combined mantle peridotites with ultramafic komatiite melts, which produced a value of -0.11 ± 0.06 ‰. These two values are similar to that originally calculated in Schoenberg et al. (2008).

Chromium isotope fractionation during core formation has been studied using the BSE value of Earth and comparing it to the $\delta^{53}Cr$ of chondrites (Bonnand et al. 2016a; Schoenberg et al. 2016). Chondritic values were found to be within the range of the BSE, suggesting no significant fractionation occurred during core formation. Experimental work exploring fractionation during metal-silicate segregation confirmed that fractionation does not occur (Bonnand et al., 2016a). The BSE value has also allowed variations between the Earth and Moon to be investigated, with Bonnand et al., (2016b) finding no difference between the two, while Sossi et al., (2018a) found a lighter $\delta^{53}Cr$ composition of lunar basalts. This difference to the BSE was explained by the loss of heavy Cr into an oxygen rich vapour (Sossi et al., 2018a). Further comparisons of the Earth with

other planets however have been limited by poor constraints on their primitive mantles as well as that of the BSE.

The impact of partial melting on the Cr isotope composition of the terrestrial mantle has been a matter of debate. Schoenberg et al (2008) found no difference between ultramafic rocks and basalts, implying limited fractionation during partial melting. Xia et al (2017) identified a melting trend in a larger suite of peridotites. Further work found fractionations between minerals, which could be a mechanism for fractionation during melting (Shen et al., 2018).

The effects of different types of alteration on terrestrial rocks, have also been investigated. Serpentinization was linked to heavy Cr isotope values up to +2 ‰ (Farkaš et al., 2013), while metamorphism did not alter the bulk rock composition (Shen et al., 2015). Metasomatism, which has been shown to have varied effects on Fe isotopes in the mantle (Weyer and Ionov, 2007), also appears to affect Cr. Xia et al (2017) showed that interactions with a basaltic melt led to heavy Cr in some peridotites. Metasomatism through other types of melts have also been invoked as a process that can alter the δ^{53}Cr composition of peridotites, in particular, loss of light Cr from olivine has been related to interactions with carbonatite melt (Shen et al., 2018). Metasomatism is a widespread process, which may have broader influences on mantle δ^{53}Cr than the limited and often extreme examples so far identified. Identifying how metasomatism may change the Cr composition of rocks will therefore be important for understanding the composition of the mantle.

Isotopic fractionation between mantle minerals provides additional constraints on the interpretation of bulk rock Cr isotope data. The relative chromium isotope

composition has been calculated using ionic models described by Young et al., (2015) to be $\delta^{53}Cr_{spinel} > \delta^{53}Cr_{cpx}$, $\delta^{53}Cr_{opx} > \delta^{53}Cr_{olivine}$ (Shen et al. 2016). This relation has been found in one suite of peridotites (Shen et al., 2018) while work on other peridotites show orthopyroxene to be the heaviest mineral (Xia et al., 2017). Therefore, questions remain regarding the behaviour of Cr isotopes in the mantle. It is unclear (a) what causes the variation in peridotites, (b) whether partial melting results in a change in the $\delta^{53}Cr$ of the mantle, and (c) the manner in which metasomatism impacts $\delta^{53}Cr$.

In this study, the stable Cr isotope compositions of peridotites from a range of locations have been measured. The $\delta^{53}Cr$ variations are interpreted using geochemical data and melting models, which provide evidence that Cr isotopic fractionation during partial melting is limited, and does not change the composition of the mantle. We agree with previous work by Xia et al. (2017) that metasomatism is able to alter the $\delta^{53}Cr$ of peridotites. We show that extensive fractionations could be produced during non-equilibrium interactions with carbonatitic liquids.

3.2. SAMPLES

Forty-two ultramafic xenoliths were selected for this study. These include 41 mantle peridotites and 1 pyroxenite. The peridotites were chosen to provide a representative sample of mantle lithosphere. In order to ensure that samples were not affected by low temperature alterations, only fresh, unweathered samples were selected. Metasomatism is widespread in the mantle, therefore a number of samples exhibiting metasomatism were included. Examples of metasomatism in these samples include; re-fertilization (KH03-3 and KH96-8),

spongy clinopyroxene (cpx) rims due to recent melt interactions (KH03-10, KH03-15, KH03-24 and KH03-27) and interstitial glass (KH03-15, KH03-16 and KH03-21) (Harvey et al., 2012). Interactions with metasomatic fluids have been recorded in other samples, e.g. Fe enrichment in 8530-24, 8531-40 and Tok 10-1 , which are due to interactions with a Fe rich melts (Weyer and Ionov, 2007). The effects of metasomatism in these samples have been shown to affect their Fe isotope composition (Weyer and Ionov, 2007).

Samples measured in this study are peridotites and pyroxenites. Both of these are ultramafic rocks, composed of clinopyroxne, orthopyroxene and olivine, as well as a high pressure aluminous phase. Peridotites are defined as having olivine contents more than 40 % (and so pyroxene contents of less than 60 %), while pyroxenites have over 60 % pyroxene (Streckeisen, 1976). Peridotites in this study have the advantage of having been well characterised in previous studies, from both the isotope and other geochemical perspectives e.g. (Reid et al., 1975; Rhodes and Dawson, 1975; Ionov, 2004; Williams et al., 2005; Ionov et al., 2006; Weyer and Ionov, 2007; Pogge von Strandmann et al., 2011; Harvey et al., 2012; Prytulak et al., 2013; Harvey et al., 2015).

3.2.1. Lherzolites

Lherzolites are peridotites with 40 to 90 % olivine (Streckeisen, 1976). Lherzolites are fertile peridotites, which have not experienced extensive melting. They are the most common lithology in the off-craton upper mantle. Twenty-nine lherzolites were included in this study. These are from Kilbourne Hole, USA; Ngaoundéré, Cameroon; Labait Hills and Lashaine, Tanzania; Massif Central, France; Vitim, Siberia; Tariat, Mongolia. The Cr_2O_3 concentrations range from 0.15 to 0.92 % and Al_2O_3 contents range from the fertile mantle to moderately refractory 1.8 to 4.6 %. The lherzolites in this study are from both spinel and garnet facies.

3.2.2. Harzburgites

Harzburgites are peridotites which have less than 5 % clinopyroxene (Streckeisen, 1976). Harzburgites are the second most common mantle peridotite, and the most common type of cratonic peridotite. They have a more refractory composition than lherzolites, being particularly depleted in clinopyroxene, as they are residues of more intensive partial melting. Nine harzburgites were selected for this study. Three are from Tariat, Mongolia, three from Kilbourne Hole, USA, and one each from Kamchatka, Russia, Dariganga, SE Mongolia, and Lashaine Tanzania. Harzburgites have lower abundances of the incompatible elements, (Ca, Al, Na) and have higher mg# (Mg/(Mg+Fe)), than lherzolites. The Cr_2O_3 concentrations range from 0.09 to 0.49 % and Al_2O_3 from 0.72 to 2.00 %.

3.2.3. Dunites

Dunites are olivine rich rocks, formed through high degrees of partial melting of the mantle or as olivine cumulates. Dunites are nearly exhausted in both clinopyroxene and orthopyroxene due to the greater degree of melting than harzburgites. Two dunites were measured in this study, both of which came from Lashaine, Tanzania. They have Cr_2O_3 of 0.09 and 0.41 % and are highly depleted in Al_2O_3 (0.16 and 0.4 %).

3.2.4. Wehrlites

Wehrlites are mantle peridotites that are relatively enriched in clinopyroxene and contain less than 5 % orthopyroxene. They are believed to have formed through refertilisation of the mantle, usually through interactions with silicate melts. One wehrlite from Tokinsky, Siberia, was measured in this study, (Tok 10-1). This sample has a Cr_2O_3 of 0.25 % and Al_2O_3

of 2.8 %. This sample is enriched in Fe with an unusual Fe isotope composition, which may reflect metasomatism (Weyer and Ionov, 2007).

3.2.5. Pyroxenites

Pyroxenites are ultramafic rocks with more than 60% pyroxene (Streckeisen, 1976). Their creation is unclear with trapped melt or recycled material both being suggested (Davies et al., 1993; Santos et al., 2002). The pyroxenite measured in this study, P6, is from Ngaoundéré, Cameroon. It has a Cr_2O_3 content of 0.15 % and Al_2O_3 of 13.3 %.

Mineral separates were also measured. These were taken from 3 spinel lherzolites and 1 spinel harzburgite.

3.3. ANALYTIC TECHNIQUES

The analytical methods used in this study follow those previously published by (Bonnand et al., 2016b). A brief summary is provided here. All acids used were purified by in-house sub-boiling distillation. Dissolutions were first carried out on hotplates, while samples with refractory material were also dissolved using high pressure Parr bombs. Hotplate dissolutions first used an HF and HNO_3 mixture followed by drying down and redissolving in 6M HCl. Parr bomb dissolutions were carried out using 6M HCl, heated in vented ovens at 200°C. Samples were checked for digestion after each run. If undissolved material remained, samples were dried down and fresh acid added before repeating the dissolution steps.

Mass bias fractionations occurring during chemical separation and isotopic measurements were corrected using the double spike method (e.g. Albaréde & Beard, 2004).

Samples were double spiked with ^{50}Cr - ^{54}Cr, prior to Cr purification, and left to equilibrate on hotplates. The ion exchange columns follows the method described in (Bonnand et al., 2016b). Two cation exchange resin columns were used to purify the Cr fraction. The first removed matrix elements, and the second cleaned isobaric interferences (^{50}Ti, ^{50}V and ^{54}Fe). Chromium blanks from this method of purifying Cr were negligible (< 4 ng) compared to the total amount of Cr processed (2 μg).

Samples were measured on a ThermoScientific Triton thermal ionisation mass spectrometer (TIMS) in static multicollection mode at the University of Oxford. Samples were loaded onto an outgassed Re filament, together with silica gel and a boric acid activator. Each measurement consisted of 54 blocks of 10 cycles, each cycle lasting 8.4 seconds, with a baseline of 50 seconds measured after every block. Long runs were possible using TIMS due to the long term stability of the beam, which allows for very high precision measurements. Along with the Cr isotopes (50, 52, 53 and 54,) isobaric interferences were monitored and corrected for using ^{49}Ti, ^{51}V and ^{56}Fe. A gain calibration was performed daily and the baseline was measured before each block. Amplifier rotations were carried out through the run. The double spike deconvolution was performed offline using an iterative procedure following that of Bonnand et al., (2011).

The Cr isotope ratios are reported using delta notation in per mille deviations from NIST SRM 979 reference material:

$$\delta^{53}Cr = \left(\frac{(^{53}Cr/^{52}Cr)_{sample}}{(^{53}Cr/^{52}Cr)_{NIST\ SRM\ 979}} - 1\right) * 1000 \qquad (1)$$

The 2 s.e. internal error for each run was typically less than 0.01 ‰. External reproducibility was assessed by repeat measurements of JP-1, over a three-year period which

yielded a value of $\delta^{53}Cr$ = -0.11 ± 0.019 ‰ (2 s.d., n=11), which closely matches previous measurements of the standard, and provides an external reproducibility comparable to that of previous work. The external reproducibility was used as the error on the measurements collected in this study, as it was nearly always larger than the internal precision. For the few samples that this was not the case, the internal precision was used instead.

3.4. RESULTS

Table 3.1.

Sample	Rock Descriptor	Location	Cr (ppm)	δ^{53}Cr	2 s.e.	Al2O3 (%)	mg#	(La/Yb)n
Vi313-1	Grnt Lhz	Vitim, Russia	2531	-0.17	0.006	4.37	0.90	1.31
Vi313-6	Grnt Lhz	Vitim, Russia	2599	-0.11	0.006	3.88	0.89	1.78
Vi313-102	Grnt Lhz	Vitim, Russia	2462	-0.14	0.007	3.23	0.89	0.61
Vi313-104	Grnt Lhz	Vitim, Russia	2551	-0.11	0.005	4.43	0.89	0.55
Vi313-106	Grnt Lhz	Vitim, Russia	2736	-0.08	0.008	3.42	0.90	2.32
Vi313-112	Grnt Lhz	Vitim, Russia	2633	-0.11	0.005	4.28	0.89	0.50
Vi314-56	Sp Lhz	Vitim, Russia	2326	-0.19	0.025	4.27	0.89	0.99
Vi314-58	Sp Lhz	Vitim, Russia	2462	-0.15	0.009	3.93	0.89	0.47
Mo-101	Sp Lhz	Tariat, Mongolia	2804	-0.09	0.005	4.33	0.91	0.46
MOG-1	Sp Lhz	Tariat, Mongolia	2736	-0.12	0.004	4.47	0.89	3.26
BN-8	Sp Lhz	Mongolia	2017	-0.14	0.004	n.d.	0.92	n.d.
PB-XEN1	Sp Lhz	Central Massif, France	n.d.	-0.13	0.014	n.d.	n.d.	2.35
KH03.02	Sp Lhz	Kilbourne Hole, USA	2051[a]	-0.17	0.004	2.76	0.92	0.54
KH03.03	Sp Lhz	Kilbourne Hole, USA	2535[a]	-0.17	0.007	4.37	0.90	0.40
KH03.6	Sp Lhz	Kilbourne Hole, USA	1765[a]	-0.22	0.003	3.32	0.91	0.34
KH03.7	Sp Lhz	Kilbourne Hole, USA	1496[a]	0.01	0.007	2.51	0.92	0.34
KH03.10	Sp Lhz	Kilbourne Hole, USA	1557[a]	-0.32	0.006	3.23	0.91	1.39
KH03.11	Sp Lhz	Kilbourne Hole, USA	2074[a]	0.00	0.005	3.55	0.91	0.25
KH03.18	Sp Lhz	Kilbourne Hole, USA	1990[a]	-0.09	0.003	3.41	0.91	0.14
KH03.21	Sp Lhz	Kilbourne Hole, USA	1812[a]	-0.10	0.004	4.41	0.90	0.31
KH03.24	Sp Lhz	Kilbourne Hole, USA	1551[a]	0.40	0.005	2.72	0.90	0.74
KH03.25	Sp Lhz	Kilbourne Hole, USA	2709[a]	0.07	0.007	2.22	0.92	0.19
KH96.2	Sp Lhz	Kilbourne Hole, USA	2336[a]	-0.11	0.007	1.83	0.92	0.22
KH96.8	Sp Lhz	Kilbourne Hole, USA	3575[a]	-0.17	0.003	3.06	0.92	1.81
KH96.18	Sp Lhz	Kilbourne Hole, USA	1549[a]	-0.10	0.005	3.46	0.91	0.03
C235D	Sp Lhz	Mt Cameroon	3984	-0.08	0.006	4.56	n.d.	n.d.
H93-X8	Sp Lhz	Laibat Hill, Tanzania	2051	-0.08	0.020	n.d.	n.d.	n.d.
P13	Sp Lhz	Ngaoundere, Cameroon	3700	-0.15	0.005	4.29	n.d.	n.d.
4500-18	Sp Hzb	Tariat, Mongolia	1778	-0.12	0.006	0.72	0.93	61.71
4500-19d	Sp Hzb	Tariat, Mongolia	2736	-0.02	0.006	1.06	0.92	6.92
8530-24	Sp Hzb	Tariat, Mongolia	2257	0.43	0.003	1.99	0.91	12.95
8531-40	Sp Hzb	Tariat, Mongolia	1984	0.39	0.007	1.37	0.91	8.70
Av-8	Sp Hzb	Kamchatka, Russia	3333	-0.14	0.005	0.78	0.91	1.43
KH03.15	Sp Hzb	Kilbourne Hole, USA	1701[a]	-0.10	0.007	1.2	0.92	1.96
KH03.16	Sp Hzb	Kilbourne Hole, USA	2302[a]	-0.02	0.004	1.13	0.93	4.74
KH03.27	Sp Hzb	Kilbourne Hole, USA	2168[a]	-0.25	0.010	1.32	0.92	0.34
BD-774	Sp Hzb	Lashaine, Tanzania	1368	0.03	0.005	0.24	0.92	n.d.
BD-822	Sp Hzb	Lashaine, Tanzania	1642	-0.06	0.007	1.85	0.93	n.d.
BD-806	Dunite	Lashaine, Tanzania	616	-0.33	0.044	0.40	n.d.	n.d.
BD825	Dunite	Lashaine, Tanzania	2804	-0.19	0.057	0.16	n.d.	n.d.
Tok-10-1	Wehrlite	Tokinsky, Siberia	1689	-0.06	0.00	2.82	0.85	n.d.
P6	Pyroxenite	Ngaoundere, Cameroon	1014	-0.35	0.04	13.27	n.d.	n.d.
JP1	Peridotite	Geological Reference	2807	-0.11	0.019 (2 s.d.)			

Table 3.1. Chemical and Cr isotope data for the samples measured in this study. a) = chromium concentrations determined using isotope dilution. The geochemical data for Cr, Al_2O_3, #mg and $(La/Yb)_n$ concentrations are taken from the literature (see main text for references).

Table 3.2.

Sample	Mineral	$\delta^{53}Cr$	2 s.e.	Cr (ppm)
KH03-24	Bulk	0.40	0.01	1553[a]
Sp Lhz	Olivine	0.43	0.01	52[a]
	OPX	0.43	0.01	3059[a]
	CPX	0.45	0.01	6097[a]
	Spinel	0.37	0.06	42040[a]
KH03-25	Bulk	0.07	0.01	2709[a]
Sp Lhz	Olivine	0.13	0.01	120[a]
	OPX	0.09	0.01	3878[a]
	CPX	0.14	0.01	8326[a]
	Spinel	-0.07	0.03	58316[a]
KH03-27	Bulk	-0.24	0.01	2168[a]
Sp Hzb	Olivine	-0.21	0.03	109[a]
	OPX	-0.01	0.01	6236[a]
	CPX	-0.19	0.01	11554[a]
	Spinel	-0.21	0.02	59251
PB-Xen	Bulk	-0.13	0.01	1842[a]
Sp Lhz	Olivine	-0.14	0.02	72[a]
	OPX	-0.07	0.01	1834[a]
	CPX	-0.07	0.01	4969[a]
	Spinel	-0.07	0.02	68664[a]

Table 3.2. Chromium concentration and stable isotope data for mineral separates from four mantle peridotites. a) = chromium concentrations determined using isotope dilution (4 sig. figs.). The Cr concentration for KH03-27 spinel is from (Harvey et al., 2012).

The $\delta^{53}Cr$ values for peridotites and mineral separates are presented in Tables 3.1. and 3.2., and Figures 3.1. and 3.2. Mantle peridotites span a range from $\delta^{53}Cr$ -0.33 to +0.43 ‰, which is within the range of published data, -0.51 to +0.74 ‰ (Schoenberg et al., 2008; Xia et al., 2017). Mantle peridotites have a wider range than mafic and ultramafic magmatic rocks

(-0.21 to -0.01 ‰ Schoenberg et al., 2008; Sossi et al., 2018a). Most mantle peridotites (30 out of 41) fall within the range of the BSE (-0.12 ± 0.10 ‰), while 8 are heavier and 3 are lighter. Compositions of lherzolites from the spinel and garnet facies are similar, with the garnet facies having a narrow range, -0.17 to -0.08‰ that falls within the middle of the range of spinel facies lherzolites. The range in compositions of the lherzolites (-0.33 to +0.40 ‰) and harzburgites (-0.25 to +0.43 ‰) are almost identical. The dunites have a range from -0.33 to -0.19 ‰, which is within error of the composition of previously measured dunites (-0.17 to -0.12 ‰ (Schoenberg et al., 2008; Xia et al., 2017)) . The wehrlite (-0.06 ‰) is within range of the BSE. The pyroxenite, P6, is lighter than the BSE (-0.35 ‰) but is within range of previously measured pyroxenites, which can be very light (-1.36 to -0.05 ‰) (Xia et al., 2017).

Figure 3.1.

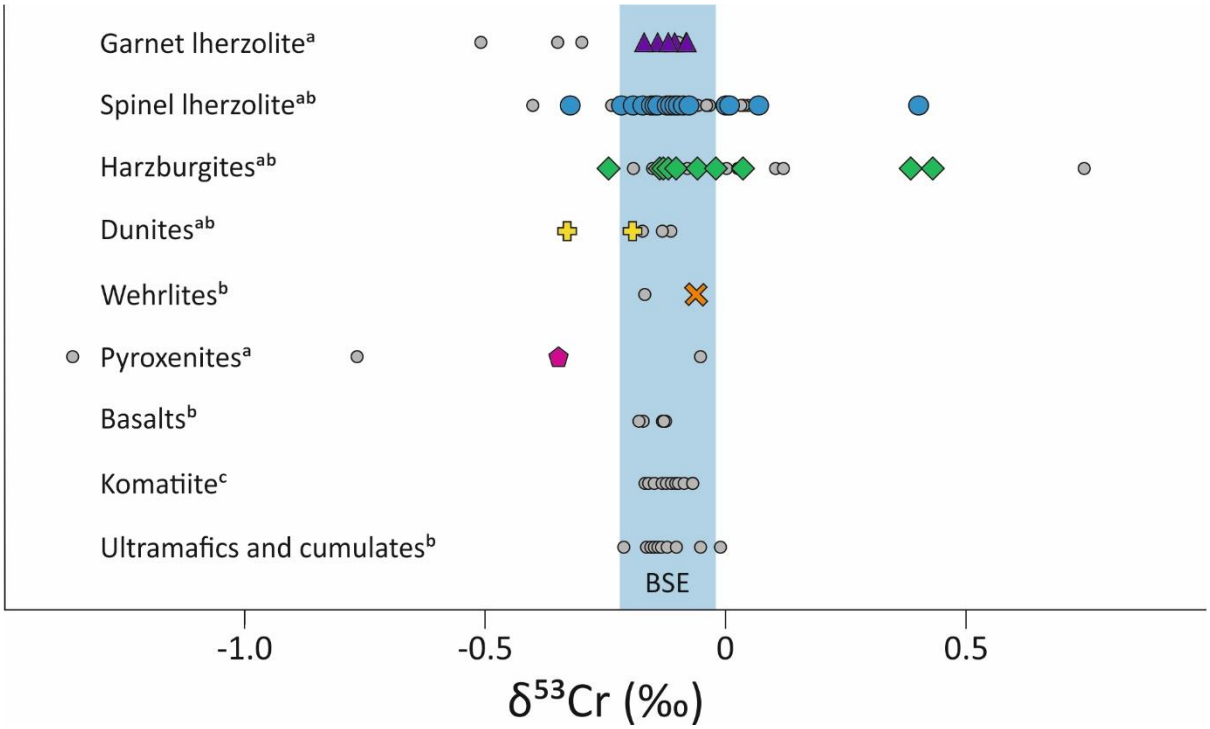

Figure 3.1. Isotopic composition of Cr in mantle xenoliths and crustal samples. Data from this study is in coloured symbols, data from previous work is shown in grey symbols, a= Xia et al., 2017; b= Schoenberg et al., 2008; c= Sossi et al., 2018a. The previously defined BSE (-0.12 ± 0.10 ‰) is shown with the blue bar. Measurements of mantle xenoliths in this study are within range of previous measurements. There is no difference between the compositions of mantle peridotites and crustal rocks. Pyroxenites have different compositions, with some extremely light values.

The $\delta^{53}Cr$ of mineral separates from 3 spinel lherzolites and 1 spinel harzburgite are presented in Table 3.2. The mineral compositions are within the range of previous studies (Shen et al., 2018; Xia et al., 2017) as shown in Figure 3.2. The composition of peridotites and the sum of their mineral separates are similar, across the range of bulk rock $\delta^{53}Cr$ values. Isotopic fractionations between phases are given using the Δ notation shown in Eq 2.

$$\Delta_{a-b} = \delta^{53}Cr_a - \delta^{53}Cr_b \quad (2)$$

Isotopic fractionations between the whole rock and mineral separates were, $\Delta_{Wr\text{-}opx}$ = -0.02 to -0.23 ‰, $\Delta_{Wr\text{-}cpx}$= -0.05 to -0.07 ‰, $\Delta_{Wr\text{-}ol}$= -0.05 to +0.01 ‰ and $\Delta_{Wr\text{-}spl}$= -0.06 to +0.14 ‰. No systematic variations are observed between mineral phases and the bulk rock composition, or between the different mineral phases. The average offset between phases is small, and unresolvable.

Indicators of degree of partial melting can be used to identify the effects of partial melting on the Cr isotope composition of the mantle. Figure 3.3 presents the δ^{53}Cr values and Al_2O_3 %, and shows no correlation. The δ^{53}Cr composition does not vary with other melt indicators (mg#, La conc, Cr conc and Ca/Al) (Fig. A1 Appendix 1).

Variations in the La/Yb ratio of mantle derived materials can be due to a number of processes from partial melting, crustal assimilation and metasomatism (McDonough, 1990). Mantle peridotites with heavy δ^{53}Cr fall into two groups based on their $(La/Yb)_n$ (Figure 3.5.). One group with a trend extending to high δ^{53}Cr and $(La/Yb)_n$ and the other trending to heavy Cr compositions with low $(La/Yb)_n$, less than that of the primitive mantle. No correlation between the δ^{53}Cr and $(La/Yb)_n$ is seen within this latter group of peridotites. High La/Yb reflects a combination of both enriched La and depleted Yb concentrations (Fig. A2 Appendix 1).

3.5. DISCUSSION

Based on the Al_2O_3 content of the mantle rocks, there is no correlation between degree of partial melt depletion and the $\delta^{53}Cr$ composition of the mantle (Fig. 3). This agrees with the previous work of (Schoenberg et al., 2008), which showed that there is no difference between the $\delta^{53}Cr$ of basaltic melts and the mantle. Other studies have attributed variations in $\delta^{53}Cr$ of mantle peridotites to partial melting, and have used melting trends between $\delta^{53}Cr$ and Al_2O_3 of mantle rocks as evidence (Shen et al., 2018; Xia et al., 2017). The causes of these contrasting conclusions is discussed below. The maximum isotopic fractionation that occurs during melting is also constrained. The correlation between $\delta^{53}Cr$ and $(La/Yb)_n$, is investigated further with this trace element ratio providing powerful insights into the processes causing Cr isotope variability.

3.5.1 Comparison with other isotope systems

Other stable isotope data are available for this suite of peridotites including Li, Mg (Pogge von Strandmann et al., 2011), V (Prytulak et al., 2013) and Fe (Weyer et al., 2005; Williams et al., 2005) which show the effects of different processes. The behaviour of these isotopes can be used to interpret our chromium isotope data (Fig. A3 Appendix 1). Lithium and Mg stable isotope ratios within mantle peridotites correlate, with the variations attributed to diffusion during the transport of the rocks to the surface (Pogge von Strandmann et al., 2011). Chromium does not correlate with $\delta^{7}Li$ and $\delta^{26}Mg$, which suggests that diffusion does not alter $\delta^{53}Cr$ in the same way. This result is expected as Cr would diffuse at a much slower rate compared to Li and Mg. The V isotope composition of peridotites is affected by

partial melting (Prytulak et al., 2013). There is no correlation between $\delta^{51}V$ with $\delta^{53}Cr$ providing further evidence against Cr fractionation during melting.

Weyer and Ionov (2007) showed that the $\delta^{56}Fe$ of peridotites can be altered by partial melting, and metasomatism. Partial melting causes a decrease in the $\delta^{56}Fe$ composition of the residue. Metasomatism does not result in extreme $\delta^{56}Fe$ compositions, but rather displaces the $\delta^{56}Fe$ values from the melting trend (e.g. 8530-24, 8531-40 (Fig. A3d Appendix 1)). These two samples have highly enriched $\delta^{53}Cr$ compositions.

3.5.2 $\delta^{53}Cr$ of mineral separates

The isotopic composition of mineral separates can provide information on how the $\delta^{53}Cr$ of a rock is expected to behave during melting. As minerals melt at different temperatures, variations in the mineral $\delta^{53}Cr$ composition would lead to differences in the $\delta^{53}Cr$ of the melt and residue. In order for mineral data to be representative of the mantle, Cr in different minerals needs to be at equilibrium. The mineral separates measured in this study show evidence that they are in equilibrium. The mantle peridotites have been transported rapidly from the upper mantle and show no sign of strong zoning or disequilibrium textures (Harvey et al., 2012). Additional evidence that samples are in equilibrium comes from the $\delta^{53}Cr$. When the $\delta^{53}Cr$ of the mantle peridotites is changed through metasomatism, minerals would not all be expected to be perturbed in the same way. Isotopic differences would decrease with time, as the isotopic composition reaches equilibrium. Mineral separates have been measured for two mantle peridotites (KH03-24 and KH03-27), that have $\delta^{53}Cr$ compositions outside the range of the BSE however, the $\delta^{53}Cr$ of the mineral separates from these samples do not show

large deviations from the bulk rock (Fig. 3). The Cr isotopes of these phases have reached equilibrium.

Figure 3.2.

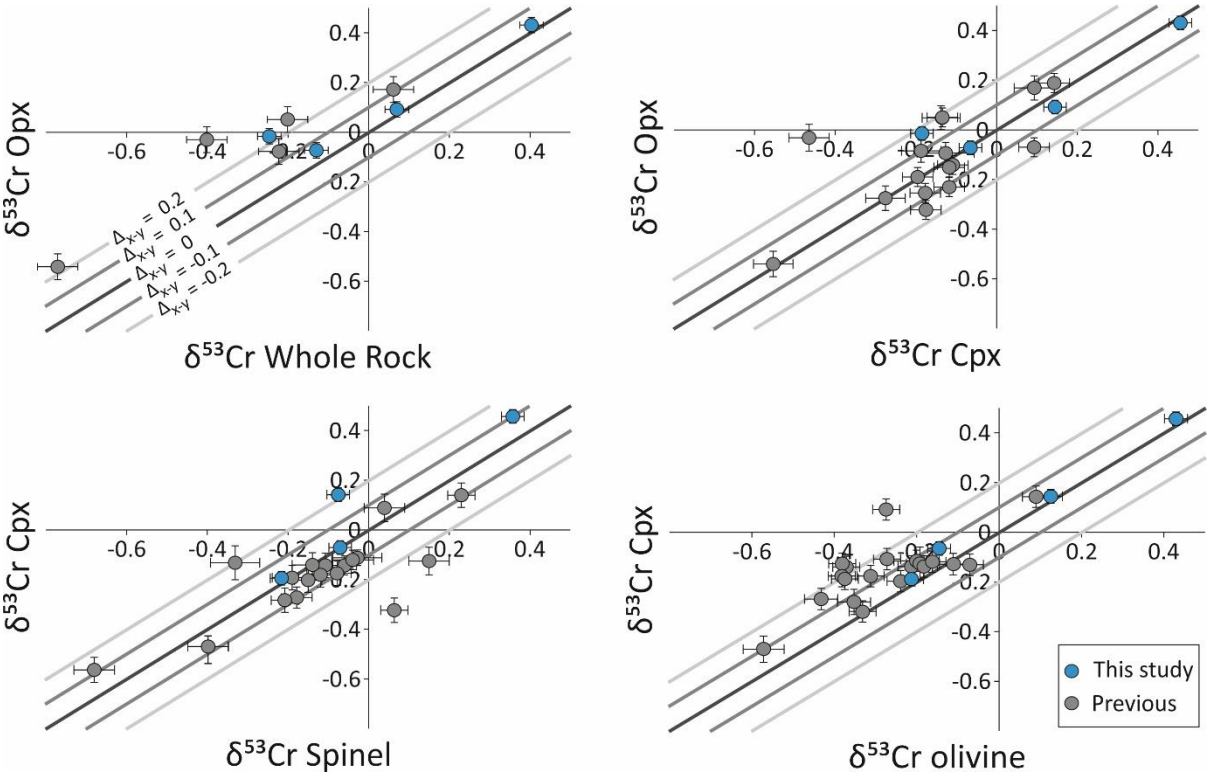

Figure 3.2. $\delta^{53}Cr$ of mineral separates. Minerals are plotted against other minerals to highlight Cr fractionations between phases. Mineral separate data from other studies is also plotted (Shen et al., 2018; Xia et al., 2017)*. The $\delta^{53}Cr$ of minerals measured within this study agree with those of previous studies. Fractionations between phases are highlighted by isolines. Fractionation between minerals measured in this study are as great as 0.23 ‰, but within range of previously measured samples. There is no consistent fractionation between phases.*

Theoretical fractionations between silicate minerals can be calculated using density functional theory (e.g. (Young et al., 2015)). Such methods have been used to predict that spinel should be heavier than coexisting minerals (Shen et al., 2016; Shen et al., 2018). Some

measurements from previous work indeed show spinels to be heavier than coexisting phases, ($\Delta_{spinel\text{-}cpx}$ = 0.10 ± 0.25 ‰ (2 s.d. n=11)) (Shen et al., 2018). However, such a fractionation has not been identified in this work, despite minerals measured being at equilibrium. When all available data are included, the $\Delta_{spinel\text{-}cpx}$ decreases. There are no resolvable differences between other mineral pairs identified in this study (Figure 3.3.).

The similar $\delta^{53}Cr$ composition of minerals, means that preferential melting of certain minerals does not lead to changes in the $\delta^{53}Cr$ of the mantle. The $\delta^{53}Cr$ of the mantle may fractionate during melting, though other processes such as different $\delta^{53}Cr$ compositions of oxidation states, equilibrium fractionations between melt and mantle. A deeper look at the effects of partial melting is investigated below.

3.5.3. Evidence for $\delta^{53}Cr$ isotope variations with melting?

If variations during partial melting exist, they may be clearly shown by comparing the $\delta^{53}Cr$ of peridotites to degree of melting. A range of melting proxies have been used to ensure that any variation with melting would be identified. Lherzolites, harzburgites and dunites represent a sequence of greater melt extraction. If partial melting caused variations within the mantle then we would expect to see the greatest variations from the primitive mantle in the $\delta^{53}Cr$ composition from lithologies representing greater melt extraction. This is not seen (Figure 3.1.).

Depending on whether an element is compatible or incompatible it will be enriched or depleted respectively in the residue of partial melting. The concentration of some elements can therefore be used as indicators of degree of melting. Melt depletion trends may be

unclear if the two elements compared, have widely different bulk distribution coefficients, e.g. an element greatly removed from the mantle within the first few percent melting will not show a clear trend with an element that is removed gradually throughout melting. Elements with a range of distribution coefficients are plotted in Figure A1 (Appendix 1), with no correlations seen.

Figure 3.3.

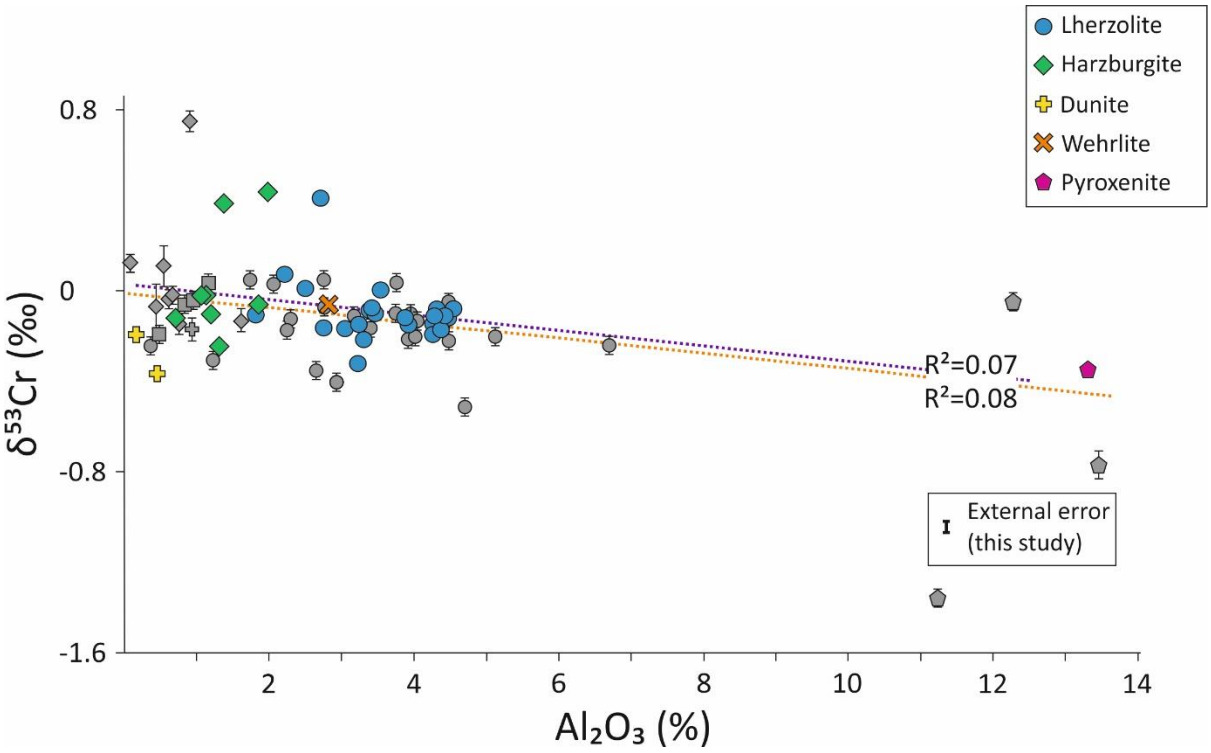

Figure 3.3. Al_2O_3 concentrations plotted against $\delta^{53}Cr$ isotope concentrations for data from this study (coloured) and Xia et al 2017 (grey). The R^2 values are for peridotites (excluding pyroxenites) in this study (0.07) and combined peridotite data of this study and Xia et al 2017 (0.08). Both R^2 values are small and show that there is no overall correlation. The Al_2O_3 content is used as this is an indicator of partial melting, with decreasing Al_2O_3 concentrations as more melting occurs. The Al_2O_3 concentrations are from numerous papers, mentioned previously.

Aluminium is a robust indicator of melting as it's bulk distribution coefficient has little variation with temperature and pressure (Herzberg, 2004; Ionov and Hofmann, 2007) and is immobile during weathering, serpenitinisation and metamorphism (Coleman and Keith, 1971; Snow and Dick, 1995). This allows mantle samples from different locations and depths to be confidently compared. The lack of correlation between the Al_2O_3 of mantle peridotites and $\delta^{53}Cr$ is shown using the R^2 value. The peridotite samples measured in this study have an R^2 value of 0.07, which is similar to the value when mantle peridotite data from previous work are included (R^2 =0.08) (Figure 3.3.), showing that there is no correlation.

Previous studies (Xia et al., 2017) have identified A_2O_3-$\delta^{53}Cr$ correlations from data sets of mantle xenoliths that include pyroxenties. Theories for the genesis of pyroxenites include, frozen melt, subduction and other arc related origins (Davies et al., 1993; Santos et al., 2002). Their origin is therefore not unequivocally related to mantle melting. Even if their origins are related to partial melting, it is incorrect to include them as an extension of the melt residue Al_2O_3 v $\delta^{53}Cr$ trend. The melt composition will be offset from the mantle source trend when the bulk distribution coefficients of the variables are not the same. Melt products should not be included in defining a fractionation trend, and the inclusion of pyroxenites has been used to infer that the variations in the residue of melting are caused by partial melting (Xia et al., 2017). Without these samples, there is no evidence of $\delta^{53}Cr$ variation with Al_2O_3 content in the data set.

3.5.4 Maximum $\delta^{53}Cr$ variations during partial melting

Figure 3.4.

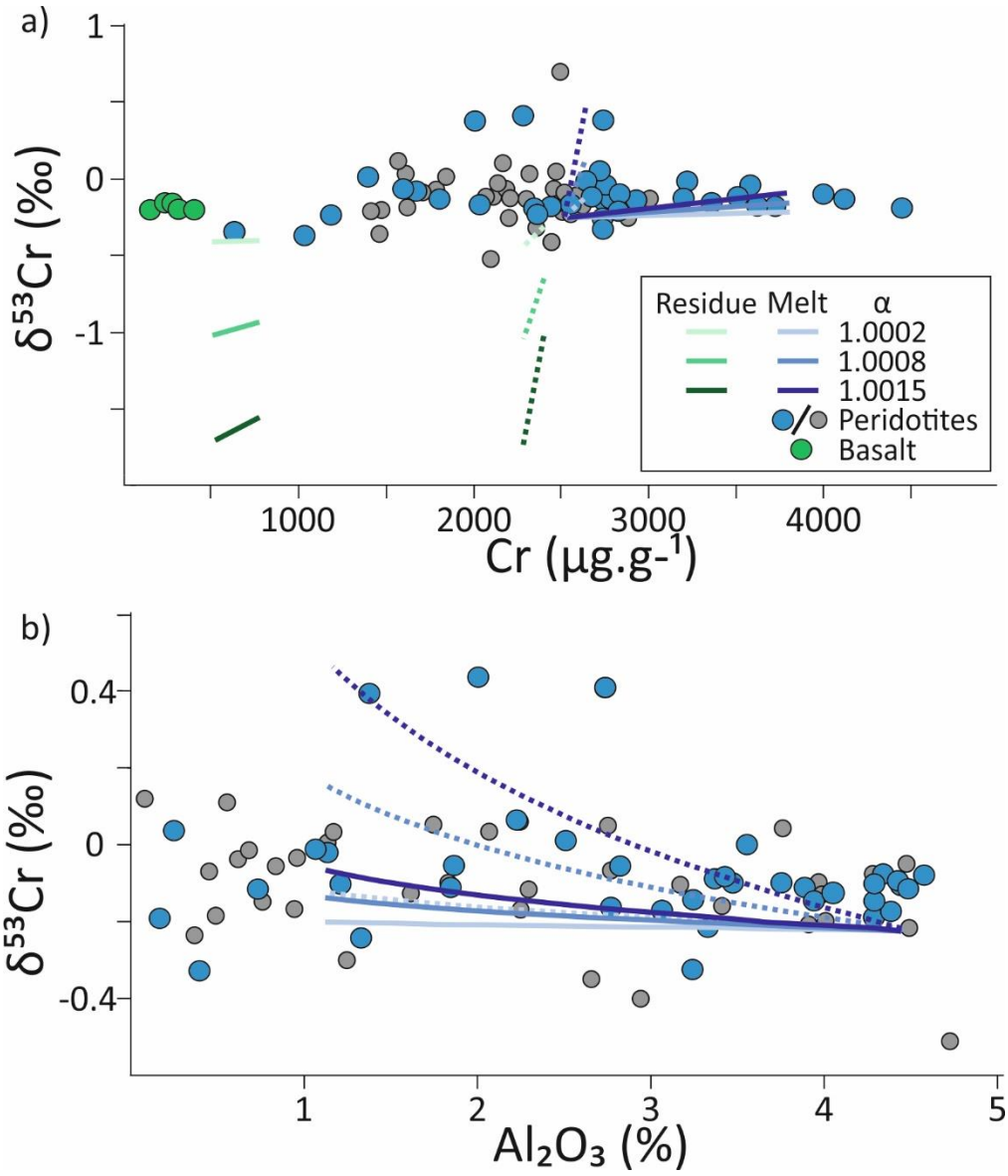

Figure 3.4. Rayleigh fractionation melting models, showing the evolution in the composition of the mantle (blue lines) and melt (green lines) with degree of melting. Different bulk coefficients for Cr have been used a Kd_{Cr} of 1.1 (dashed lines) and a Kd_{Cr} of 1.1 (solid line). The mantle composition evolves from a fertile composition at 4.45% Al_2O_3 to lower Al_2O_3 compositions. Larger variations in $\delta^{53}Cr$ are created using a smaller Kd_{Cr}. A KD_{Cr} of 5 cannot

recreate the spread in mantle peridotites using the fractionation factors illustrated here. The Cr concentration of basalts can only be recreated using a KD_{Cr} *of 5. The starting conditions of the mantle are the same as previous work* (Xia et al., 2017)*,* $\delta^{53}Cr$ *= -0.22 ‰, Cr= 2500 ppm,* Al_2O_3 *= 4.45 %. A range of fractionation factors are used (α=1.0002, 1.0008 and 1.0015). Data for mantle peridotites are taken from this study and* (Xia et al., 2017) *and data for basalts are from* (Schoenberg et al., 2008)*.*

Models presented here expand on those of Xia et al (2017), in particular by investigating the effect of the bulk distribution coefficient of Cr on the resulting melts and residues. This study uses a higher DCr of 5, than that used in Xia et al (2017) (DCr = 1.1). Past work on chromium's behaviour in the mantle suggests that the higher value is more representative. Hanson & Jones (1998) found that the amount of Cr present in melts under normal circumstances was limited by oxygen fugacity, preventing high Cr concentrations in basaltic melts. A series of experiments with a range of starting conditions found the Cr distribution coefficient during melting varies from DCr 5 to 10 (Liu and O'Neill, 2004). A higher bulk distribution coefficient can more accurately recreate the products of partial melts (basalts), which have Cr concentrations of <500 ppm.

Melting models were calculated using Rayleigh fractionation equations (Eq 3. and Eq 4), (Shaw, 1970; Xia et al., 2017). Equation 3 is used to describe the variation in elemental abundances, where F is the fraction of the rock that was melted and D is the bulk distribution coefficient between the solid and liquid ($D = [C]_s/[C]_l$). Equation 4 describes the change in the isotopes of Cr with *f* as the amount of Cr remaining in the residue, and α is the isotopic fractionation factor between melt and solid ($\alpha = (^{53}Cr/^{52}Cr)_{solid}/(^{53}Cr/^{52}Cr)_{melt}$).

$$\frac{[C]s_x}{[C]s_0} = (1 - F)^{1/D-1} \quad (3)$$

$$\left(\frac{^{53}Cr}{^{52}Cr}\right)_r = \left(\frac{^{53}Cr}{^{52}Cr}\right)_0 * f^{1/\alpha-1} \quad (4)$$

The α values used were kept constant at all stages of melting and set at $\alpha_{rock\text{-}melt}$ = 1.0002, 1.0008 and 1.0015, which creates a difference in the Cr composition between rock and melt of $\Delta_{rock\text{-}melt}$ = 0.2, 0.8 and 1.5 ‰. The fractionation factors were set to make the composition of melts lighter than the rock from which they formed, by 0.2 to 1.5 ‰. This follows the choice of previous studies, and the widely held view that less compatible Cr (Cr^{2+} (Roeder and Reynolds, 1991)) will be isotopically light (Schauble, 2004).

Changing the bulk distribution coefficient to a higher value decreases the rate at which Cr is removed from the mantle. The amount of Cr removed from the mantle affects the progress of isotopic Rayleigh fractionation, as described in Equation (4), which shows greater variations in the $\delta^{53}Cr$ composition when a greater fraction of the element of interest is removed. The effect on the $\delta^{53}Cr$ of the residue, for different bulk coefficients, using the same fractionation factor, is highlighted in Figure A4 (Appendix 1). For a bulk distribution coefficient of 1.1, 27.8 % of the Cr is lost over 30 % of melting, whereas with DCr = 5 only 6.9 % of Cr is lost through the same amount of melting. The smaller fraction of Cr removed using a higher bulk distribution coefficient results in suppressed variation in the $\delta^{53}Cr$ of the residue. The variation in $\delta^{53}Cr$ is reduced proportionally to the increase in the bulk distribution coefficient; with DCr = 5, there is 4.5 times less variation in the $\delta^{53}Cr$ of the residue than when DCr = 1.1. By using a bulk distribution coefficient that is higher, large variations within the residue cannot be created.

The variations created within the mantle, as described by our melting models, are much smaller than the range in the $\delta^{53}Cr$ composition of mantle peridotites (Figure 3.4.a. and b.). The highest fractionation factors modelled ($\alpha = 1.0015$), will create a maximum change in $\delta^{53}Cr$ of 0.11 ‰, over 30 % of melting, which is smaller than the spread in the compositions of mantle peridotites (-0.33 to +0.43 ‰). In order to explain the mantle peridotite compositions through partial melting, much larger isotopic fractionation factors would be required. The $\delta^{53}Cr$ composition of melt products can be used to place limits on the magnitude of mantle-melt isotopic fractionation factors. For compatible elements, Figure 3.4.a. shows the composition of melts can be estimated by the fractionation between mantle and melt. Even when using small fractionation factors, resolvable differences would be created. The isotopic composition of basalts falls within the range of the BSE (Schoenberg et al., 2008), while melts created within the model are 0.2 to 1.5 ‰ lighter depending upon the fractionation factor used (Figure 3.4.a). In order to match the basaltic isotope composition of the model to real samples, the fractionation factor must be $\alpha < 1.0001$, or $\Delta_{mantle\text{-}melt} < 0.1$ ‰.

The choice of bulk distribution coefficient on the composition of melts is examined in Figure 3.4.a. Melts created with a DCr = 1.1, have Cr concentrations 5 times greater than those of basalts. The Cr concentration of melts created using DCr = 5 are closer to the compositions of basalts but still slightly high. The bulk distribution coefficient of 5 provides a better match, however it should be considered a lower estimate. If higher bulk coefficients are used, then this will further reduce the $\delta^{53}Cr$ variation seen within the mantle from partial melting.

The lack of correlation in the melting trends with $\delta^{53}Cr$, and the similarity between the $\delta^{53}Cr$ composition of melts and mantle impose strict limits on the possible fractionation between the mantle and melt of <0.1 ‰. A fractionation of <0.1 ‰ between mantle and melt

is not large enough to create observable differences within the mantle. Therefore, alternative processes need to be investigated to explain the observed variations in the $\delta^{53}Cr$ of mantle peridotites.

3.5.5 Metasomatic alterations to Cr stable isotopes in the mantle

3.5.5.1 Carbonatite metasomatism evidence

Mantle peridotites with $\delta^{53}Cr$ compositions heavier than the mantle are separated into two groups determined by the $(La/Yb)_n$ (Figure 3.5.). One group extends to heavy $\delta^{53}Cr$ with high $(La/Yb)_n$, and the other to heavy $\delta^{53}Cr$ with $(La/Yb)_n$ lower than the primitive mantle. The covariation between $(La/Yb)_n$ and $\delta^{53}Cr$ within group 1 peridotites suggest that the excesses are caused by the same process. The La and Yb concentrations of the group 1 peridotites (Figure A2 Appendix 1) show that the increase in the $(La/Yb)_n$ ratio is due to an increase in La as well as a decrease in Yb.

The La/Yb ratio is sensitive to a number of processes, including partial melting, crustal assimilation and metasomatism. Partial melting fractionates La and Yb as they have different distribution coefficients, which depend upon the mineral assemblage. However for both garnet and spinel peridotites, La is more incompatible than Yb, and the $(La/Yb)_n$ of residues will be reduced to less than the La/Yb ratio of the BSE. Partial melting cannot explain the increase in the $(La/Yb)_n$ of group 1 peridotites.

Figure 3.5.

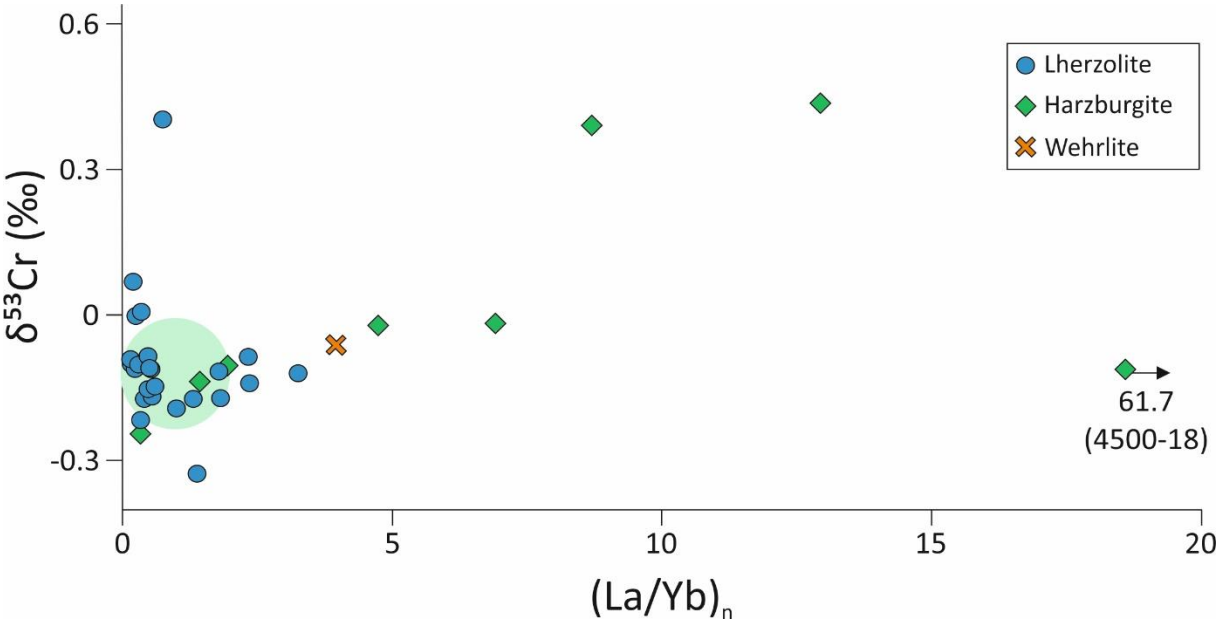

Figure 3.5. $(La/Yb)_n$ is normalised to the composition of the BSE and plotted against the $\delta^{53}Cr$ of peridotites from this work. $(La/Yb)_n$ variations from the primitive mantle can be affected by a number of processes including metasomatism. Peridotites with high $\delta^{53}Cr$ populate two trends, one trend extends to high $\delta^{53}Cr$ and $(La/Yb)_n$, while the other has high $\delta^{53}Cr$ but without any correlation to the $(La/Yb)_n$. REE data are taken from the previously cited references.

Addition of recycled material could alter the $(La/Yb)_n$ and $\delta^{53}Cr$ of peridotites to create the trend. Crustal material is recycled into the mantle and incorporated into peridotites where it alters the bulk chemistry. Crustal material is enriched in REEs, especially LREEs, compared to the primitive mantle. Low temperature processes can lead to heavy $\delta^{53}Cr$ compositions in sediments (Frei et al., 2011; Bonnand et al., 2013). Addition of sediments with heavy Cr and high $(La/Yb)_n$ would create a positive trend like that within Figure 3.5. However, the amount of material that would need to be added would alter the composition of peridotites in other ways that are not seen. Additionally, subducted sediments have low Cr concentrations, (6-

130 ppm) (Plank and Langmuir, 1998), which would require $\delta^{53}Cr$ compositions far more extreme than any natural material.

Metasomatism has been previously suggested as an alternative to explain the heavy $\delta^{53}Cr$ in peridotites, (Shen et al., 2018; Xia et al., 2017). Metasomatism refers to a chemical change of a rock, through either addition or loss of material (Menzies and Hawkesworth, 1987). Two types of metasomatism are distinguished depending on whether changes to the rock are visible (modal metasomatism) or if the variations occur only in the chemical composition (cryptic metasomatism) (Dawson, 1984). There is limited evidence for modal metasomatism in the group 1 peridotites (Harvey et al., 2012), so variations to the $\delta^{53}Cr$ would have resulted from cryptic metasomatism. Previous cryptic metasomatic alterations of $\delta^{53}Cr$ have been proposed, with interactions with a basaltic melt suggested to lead to the loss of light Cr, as seen within isotopically heavy harzburgites (Xia et al., 2017) and olivine (Shen et al., 2018).

Widespread enrichments of $(La/Yb)_n$ within the continental lithospheric mantle are attributed to metasomatism by low degree partial melts (McDonough, 1990). A variety of low degree partial melts with high $(La/Yb)_n$ ratios could act as the metasomatic agents, including shoshonites, lamproites, nephelinites and carbonatites. These low degree partial melts are enriched in a range of other elements. Enrichments of these elements in the group 1 peridotites can be used to identify if they have interacted with low degree partial melts.

Shoshonitic and lamproitic melts are enriched in K as well as the REEs. They have K_2O on the percent level, which is around a 100 times increase compared to the mantle (Morrison, 1980; Paul C. Hess, 1989). The elevated K levels is similar to the elevation in $(La/Yb)_n$ in these melts compared to the primitive mantle. If these melts affected the $(La/Yb)_n$ a change would

also be seen in the K concentration. However, there is no correlation between K_2O and La/Yb ratios or $\delta^{53}Cr$. Most samples have K_2O concentrations in the range 0.01-0.03 % with only one sample, spinel harzburgite 4500-18, with a higher K_2O% of 0.07 %. This sample also has an anomalously high $(La/Yb)_n$ value of 61.7, but with a $\delta^{53}Cr$ composition similar to the BSE. This highly enriched $(La/Yb)_n$ sample could be altered through interactions with K enriched partial melts, without the interaction altering the $\delta^{53}Cr$ composition. There is however, no suggestion that such high K melts have interacted with the mantle peridotites that carry high $\delta^{53}Cr$.

Nephelinites are ubiquitous small scale melts anomalously enriched in the incompatible elements, including high Sr up to 10,000s ppm e.g.(Cheng et al., 2015; Ntoumbé et al., 2016). There is no correlation between Sr and $\delta^{53}Cr$ or $(La/Yb)_n$, excluding these melts from being the metasomatic agent.

Carbonatites are melts with over 50 % carbonate material. Carbonatites have been linked extensively to mantle metasomatism (Green and Wallace, 1988). In the region of the upper mantle between 80-150 km, where CO_2 and oxidised carbon is stable in melts, carbonatite metasomatism is widespread. The low viscosity of the melts and their fractionated composition would make them able to alter mantle composition.

Figure 3.6.

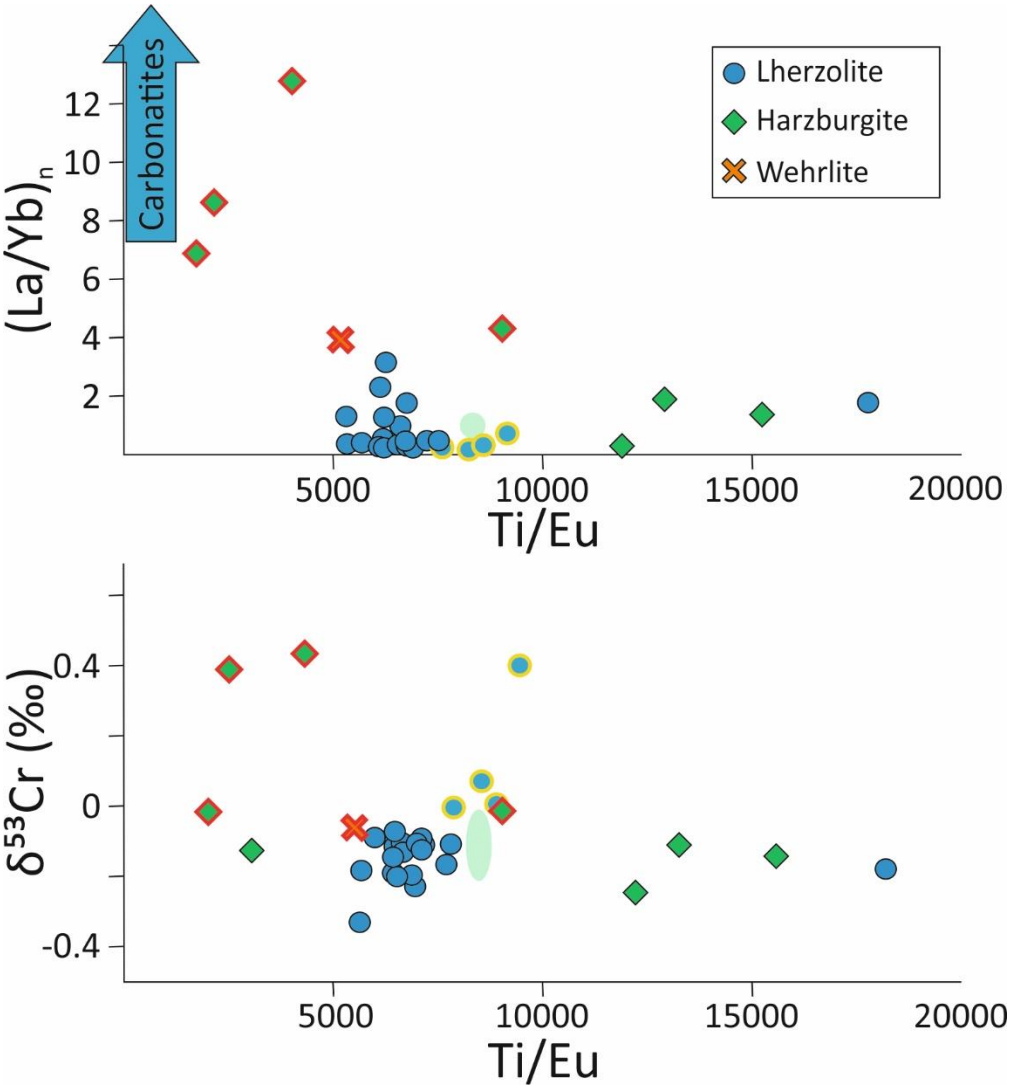

Figure 3.6. The Ti/Eu concentration plotted against $(La/Yb)_n$ and $\delta^{53}Cr$. The Ti/Eu ratio can be used as an indicator of carbonatite interaction, as carbonatite melts have very low Ti/Eu ratios. Data points with red outlines and yellow outlines are group 1 and group 2 peridotites respectively. The group 1 peridotites with high La/Yb and $\delta^{53}Cr$ have the lowest Ti/Eu ratios, indicating interactions with carbonatite liquids.

Calcium is a dominant element in carbonatites, (up to 40 % CaO), but is enriched by less than a factor of 10 compared to the mantle, whereas their $(La/Yb)_n$ ratio is more extreme,

100 times that of the mantle. Calcium variations from the interaction of carbonatites and the mantle, may be swamped by other variations in the Ca concentration. The Ti/Eu ratio, coupled with La/Yb ratios is a useful indicator of carbonatitic metasomatism (Nelson et al., 1988; Sweeney et al., 1992; Rudnick et al., 1993). Carbonatites can have highly fractionated Ti/Eu ratios as low as 3, with an average ratio of 574 (Nelson et al., 1988), much lower than the primitive mantle Ti/Eu =7740 (Sun and McDonough, 1989). The Ti/Eu ratio is not commonly fractionated in the mantle, other melts have ratios similar to the mantle composition (Yaxley et al., 1998). The group 1 peridotites have the lowest Ti/Eu ratios, suggesting that these peridotites have interacted with a carbonatitic melt (Figure 3.6.).

However, carbonatite melts are enriched in both La and Yb, compared to the mantle. They cannot therefore, explain the Yb concentrations of the group 1 peridotites which are depleted compared to the primitive mantle. This can be explained if the group 1 peridotites had undergone partial melting prior to metasomatism, which would deplete both La and Yb. Later, interactions with a carbonatitic melt containing one hundred times more La than Yb would increase the La concentrations while only causing a small change to the Yb concentration.

3.5.5.2 Effects of carbonatite metasomatism on $\delta^{53}Cr$ of mantle peridotites

Carbonatite metasomatism is a widespread process in the Earth's mantle, so would be able to explain the diverse geographical settings of the group 1 peridotites. However, the mechanism through which carbonatites altered the mantle is not obvious. Carbonatites contain low concentrations of Cr, therefore interactions between them and the mantle may not be expected to cause any large $\delta^{53}Cr$ variations. Trapped carbonatitic melt can alter the

composition of peridotites if carbonatites have different $\delta^{53}Cr$ isotope compositions to the peridotite. Erupted carbonatites have low Cr concentrations, averaging 13 ppm for calicocarbonatites (Wooley and Kempe, 1989), while magnesio- and ferrocarbonatites have only slightly higher Cr concentrations. A mass balance can be used to calculate how much carbonatite melt would be needed to create the enriched REE and $\delta^{53}Cr$ compositions of group 1 peridotites. Using the peridotite 8530-24 (La = 2.63 ppm and $\delta^{53}Cr$ = 0.43 ‰) and assuming that its unmetasomatised composition was depleted in La due to partial melting, the amount of trapped carbonatite required to alter the composition is calculated to be 0.45 %, of the total rock. The trapped melt $\delta^{53}Cr$ composition would be over 1000 ‰, an unrealistic composition.

Carbonatite melts could change the mantle composition through equilibrium interactions in one of two ways. If there is a fractionation at equilibrium between the melt and the mantle, with the carbonatite melt having a lighter equilibrium composition, the mantle will become enriched in heavy Cr. Isotopic fractionation factors between carbonatites and the mantle may be expected to exist, due to the different energy of sites that Cr will inhabit (Schauble, 2004). Alternatively, if the carbonatite melt has an initial composition that is heavier than the mantle, then equilibrium between the two could increase the $\delta^{53}Cr$ composition of the mantle. Heavy Cr isotope composition of carbonatites of up to 1 ‰ have been suggested by (Shen et al., 2018) (a value taken from the composition of carbonates (Frei, Gaucher, Døssing, & Sial, 2011)). These two methods will not greatly alter the composition unless multiple parts carbonatite alter one part of mantle, due to the low Cr concentration of carbonatites.

The effects of these interactions are explored in mass balance models in Figures A5 and A6 (Appendix 1). These models were created by iteratively adding one part of carbonatite material, and altering the composition of the mantle appropriately. The models show that for equilibrium metasomatism that carbonatitie melts must have extreme $\delta^{53}Cr$, or that larger amounts of carbonatite melt must flux through the mantle in order to alter the $\delta^{53}Cr$ composition of the mantle. Both options are unlikely.

An alternative explanation is disequilibrium interactions leading to kinetic isotope fractionation of Cr between a carbonatite melt and the mantle. These non-equilibrium melt-mantle interactions would preferentially transport light Cr isotopes into the component that is less saturated in Cr. To create the $\delta^{53}Cr$ compositions seen, the less saturated phase would need to be the carbonatite melt. Erupted carbonatites have low Cr concentrations, with experiments suggesting that they are undersaturated. Partition coefficients of carbonatite melts generated from low degrees of partial melting have previously been calculated for depths of 6.6 to 8.6 GPa (Dasgupta et al., 2009). The bulk distribution coefficient for Cr at these pressures is 12.7, which relates to a Cr concentraiton of the melt of 200 ppm, when in equilibrium with fertile mantle. The most common form of carbonatites, Calciocarbonatites, have variable Cr concentrations at the surface, 2-479 ppm with an average concentration of 13 ppm (Wooley and Kempe, 1989), suggesting that erupted carbonatites are frequently undersaturated in Cr. If these melts interacted with the mantle prior to eruption, then they would have experienced increases in their Cr content.

The La concentation of the mantle also varies with interactions by carbonatite melts. This leads to an increase in the concentations of La in peridotites. The partition coefficient of La in carbonatites is 0.002 (Dasgupta et al., 2009), which would generate melts of 343 ppm

La. This is lower than the composition of erupted carbontaties (average 900 ppm (Wooley and Kempe, 1989)). Interactions between La oversaturated carbonatites and the mantle would increase the La concentraiton of the mantle. Disequilibrium interactionations with carbonatite melts, would lead to the geochemical characteristics of the group 1 peridotites as seen within our samples.

Similar Cr isotope variations to those described here have previously been identified within different mantle settings (Xia et al., 2017). This study showed that high $\delta^{53}Cr$ values could be created due to diffusive loss of light Cr to a basaltic melt. We agree that non-equilibrium loss of Cr is a viable process for altering $\delta^{53}Cr$ on the bulk rock scale. The effects of carbonatite metasomatism on the Cr composition of the mantle are more widespread than previously considered.

3.5.5.3 Metasomatism by other low Cr melts?

The group 2 samples with heavy $\delta^{53}Cr$ do not have elevated $(La/Yb)_n$. Their La and Yb concentrations as well as the $(La/Yb)_n$ ratio are less than the mantle, which is characteristic of partial melting. These samples do not show the alteration effects associated with carbonatite metasomatism.

The group 1 and group 2 peridotites have a similar range in $\delta^{53}Cr$ compositions, and apart from the REE and Ti/Eu have similar chemical compositions. That group 2 peridotites do not show carbonatite melt signatures does not mean that the same Cr isotope fractionating process could not have been carried out by a different melt. A different Cr undersaturated melt could have interacted with the group 2 peridotites, resulting in the preferential transfer

of light Cr isotopes from the mantle into the melt, and leaving behind a mantle with heavy $\delta^{53}Cr$. If the melt is not as enriched in REE as the carbonatitic melt, then a trend between $(La/Yb)_n$ and $\delta^{53}Cr$ would not exist.

3.5.5.4 Isotopically light Cr liquids

There are a number of samples with isotopically light $\delta^{53}Cr$ outside the ranges of the BSE (-0.12 ± 0.10 ‰), BD-806, KH03-10 and KH03-27 with $\delta^{53}Cr$ of (-0.33 to -0.25 ‰). The light $\delta^{53}Cr$ is not related to lithology, as samples include a dunite, spinel lherzolite and spinel harzburgite respectively. Similarly, there is no correlation with Al_2O_3 compositions, so the light composition is not related to partial melting. Non-equilibrium interaction within these rocks would not be able to lead to these light compositions, as heavy Cr would not be preferentially removed.

A possible explanation for light $\delta^{53}Cr$ values is that they are instead the result of addition of Cr from the metasomatising melts proposed above. After the Cr undersaturated melts have interacted with the mantle they will become enriched in light Cr. Once such melts equilibrate with the mantle then their effect on mantle $\delta^{53}Cr$ will be different to that explained above. Equilibrium exchange will lead to an offset in the isotopic composition equal to the isotopic fractionation factor between the two phases, which would decrease the $\delta^{53}Cr$ of the mantle peridotites.

3.6. CONCLUSIONS

Data from 42 mantle samples are presented with a range from -0.35 to 0.43 ‰, compositions that agree with previous studies. Mineral separates from 4 peridotites were measured, with only small differences in $\delta^{53}Cr$ between phases identified. There is no evidence that any phases are isotopically distinct

Geochemical trends (Al_2O_3 %, etc.) show that there is no correlation between the degree of melting and $\delta^{53}Cr$. The modelled behaviour of Cr isotope fractionation during melting shows that variations in the mantle can only be created by unreasonably large fractionations, which are not expected in the mantle. The similarity between the composition of melts and the mantle suggest that only small fractionations occur during melting. The small fractionations that are allowed from the composition of melts mean that only a small contribution to the $\delta^{53}Cr$ variation can be accounted for by melting.

Evidence of interactions between mantle peridotites with high $\delta^{53}Cr$ and carbonatite melts were provided through high La concentrations and $(La/Yb)_n$ ratios, and low Ti/Eu ratios. The high $\delta^{53}Cr$ composition of these samples can be explained by the non-equilibrium fluid melt interactions, with Cr undersaturated melts. Non-equilibrium fluid melt interactions between the mantle and other Cr deficient melts may occur, without having the same trace element variations. The creation of an isotopically light phase through this process can also explain light $\delta^{53}Cr$ compositions within peridotites through later interactions.

The variations seen within the mantle, mean that the use of mantle peridotites to calculate the BSE will not provide an accurate composition. Variations in the mantle from metasomatism are difficult to identify. Mantle peridotites with metasomatic $\delta^{53}Cr$ variations

will likely be included in any selection of samples. This will create BSE estimates with large uncertainties.

Chapter 4: $\delta^{53}Cr$ variations in komatiite flows and a new value of the BSE

4.1. INTRODUCTION

Komatiites are enigmatic igneous rocks first described by (Viljoen and Viljoen, 1969). They represent high degree partial melts, enriched in compatible elements such as Mg, Ni and Cr, and are of particular interest because they provide a method for studying the evolution of the mantle from the Archean to today. The first identified komatiites were from the Proterozoic and Archean, suggesting that the conditions necessary for their formation no longer persist within the modern mantle. Then, Phanerozoic examples were recognised with the identification of the Gorgona komatiites (Echeverria, 1980) which formed at 89.2 ± 5.2 Ma (Walker et al., 1999).

4.1.1. Komatiite genesis

In order to produce the compatible element rich composition of komatiites, high degrees of partial melting are required. This can be achieved by increasing the temperature of the mantle beyond the solidus (which requires temperatures up to 1650°C (Kushiro and Yoder, 1969; Arndt et al., 1997; Arndt et al., 1998)). Alternatively, high degree melts can be created by adding water and thereby moving the solidus. Melting with 10 % of water in the source can lower the solidus by 300°C, which can create high degree partial melts at ambient mantle temperatures (Brooks and Hart, 1974). The melts created under these different conditions should have distinct characteristics. However, evidence to support both theories have been identified within komatiites.

Early evidence presented for the hydrous melting hypothesis included the ‘quenched’ spinifex texture of olivine. This unusual texture, ubiquitous in komatiites, was initially explained by rapid cooling from the dehydration of the melt at low pressures (Brooks and Hart, 1974). However, an alternative hypothesis is that the spinifex texture is created by

localised Mg depletion within the flow (Arndt, 1986). The spinifex texture has been recreated in anhydrous experiments with slow cooling rates (Faure et al., 2006), showing that there is no need to invoke hydrous melting.

In a series of papers by Parman, Grove and co-workers a hydrous melting hypothesis was developed (Grove et al., 1997; Parman et al., 2004). In this model the source of the komatiites was a subduction zone, which provided the higher water contents. The hydrous melting theory is hard to reconcile with the interpretation of komatiites as extrusive rocks. During the ascent of a hydrous magma, the lower pressures would reduce the solubility of water and lead to dehydration of the magma, thereby raising the solidus and freezing the melt within the crust (Brooks and Hart, 1974). A new model for intrusive formation within subduction zones was developed to allow hydrous melting. This theory was developed around the Barberton komatiites, which had been interpreted as intrusive rocks (Parman et al., 1997; Grove et al., 1999; Parman et al., 2004). The similarities of komatiites to boninites (Parman et al., 2004), a hydrous high degree partial melt found in recent volcanism (Crawford et al., 1989), was used to suggest that komatiites formed in the same setting (Parman et al., 2004). Geobarometers using pyroxenes from Barberton komatiites were used to calculate the depth of formation at 190 MPa (Parman et al., 1997). However there are extensive studies that conclude that komatiites are extrusive lava flows (Pyke et al., 1973; Aitken and Echeverria, 1984; Wilson et al., 1989 etc.), including the Barberton komatiites, which had previously been described as intrusive (Dann, 2001).

Recently, extensive work has been carried out to determine the water content of komatiites. Berry et al., (2008) measured the $Fe^{2+}/\Sigma Fe_{TOT}$ to determine how much dehydration occurred, while other studies have measured the H_2O content of inclusions within minerals

(Shimizu et al., 2001; Sobolev et al., 2016; Asafov et al., 2018). These methods have shown that there is some water present, but it is less than 1 %. This is insufficient to decrease the solidus of the ambient mantle enough to create komatiites. Evidence previously presented in favour of hydrous melting, has now been explained through other methods, leading to the conclusion that the high degree of melting of komatiite magmas was caused by higher temperatures.

4.1.2. Komatiites as tools for investigating the mantle

Komatiites, being high degree melts, have a composition closer to that of the mantle than basalts and other mantle derived melts. The temporal range of komatiites renders them particularly useful for studying how the Earth has evolved over much of the history of the planet. Komatiites have been used to demonstrate that there has been no significant change in mantle oxidation state over time, e.g. (Canil, 1997; Canil, 1999; Hibbert et al., 2012).

The high temperatures that are required for komatiite formation allow the stable isotope composition of the mantle to be explored. Equilibrium isotope fractionation decreases with temperature, following the relation $\Delta_{a-b} \propto \frac{1}{T^2}$ (e.g. Schauble, 2004). Higher degrees of melting will in any case have a more limited amount of isotopic fractionation during melting, as the liquid more closely approaches the bulk composition of the source. Komatiites have previously been used to estimate the stable isotope composition of the mantle for a number of elements including; Fe, Ni, Mo, Sn and Zn (Hibbert et al., 2012; Greber et al., 2015; Badullovich et al., 2017; Gall et al., 2017; Sossi et al., 2018b). These studies selected komatiites that were most representative of the initial liquid. The same method has been used to calculate the BSE δ^{53}Cr (Sossi et al., 2018a). Archean komatiites with spinifex textures from five cratons were used as they were thought to most likely to represent

quenched liquids (Faure et al., 2006; Sossi et al., 2016). Sossi et al., (2018a) combined their komatiite data with the $\delta^{53}Cr$ of fertile unmetasomatised samples, to provide a value of the BSE (0.11 ± 0.06‰, n = 36). The $\delta^{53}Cr$ BSE value obtained using komatiites shows an improvement in the precision over other methods, which only used mantle peridotites, whose composition can be affected by metasomatism ((Xia et al., 2017; Shen et al., 2018) and chapter three of this work).

Further refinement of the BSE composition may be possible through developing an understanding of the behaviour of Cr stable isotopes during komatiite crystallisation. The composition of komatiite liquid does not fractionate during melting (Sossi et al., 2018a) which means their composition is that of the mantle. However, Cr isotopes can fractionate during basalt crystallisation (Bonnand et al., 2016a). To improve our knowledge of the Cr isotope composition of komatiite liquids, the effect of crystallisation needs to be understood.

4.2. SAMPLES

Komatiites from three suites were analysed representing diverse ages, locations and compositions. The komatiites within this study are among the least altered thus far discovered, in order to reduce the likelihood of post emplacement changes to the stable Cr isotope composition. Samples were chosen from particularly well studied flows.

4.2.1. Tony's Flow, Reliance Formation, Belingwe

Tony's Flow is one of a number of komatiite flows from the Reliance Formation within the Belingwe Greenstone Belt. The flow is dated at 2.7 Ga (Puchtel et al. 1997; Chauvel et al. 1993). Samples in this study were collected on two sampling expeditions and are from the spinifex and cumulate layers of the same flow (Puchtel et al., 2009). The MgO concentration of the parental liquid has been estimated at 27.5 %, by calculating the composition of melt in

equilibrium with the most magnesium rich olivines (Asafov et al., 2018). Tony's Flow REE abundances show that the mantle source was strongly depleted in incompatible trace elements. The flow is described as being uniquely fresh for Archean komatiites (Nisbet et al., 1987). The oxidation state of the Tony's Flow lava has been given as ΔFMQ= +0.48 ± 0.27 (Nicklas et al., 2018).

4.2.2. Victoria Lava Lake, Vetreny Belt

Komatiites from Victoria Lava Lake are from a thick flow, interpreted as a lava lake (Puchtel et al., 1996). The komatiite flow is dated at 2.4 Ga (Puchtel et al., 1997). The current study used samples described in (Puchtel et al., 2016b) from a recent sampling expedition. The parental liquid for these samples is estimated to contain 15 % MgO (Puchtel et al., 1996), consistent with a lower degree of melting than Tony's Flow komatiites. Samples from the Vetreny Belt encompass a range of komatiite types. Chromite separates were taken from two samples in this suite. The only minerals present as phenocrysts are olivine and chromite (Puchtel et al., 1996). Lithophile trace element and Sm-Nd isotopic studies show that the samples come from a depleted mantle (Puchtel et al., 1997). Most elements were shown to be immobile within Victoria Lava Lake, even during low grade metamorphism (Puchtel et al., 1996). Contamination from a crustal source is recognized within the Hf and Nd isotope compositions, and calculated to be 4 % (Puchtel et al., 2016). The initial oxidation state of the lavas has been calculated using V partitioning in olivine (ΔFMQ= +0.43 ± 0.26) and chromite (ΔFMQ= +0.37 ± 0.15) (Nicklas et al., 2016; Nicklas et al., 2018).

4.2.3. Gorgona Island

The youngest samples come from the Isle of Gorgona, off the coast of Colombia, which are unique Phanerozoic komatiites dated at 89.2 ± 5.2 Ma by Re-Os (Walker et al., 1999). The

initial MgO % composition of the Gorgona Island komatiites was calculated using the melt in equilibrium with the composition of olivines to be 18 % (Nisbet et al., 1993). The Isle of Gorgona is made up of a range of intrusive and extrusive rocks, and is believed to have been emplaced from the sea floor (Kerr, 2005). The Gorgona island rocks have been related to the Caribbean flood basalts (Arndt et al., 1997; Révillon et al., 2000; Kerr, 2005). Samples from Gorgona were collected from around the edge of the island and from different lava flows. The heavily faulted and poor exposures of the komatiites mean that relations between flows are uncertain (Kerr, 2005).

4.3. ANALYTIC TECHNIQUES

4.3.1. Sample Dissolution

Aliquots of the komatiite powders were initially dissolved in HF and HNO_3 before slowly drying to prevent fluoride formation. Residues were then dissolved in 6M HCl. If undissolved material remained, high pressure dissolutions, using a HPA-S high pressure asher, were carried out. Samples were taken up in 6M HCl and then pressurised within the asher to 100-130 bar and heated to 250°C for 5 hours. The blanks from the high-pressure dissolution were <3 ng. The total procedural blank was <4 ng, which is negligible compared to the amount of Cr processed (2 μg).

4.3.2. Sample Preparation

Two micrograms of Cr were prepared by chemical purification. A double spike of ^{50}Cr-^{54}Cr, was used to correct for experimentally induced fractionation and was added to samples prior to chemical separation. A two-stage cation exchange column chemistry was used to produce purified Cr. The first column removes matrix elements, while the second column was

designed to further remove elements that create isobaric interferences of Ti, V and Fe with Cr. The column procedure follows that described in (Bonnand et al., 2016b). After Cr separation, the samples were oxidised with H_2O_2 to remove any organic material from the columns.

4.3.3. Thermal Ionisation Mass Spectrometry

A Thermo Scientific Triton Thermal Ionisation Mass Spectrometer (TIMS) was used to measure isotopic compositions. Samples were heated on rhenium (Re) filaments. Chromium was loaded on the filaments in 6M HCl along with a silicon boride activator. Filaments were flashed to a dull red to ensure that a homogeneous glass was formed. Measurements were made with an ion current of 3-7x10^{-11} Amps on the largest beam (^{52}Cr). The cup configuration measured all isotopes of Cr (^{50}Cr, ^{52}Cr, ^{53}Cr and ^{54}Cr) and elements with isobaric interferences ^{49}Ti, ^{51}V and ^{56}Fe in static mode. A run for one sample consisted of 540, 8.4 second measurements. The run was split into 54 blocks, with a 50 second baseline taken after each block. Amplifier gains were taken before the measurements every day.

The reproducibility of measurements was calculated by repeat measurements of geological standard JP-1 over a year. This gave a value of δ^{53}Cr= -0.107 ± 0.019 ‰ (2std), which agrees well with previous studies (−0.128 ± 0.022 (Bonnand et al., 2016a)). The external reproducibility, 19 ppm, is as good as, or better than, previous measurements (22 ppm (Bonnand et al., 2016a) and 35 ppm (Schoenberg et al., 2016)). The internal precision of the run is calculated using the 2x standard error of the 540 blocks, with a 6 s.e. filter to remove outliers. External reproducibility was used to report the uncertainty on the measurements as it was greater than the internal precision.

4.4. RESULTS

Komatiites measured in this study range from $\delta^{53}Cr$ = -0.16 to -0.01 ‰ with substantial overlap between locations (Figure 4.1.). Gorgona samples range from -0.15 to -0.06 ‰, Victoria Lava Lake from -0.16 to -0.14‰ and Tony's Flow from -0.14 to -0.01‰ (Table 4.1. and Figure 4.1.). The composition of chromite separates from Victoria Lava Lake komatiites 12001 and 12105 were within error of the bulk rock compositions, $\delta^{53}Cr$ = -0.14 to -0.13‰ (Figure 4.2.). Komatiites measured in this study agree with those reported in previous studies, $\delta^{53}Cr$= -0.17 to -0.07 ‰ (Sossi et al., 2018a).

Resolvable differences occur within samples from two locations, Gorgona Island and Tony's Flow. The $\delta^{53}Cr$ within these flows vary with MgO (%) content, both of which become isotopically heavy at lower MgO, (Figure 4.1.). Victoria Lava Lake does not show any variations in $\delta^{53}Cr$ even across a large range of MgO (%).

Table 4.1.

Sample	Location	Type	$\delta^{53}Cr$	2 s.e.	Cr (ppm)
GOR 94-3	Gorgona	Cumulate	-0.14	0.01	2745
GOR 94-17	Gorgona	Cumulate	-0.12	0.01	932
GOR 94-44	Gorgona	Cumulate	-0.15	0.01	2598
GOR 94-19	Gorgona	Spinifex	-0.06	0.02	514
GOR 94-43	Gorgona	Spinifex	-0.12	0.01	1340
TN-16	Tony's Flow	Cumulate	-0.12	0.01	2247
TN-19	Tony's Flow	Cumulate	-0.07	0.01	2223
ZV-10	Tony's Flow	Cumulate	-0.14	0.01	2284
TN-01	Tony's Flow	Spinifex	-0.14	0.03	2332
TN-03	Tony's Flow	Spinifex	-0.06	0.01	2455
TN-05	Tony's Flow	Spinifex	-0.13	0.01	2369
TN-06	Tony's Flow	Spinifex	-0.09	0.01	2191
ZV-14	Tony's Flow	Spinifex	-0.01	0.01	2023
12001	Victoria Lava Lake	Cumulate	-0.14	0.01	3146
12105	Victoria Lava Lake	Cumulate	-0.14	0.01	3170
12106	Victoria Lava Lake	Cumulate	-0.15	0.01	1933
12101	Victoria Lava Lake	Spinifex	-0.16	0.01	607
12110	Victoria Lava Lake	Spinifex	-0.15	0.01	1277
12117	Victoria Lava Lake	Spinifex	-0.15	0.02	818
12124	Victoria Lava Lake	Spinifex	-0.15	0.01	372
12001 Chr 1	Vetreny Belt	Chromite	-0.14	0.01	242400
12001 Chr 2	Vetreny Belt	Chromite	-0.14	0.04	239000
12105 Chr 1	Vetreny Belt	Chromite	-0.13	0.02	202200
12105 Chr 2	Vetreny Belt	Chromite	-0.13	0.02	249800

Table 4.1. Composition of $\delta^{53}Cr$ and [Cr] for komatiites and chromite separates. Chromium concentration data is taken from the literature (Puchtel et al., 2009; Puchtel et al., 2016)*, through analysis using the Department of Earth Sciences, Oxfords Quad, or by isotope dilution.*

Figure 4.1.

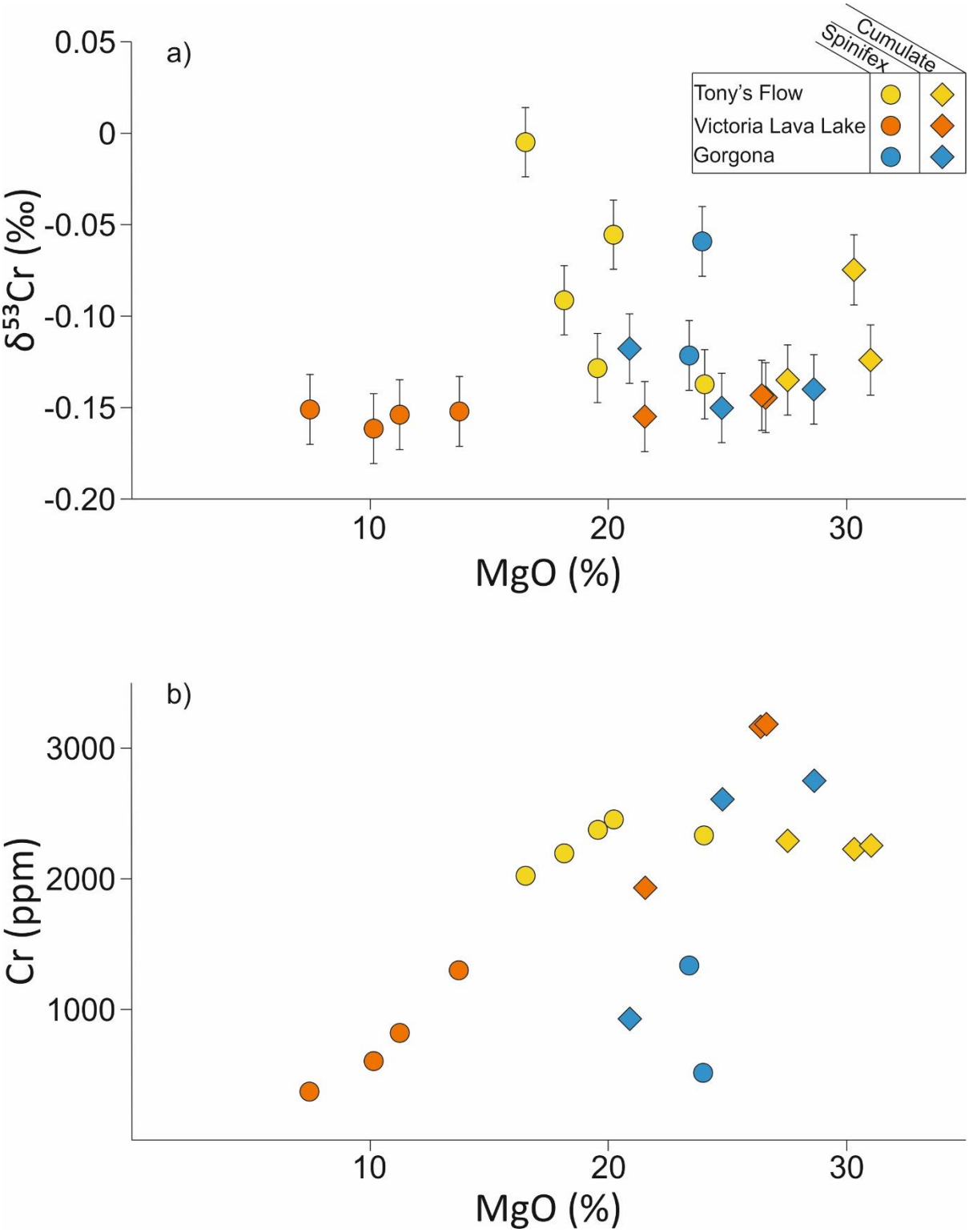

Figure 4.1. Variations in $\delta^{53}Cr$ and [Cr] plotted against MgO (%), which can be used as a proxy of crystallisation. The $\delta^{53}Cr$ of all komatiite flows overlap. Resolvable variations in $\delta^{53}Cr$ are

identified in Gorgona and Tony's Flow komatiites, while Victoria Lava Lake has no resolvable difference in δ^{53}Cr. Gorgona and Tony's Flow show an increase in δ^{53}Cr at lower MgO (%), suggesting isotope fractionation during crystallisation. A positive correlation is seen between the [Cr] and MgO(%), suggesting that Cr acts as a compatible element.

Figure 4.2.

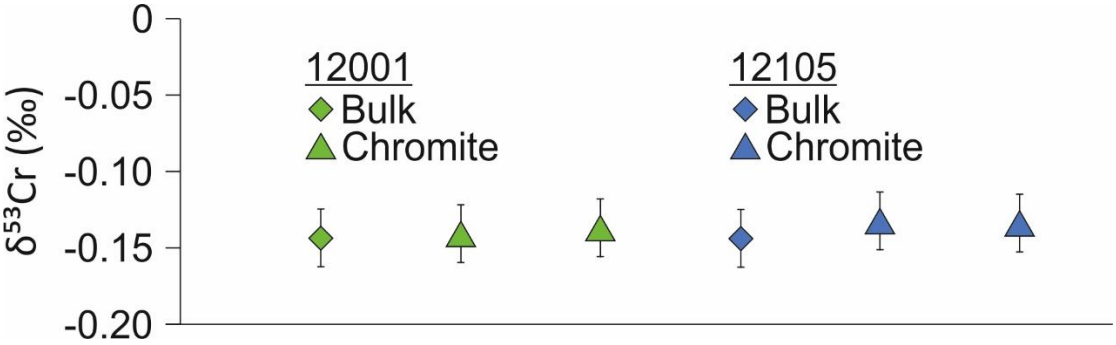

Figure 4.2. The δ^{53}Cr of chromites from Victoria Lava Lake komatiites plotted alongside the bulk rock compositions. The komatiites are indistinguishable from their chromite separates.

4.5. DISCUSSION

Resolvable δ^{53}Cr differences within komatiite flows have been identified. Magmatic Cr isotope fractionation processes have previously been identified (Bonnand et al., 2016a, in review). Therefore, fractional crystallisation may affect the δ^{53}Cr of komatiites as well. The δ^{53}Cr variations within the komatiite flows cannot be due to isotopic fractionations during partial melting, as any variation within the komatiite liquid would not be preserved during transportation. The major minerals that control the chemical composition of komatiites are first considered and then used to understand the behaviour of Cr within the komatiite suites.

4.5.1. Crystallisation of komatiite flows

The composition of komatiite lava flows evolve through in situ crystallisation. Olivine is the major solidus phase and crystallises throughout, changing the composition of the liquid in the flow. The typical olivine modal abundance is 20-50 %, but can be up to 80 % (Arndt, 2008). Olivine in komatiites is MgO rich (~50 % (Renner et al., 1994)), which leads to a lower MgO content in komatiites that form later. The MgO content of komatiites can be used as a proxy for the degree of crystallisation.

Figure 4.3.

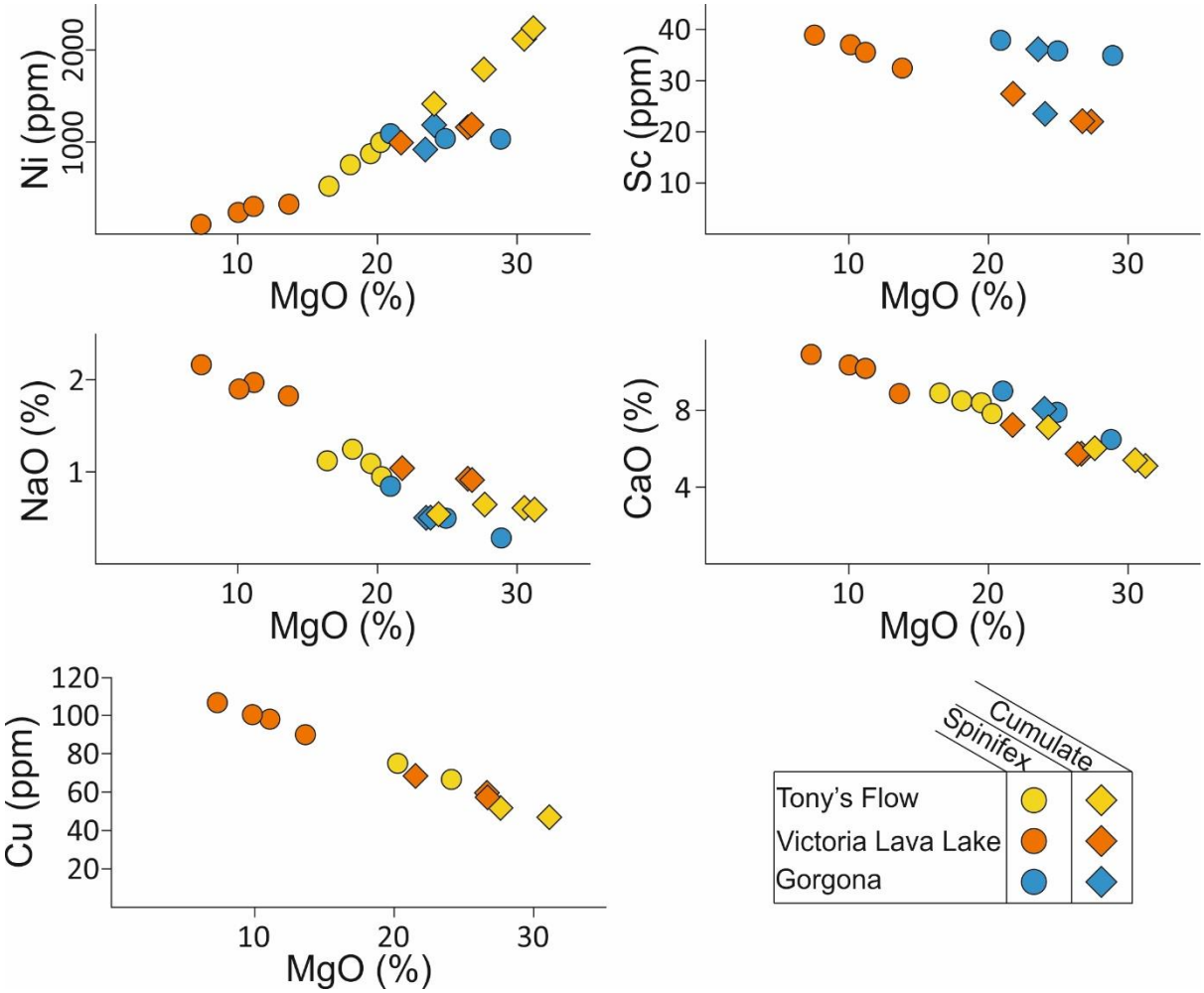

Figure 4.3. Major element variations plotted against MgO. MgO here is used as an indicator of crystallisation, as it is compatible within olivine, the major phase found in komatiites. Figure

6a confirms that olivine is the major phase crystallising, with a strong correlation against the MgO content seen throughout. Negative correlations between MgO and Sc, NaO, CaO and Cu shows that these elements are incompatible and minerals such as orthopyrene, amphibole, clinopyroxene, plagioclase and sulphides are not major phases in the komatiites in this study.

In order to further understand the behaviour of Cr it is necessary to constrain the major phases within the komatiites. Nickel is highly compatible within olivine. The Ni content of the komatiites can be used to ascertain if olivine is the main Mg phase forming, or if the MgO contents are controlled by multiple phases. Deviations away from a simple Ni-Mg trend will show that either element is crystallising within another phase. The strong correlation between Ni and MgO, without any inflections (Figure 4.3.a.), shows that olivine is the major MgO rich phase crystallisation throughout, confirming that variations in MgO (%) is simply due to the crystallisation of olivine.

Pyroxenes are common within komatiite flows. They usually have higher Cr concentrations than olivines, and are an important host of Cr in mantle rocks and basalts. Scandium is compatible within orthopyroxene, but is shown to behave incompatibly within Victoria Lava Lake and Gorgona (Figure 4.3.b.). As Sc behaves incompatibly, orthopyroxene is not a major mineral, and will not influence the behaviour of Cr. Clinopyroxenes are enriched in NaO and CaO. These elements are also enriched in other minerals, such as amphiboles and plagioclase, which can also occur within komatiites. Figure 4.3.c. and d. show that both elements behave incompatibly. Clinopyroxenes, amphiboles and plagioclases can also be discounted as phases that will influence the behaviour of Cr.

Sulphides in komatiites could fractionate $\delta^{53}Cr$ as they have large equilibrium fractionation coefficients with silicate minerals (Moynier et al., 2011b). Sulphides found

within komatiites are Cu and Ni rich, and can also be enriched in Cr (Arndt, 2008). Nickel is controlled by the crystallisation of olivine, leading to the positive correlations seen within Figure (4.3.a.), however if sulphides crystallise at low temperatures, they will rapidly consume the remaining Ni (Arndt, 2008). The crystallisation of sulphide at lower temperatures would cause an inflexion within the trends, not seen in these graphs. Furthermore, Cu behaves incompatibly in the komatiites but would be removed if sulphides crystallised (Figure 4.3.e.).

Chromites within komatiites, are usually present in a few percent or less although in some extreme cases they can make up 10 modal percent (Barnes, 1998). They contain 10s of percent of Cr, so are likely to be an important reservoir. At high MgO contents, Cr behaves slightly incompatibly, with a small increase in concentration. At lower MgO, Cr behaves compatibly. As other Cr rich phases, (e.g. pyroxenes and sulphides) are not crystallising in large amounts, the inflexion in the Cr-MgO trend is best explained by the initiation of chromite crystallisation (Figure 4.1.b.).

During crystallisation of komatiites, olivine excesses and deficits occur (Arndt, 1986). For the Reliance Formation komatiites, including Tony's Flow, there is a strong correlation between the MgO content and the amount of olivine (Figure 4.4.a.). MgO concentrations that are higher than the initial composition show an excess of olivine, while those with lower have olivine deficits. The composition of the komatiite can be used to calculate the amount of olivine that has crystallised out of the melt, (Figure 4.4.a.) which shows that those with lower MgO have a combination of higher olivine crystallisation as well as lower modal olivine (Arndt, 2008).

4.5.2. Chromium variations within komatiite flows

From the previous discussion, it is clear that the main minerals within the komatiite flows and samples studied here are olivine and chromite. Olivines usually contain low concentrations of Cr, within the mantle and in mafic lavas the concentration can be 100 ppm or less. However, in komatiites the Cr concentration of olivine is higher (500-2000 ppm (Arndt, 2008)). This is due to a combination of; greater compatibility of Cr at high temperatures and Mg contents, delayed crystallisation of chromites and higher $Cr^{2+}/\Sigma Cr_{TOT}$ (Donaldson, 1982; Shore, 1996). The higher Cr contents of olivines and the dominance of olivine within komatiites, makes them a major host of Cr.

The behaviour of Cr within the komatiite flows within this study differ (Figure 4.1.b.). Tony's Flow and Victoria Lava Lake both show that Cr is compatible at low Mg, but within Tony's Flow Cr behaves incompatibly at high Mg contents. This behaviour is not seen in Victoria Lava Lake, due to the lower Mg contents within the flow. The Mg and Cr trends are displaced from each other, with Tony's Flow crossing the x-axis at a lower MgO content than Victoria Lava Lake (Figure 4.1.b.), showing that Cr is behaving less compatibly in this flow. Gorgona Island komatiites do not show a clear trend, due to komatiites coming from a number of flows.

The different behaviour of Cr in Tony's Flow and Victoria Lava Lake can be explained by crystallisation of olivine and chromites. Olivine is the liquidus phase in komatiite flow crystallisation, but the liquidus temperature is dependent upon the Mg content of the magma; Mg-rich lavas begin to crystallise olivine at higher temperatures. Experimental studies have shown that the change in liquidus temperature can vary by over 100°C. Tony's Flow and Gorgona, with MgO contents of 25 % will have an olivine liquidus temperature of

1500°C (Arndt, 1976), while Victoria Lava Lake komatiites, with an initial MgO content of 15-17 % will begin to crystallise at 1350°C (Murck and Campbell, 1986). The same studies found that the liquidus temperature of chromites was consistently at 1300°C and did not depend on the Mg content. Komatiite lava flows with low Mg contents (such as Victoria Lava Lake) will have only a small temperature difference between olivine and chromite crystallisation. Higher Mg lavas (such as Tony's Flow) will have a larger difference in liquidus temperatures. The early crystallisation within Tony's Flow will only have experienced the formation of olivine, which is expressed by the MgO and Cr variations within Figure 4.1.b. The initial olivine-only crystallisation results in a slight increase in the Cr concentration. At ~21 % MgO, chromite begins to crystallise which decreases the Cr concentration. In Victoria Lava Lake, olivine and chromite begin to crystallise almost at the same time, resulting in the positive correlation between Cr and MgO (Figure 4.1.b.).

Chromite will crystallise once the flow is saturated in Cr. Chromium is less soluble under more oxidised conditions and lower MgO (Murck and Campbell, 1986; Barnes, 1998). During olivine crystallisation, the MgO content of the komatiite magma is decreased and Cr saturation is eventually reached. Once saturation has been reached the chemical composition of the magma will evolve along the Cr saturation curve. The position of the chromite saturation curve in MgO vs Cr space will be controlled by the oxidation state of Cr. Figure 4.7. shows that chromite saturation is suppressed in Tony's Flow compared to Victoria Lava Lake, which suggests that the Cr^{2+}/Cr_{TOT} is lower. The Cr^{2+}/Cr_{TOT} is controlled by the oxygen fugacity of the lava, and the temperature (Li et al., 1995). The oxygen fugacity of the two komatiite flows is indistinguishable (Nicklas et al., 2016; Nicklas et al., 2018), therefore the difference arises from the temperature. Tony's Flow will have higher temperature, as shown by the higher MgO content, due to a higher degree of melting and temperature.

Figure 4.4.

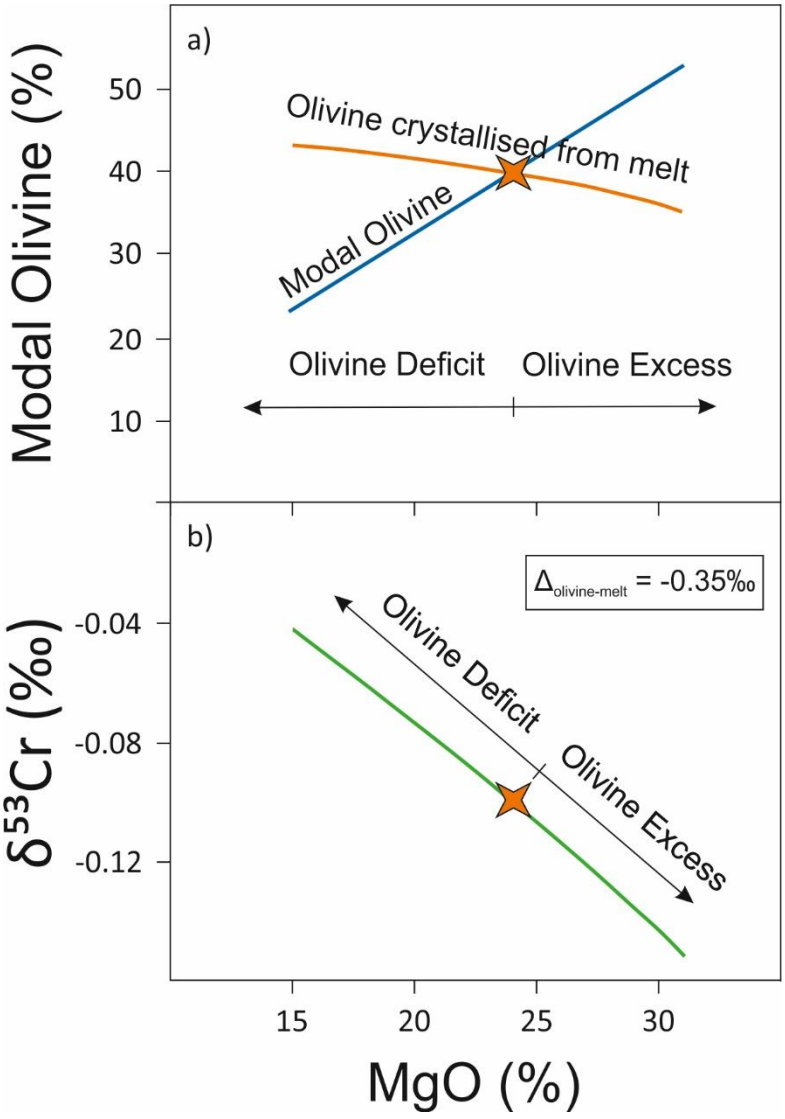

Figure 4.4. Model of olivine excess and deficits. Figure 8a shows the measured modal olivine concentration (blue line), and the modelled amount of olivine that has crystallised out of the melt (orange line, see the appendix for calculations). Olivine excesses occur in komatiites with high MgO contents. The initial composition of the melt is given by the orange star. Figure 8b shows the modelled variation of the melt, with a difference in the isotopic composition and the rest of komatiite of -0.35 ‰. The [Cr] of olivine used within the model is 1500 ppm. Komatiites that have lower MgO contents, have heavier δ^{53}Cr compositions due to deficits of isotopically light olivine.

Gorgona komatiites do not show clear trends unlike the other two komatiite flows studies here. However, there is a decrease in the Cr content with MgO composition. The plots of major elements show that the major minerals, within these komatiite are also olivine and chromite. Although it is not possible to tell when chromite crystallisation began, lower Cr contents at lower MgO, suggests that crystallisation proceeded in a similar way to the other flows.

4.5.3. External alteration of the δ^{53}Cr of komatiites

In order to ascertain the manner in which Cr isotopes are fractionated during crystallization it is first necessary to ascertain whether secondary or open system processes may have influenced the values obtained. Komatiites from the Archean, measured within this study, are described as remarkably fresh (Nisbet et al., 1987; Renner et al., 1994; Puchtel et al., 1996). This is relative to Archean rocks that, due to being billions of years old, are commonly highly altered, by processes such as weathering and serpentinisation, both of which can change δ^{53}Cr (Farkaš et al., 2013; Frei et al., 2014). The transport of komatiite magmas through the crust can also lead to entrainment of material, which may modify the composition of the initial magma (Puchtel et al., 2016). Before the effects of fractional crystallisation on δ^{53}Cr can be considered the extent to which these non-magmatic processes overprint the isotope composition must be addressed.

4.5.3.1. Crustal Assimilation

The amounts of crustal assimilation for komatiites have previously been calculated using Nd and Pb isotopes. Victoria Lava Lake is calculated to have had 4 % assimilation of

crustal contamination (Puchtel et al., 2016). The isotopic composition of Tony's Flow and Gorgona shows no evidence of significant crustal assimilation (Chauvel et al., 1993).

The $\delta^{53}Cr$ compositions of sedimentary rocks have a large range due to the greater fractionations at low temperatures (Bonnand et al., 2013; Frei et al., 2014). The inclusion of such material could in principle change the $\delta^{53}Cr$ of the magma. However, the crust contains much less Cr than komatiites (200 ppm compared to 2000 ppm), so the contribution to the Cr budget of komatiites from crustal material will be less than <1 %. In order to lead to variations within the komatiite melt, the crustal material would have to be highly fractionated. Victoria Lava Lake is the one sample suite with evidence of significant crustal assimilation, however no $\delta^{53}Cr$ variations can be resolved within the flow (Figure 4.1.a.). Crustal assimilation within the Victoria Lava Lake komatiites have not led to variations within the flow, however if the material was well mixed in, then the overall composition of the flow may have been altered. This is not the case, with a range of $\varepsilon^{143}Nd$ values of the flows (-0.52 to -1.00) showing that there the Victoria Lava Lake komatiites have varying amounts of sediment added.

4.5.3.2. Weathering

Weathering can alter the stable Cr isotope composition of rocks (Frei et al., 2014). The removal of more soluble and isotopically heavy Cr^{6+} results in weathered rocks becoming isotopically light (Frei et al., 2014). Fluid mobile elements, can be used as a proxy for weathering. The K_2O/SiO_2 will decrease with loss of mobile K, while Si will be unaffected. There is no such systematic variation within any of the flows (Figure 4.5.). Komatiites from Victoria Lava Lake show a large range in K_2O/SiO_2, but no decrease in $\delta^{53}Cr$ (Figure 4.5.a.). Tony's Flow and Gorgona peridotites have lower K_2O/SiO_2 ratios than Victoria Lava Lake and have a greater range in $\delta^{53}Cr$ (Figures 4.5.a. and b.). However, there is no variation between

K_2O/SiO_2 and $\delta^{53}Cr$ within suites, which would be expected if loss of K through weathering was related to a variation of the $\delta^{53}Cr$.

Figure 4.5.

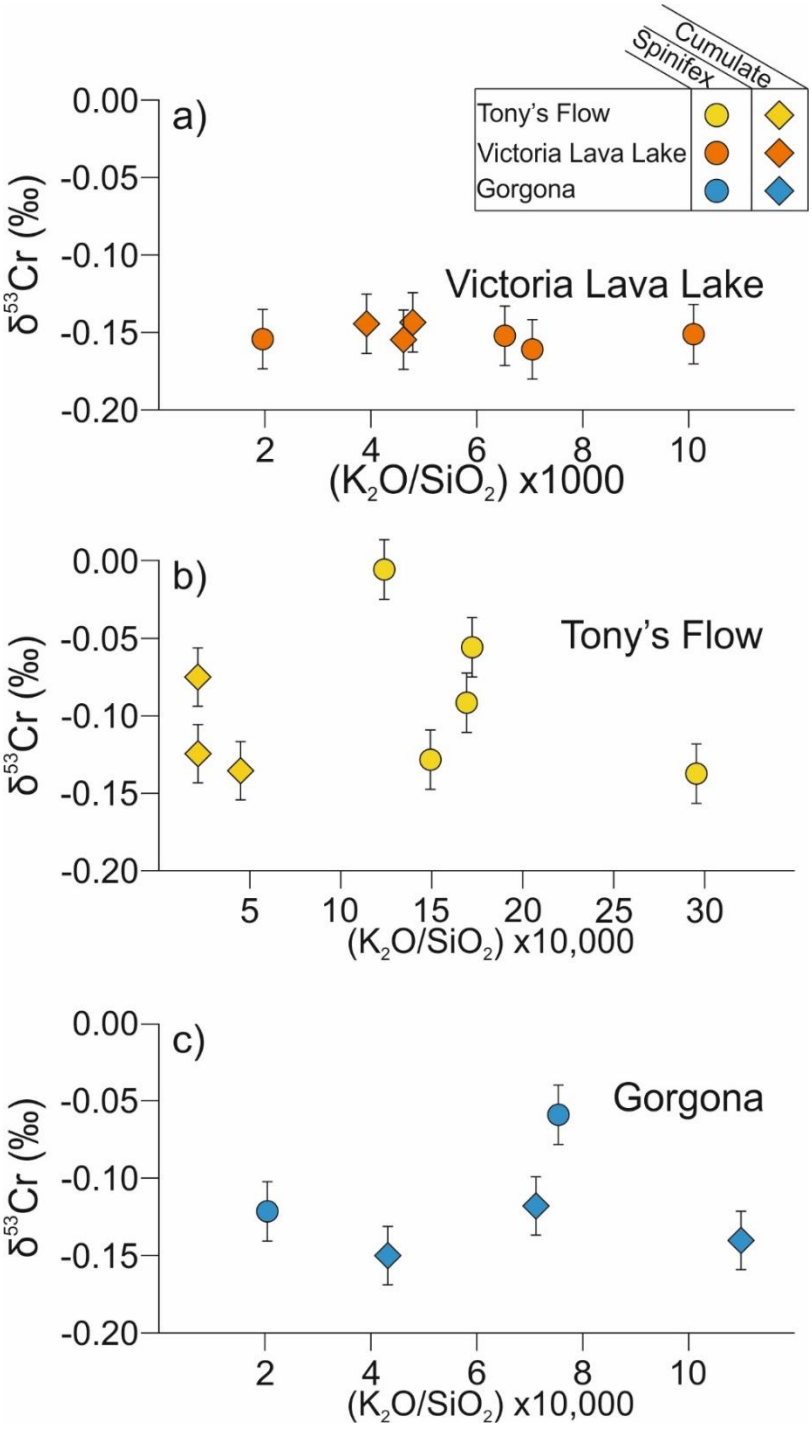

Figure 4.5. $\delta^{53}Cr$ plotted against weathering proxy K_2O/SiO_2. Lower K_2O/SiO_2 ratios indicate loss of fluid mobile K_2O during weathering. There is no change in the $\delta^{53}Cr$ with the K_2O/SiO_2 ratio in any of the komatiite suites, showing that weathering does not alter the composition.

4.5.3.3. Serpentinisation

Serpentinisation is common within komatiites, in which olivines and some other minerals react with high temperature fluids. Tony's Flow and Victoria Lava Lake both show evidence of this alteration (Nisbet et al., 1987; Puchtel et al., 1996). Farkaš *et al.*, (2013) has shown that serpentinisation can lead to increases in the δ^{53}Cr composition of rocks. The loss on ignition (LOI) index is used to quantify the amount of serpentinisation that has occurred. No variations between LOI and δ^{53}Cr are seen for the samples within this study.

Figure 4.6.

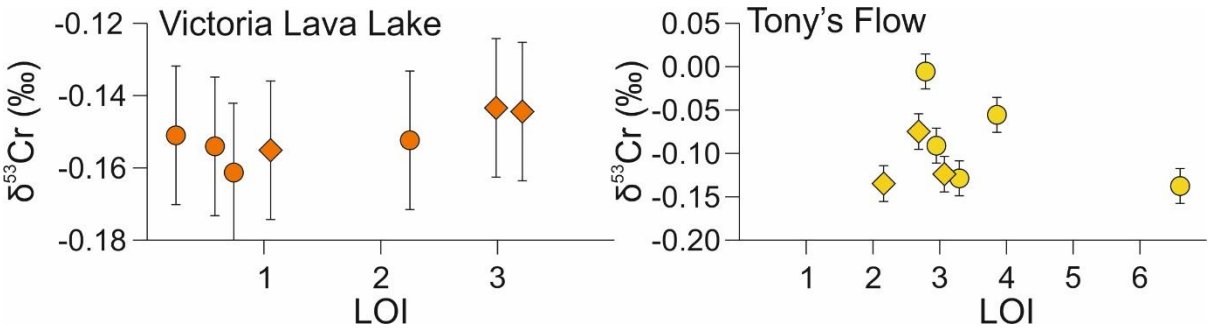

Figure 4.6. a and b showing δ^{53}Cr plotted against loss on ignition, an indicator of serpentinisation. There is no correlation in either of the flows. LOI data from Puchlet et al (2009, 2016).

Having ruled out the possibility that the δ^{53}Cr of komatiites have been altered by secondary processes, the variations within the flows are explained in terms of magmatic processes in the following.

4.5.4. Magmatic Cr isotope fractionation within komatiite flows

Fractional crystallisation has previously been shown to alter the δ^{53}Cr of terrestrial and extra-terrestrial magmas, through crystallisation of isotopically heavy phases (Bonnand et al., 2016a; Bonnand et al., in review). Within lunar samples, crystallisation of isotopically

heavy chromite led to more evolved melts becoming isotopically light (Bonnand et al., 2016a). A similar trend was seen within terrestrial basalts (Bonnand et al., in review), with the small variation within the $\delta^{53}Cr$ explained by the crystallisation of pyroxene along with spinel.

Chromium isotope compositions of the komatiite flows show different behaviour to that identified in previous studies, and between flows. Victoria Lava Lake komatiites have no variation in $\delta^{53}Cr$ during crystallisation (Figure 4.1.a.) whereas Tony's Flow and Gorgona Island komatiites change to heavier $\delta^{53}Cr$ as crystallisation progresses (Figure 4.1.a.). The changes in Tony's Flow and Gorgona Island suggest that a light phase is being removed from the magma. Equilibrium fractionation will lead to light Cr isotope compositions in phases that have lower oxidation states, and higher coordination numbers (Schauble, 2004). The two minerals that host Cr within komatiites are olivines and chromite. Olivine contains Cr within octahedral sites (C.N. = 6) and can hold Cr^{2+}, while spinel hosts Cr within tetrahedral sites (C.N. = 4) and only contains Cr^{3+} (Roeder and Reynolds, 1991), which suggests that olivine should be lighter than chromite (Shen et al., 2016; Shen et al., 2018).

Tony's Flow has olivine excesses and deficits within different komatiites. Removal of isotopically light olivines could increase the $\delta^{53}Cr$ of these komatiites. The expected variations have been modelled, and are presented in Figure 4.4.a. In order to recreate the variations seen within the Tony's Flow komatiite lavas a minimum fractionation factor of $\alpha_{melt\text{-}olivine}$ = 1.00035 is required. The inclusion of isotopically light olivine can explain the majority of $\delta^{53}Cr$ variations identified within the komatiite lava flows.

Olivine excesses and deficits would also be expected to lead to different $\delta^{53}Cr$ within Victoria Lava Lake, if these komatiites have the same inter-mineral isotope fractionation as in Tony's Flow. However, no $\delta^{53}Cr$ variations are seen. This either means there is no isotopic

fractionation between the phases within this flow or olivine excesses / deficits did not occur. The $\delta^{53}Cr$ composition of chromites have been measured for komatiites from Victoria Lava Lake (Figure 4.2.), and have the same composition as the bulk rocks. In order for the composition of the chromites to be the same as the bulk rock, the $\delta^{53}Cr$ composition of olivine must also be the same. The lack of variation of $\delta^{53}Cr$ within Victoria Lava Lake, is therefore due to no isotopic fractionation between phases.

The difference between the behaviour of the Victoria Lava Lake and Tony's Flow may be explained by differences in the $Cr^{2+}/ \Sigma Cr_{TOT}$ of the komatiites. Inter-mineral fractionations are caused by the different oxidation state of Cr, and the coordination number. There will not be any difference in the coordination number between olivines within Tony's Flow and Victoria Lava Lake hence this cannot be a cause of the differences in inter-mineral fractionation.

It is shown in Figure 4.7. that Tony's Flow has a higher Cr^{2+}/Cr_{TOT} ratio than Victoria Lava Lake, which suggests that the different spinel-olivine fractionation of the komatiite flows are due to the Cr oxidation state. A lower Cr^{2+}/Cr_{TOT} ratio will cause smaller inter-mineral fractionations within the Victoria Lava Lake komatiites, and lead to the constant $\delta^{53}Cr$ composition of these komatiite samples.

Figure 4.7.

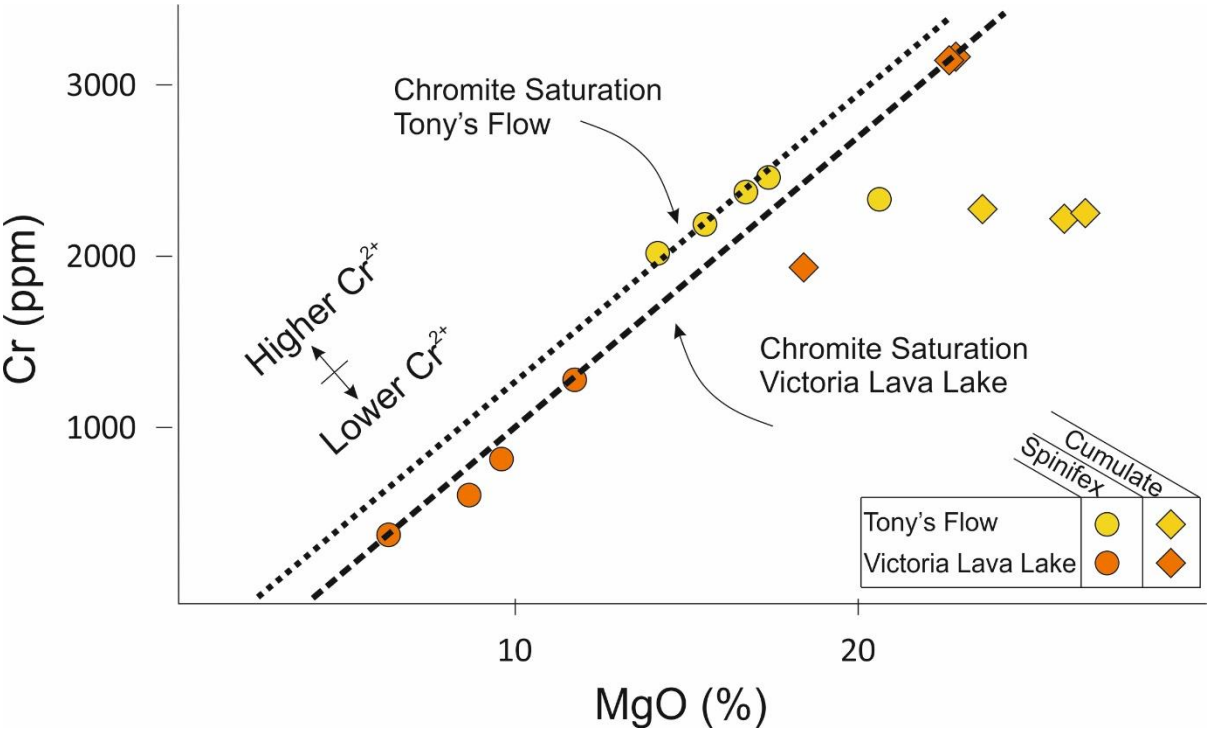

Figure 4.7. Comparison of chromite saturation curves of Tony's Flow and Victoria Lava Lake, as shown by MgO and [Cr] correlations. Tony's Flow has a chromite saturation line that is at lower MgO contents compared to Victoria Lava Lake. This is due to the higher temperatures within this flow, which causes Cr to be more compatible.

There is a general trend to lighter $\delta^{53}Cr$ with magmatic evolution for Gorgona Island komatiites (Figure 4.1.a). As with the Cr concentrations, the trend within Gorgona komatiites is not clearly defined, because the measurements come from numerous komatiite flows. The increase in $\delta^{53}Cr$ to heavier values is similar to that seen in Tony's Flow, suggesting that a similar process may be occurring within both flows

4.5.5. Differences in crystallisation behaviour between komatiitic and other magmas

Previous studies have investigated $\delta^{53}Cr$ isotope fractionation during crystallisation of lunar and terrestrial basalts (Bonnand *et al.*, 2016, in review). Both studies found that during crystallisation the melts became increasingly light, due to a heavy phase crystallising out, in contrast to komatiites, which become heavier.

There are similarities between lunar basalts and komatiites, with higher $Cr^{2+}/\Sigma Cr_{TOT}$ and Cr concentrations than basalts (Papike et al., 2005). However, pyroxene is a more important phase within lunar basalts. The fractionation in the lunar basalts is affected by the crystallisation of heavy spinels, increasing the $\delta^{53}Cr$ composition of the residue (Bonnand et al., 2016a).

Crystallisation has also been studied within the Fangataufa ocean island basalts (Bonnand *et al*., in review). The Cr concentrations and $Cr^{2+}/\Sigma Cr_{TOT}$ are both lower in these OIBs than komatiites. The $\delta^{53}Cr$ decrease in the Fangataufa OIBs, is less than within lunar basalts, but still requires the removal of a heavy phase. This is explained by the crystallisation of heavy spinel, and slightly heavy pyroxene (Bonnand *et al*., in review).

The different behaviour reported here reflects the high Cr content of olivines in komatiites. They contain a greater fraction of the Cr budget compared to that found in any other melt. As they can include Cr^{2+} within their crystal lattice, they can crystallise light Cr, leading to an evolution to heavier Cr in the melt.

4.5.6. BSE estimates

Komatiites can be used to estimate the $\delta^{53}Cr$ value of the BSE (Sossi et al., 2018a). They are melts that have similar compositions to the mantle, with the benefit over peridotites of sampling a larger volume, and so diluting the variable effects of localised metasomatism. No fractionation is expected during melting of the komatiite source, as other melt products have $\delta^{53}Cr$ compositions similar to the BSE (Schoenberg *et al.*, 2008; Sossi 2018a, Bonnand et al, in review), with any fractionation occurring during melting further reduced at the high temperatures of komatiite genesis. The BSE value of $\delta^{53}Cr$ can be calculated by using the initial komatiite liquid composition.

Calculations of the BSE were made using the three komatiite suites measured in this study, and samples from Sossi et al. (2018a). The komatiites from Sossi et al. (2018a) have the same $\delta^{53}Cr$ range as samples measured within this study (Figure 4.8.). The komatiites measured in Sossi et al. (2018a) are from the Archean with ages of 2.7 to 3.5 Ga and from the A1 and A2 spinifex zones, which were selected as they most closely represent the chemical composition of quenched liquids. This selection of komatiites, on average, have higher Cr concentrations. In order to account for variations within komatiite lava flows, only the Komatii and Munro komatiite flows from Sossi et al (2018a) were used, as these flows included multiple samples.

Figure 4.8.

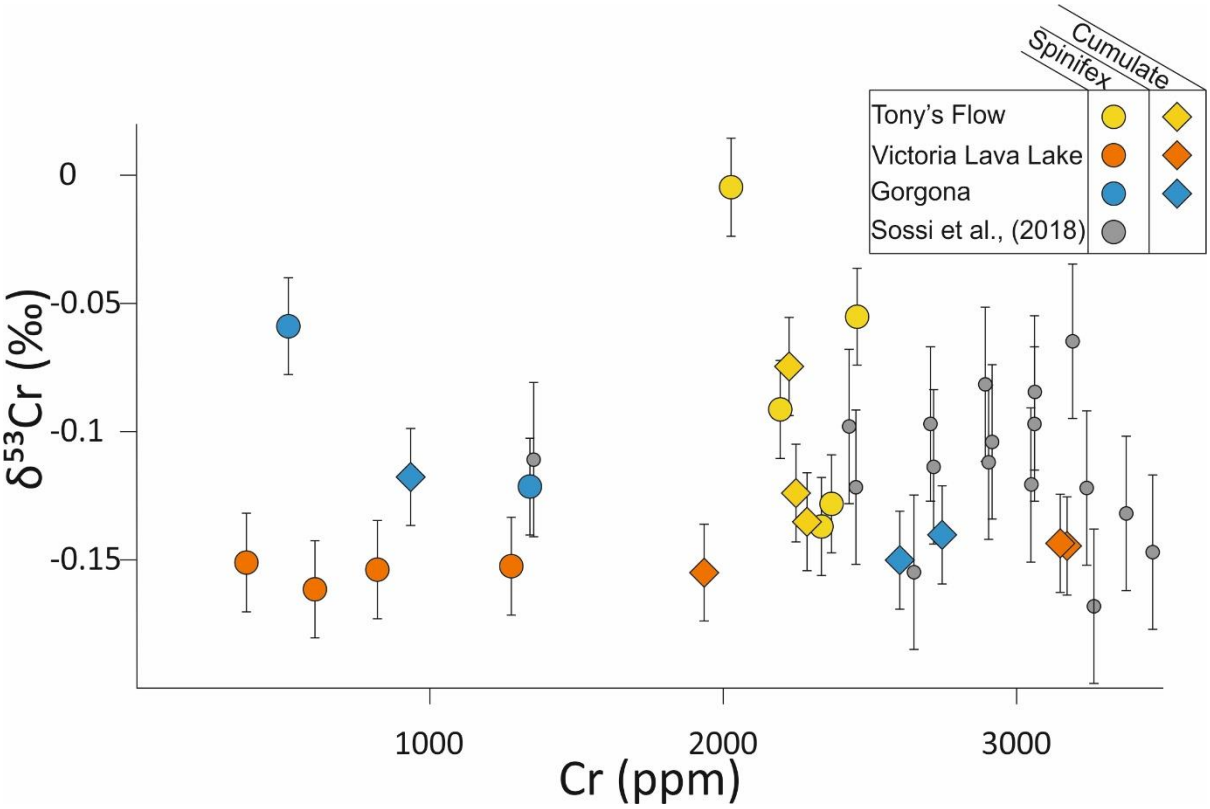

Figure 4.8. $\delta^{53}Cr$ variations against Cr concentrations. Victoria Lava Lake show no variations while Tony's Flow and Gorgona Komatiites have heavier $\delta^{53}Cr$ at lower Cr concentrations. Samples measured here show the same $\delta^{53}Cr$ composition of komatiites as previous work (Sossi et al., 2018a)*. Samples from Sossi et al., (2018a) are all Archean spinifex komatiites. The high [Cr] of komatiites from Sossi et al., (2018a), are due to the choice of samples, that were chosen to represent quenched liquids.*

Previous calculations of the BSE using komatiites have been carried out with samples that best represent the initial liquid composition (e.g. (Gall et al., 2017; Sossi et al., 2018a)). The initial composition method has the benefit over using an average by discarding samples with extreme values. The initial liquid composition can be calculated a number of ways, one of which is by using the MgO content. The initial MgO content of the komatiite liquid can be

obtained by calculating the liquid that would be in equilibrium with the most magnesium rich olivine (Bickle, 1982; Nisbet et al., 1993). The komatiites with the MgO closest to this value are then assumed to represent the chemical composition of the initial melt (e.g. Hibbert et al., 2012).

The BSE was calculated using the $\delta^{53}Cr$ of the komatiite samples with an MgO composition closest to the initial liquid, providing a value of -0.13 ± 0.07 ‰ (n =5). This value agrees with previous attempts, but does not improve on the uncertainty. This method selects some of the heaviest and lightest $\delta^{53}Cr$ measurements for the Komati, Munro and Tony's Flow komatiites (Table 4.2.). The value of the BSE is unable to be precisely recreated as the method assumes that the fractionation of Cr isotopes is linear with MgO, which is not the case. When the MgO of the komatiite has the initial value of the melt, it does not have the initial $\delta^{53}Cr$ value.

Calculating the BSE composition of the Earth through an average of A1 and A2 spinifex's has the same limitation. All but one of the spinifex komatiites, in this study are characterised type A1 or A2. Figure 4.8. shows that there is a large scatter in $\delta^{53}Cr$ in the spinifex komatiites, as great as that for the cumulates. Although the chemical composition of the A1 and A2 spinifex komatiites is close to that of the initial melt, the fractionation during crystallisation results in a highly variable $\delta^{53}Cr$ of spinifex komatiites. The average composition of the A1 and A2 spinifex komatiites from this study and Sossi et al (2018a) is -0.12 ± 0.06 ‰ (2 s.d., n = 26), which does not provide an improvement to the precision of the BSE. Both methods recreate the composition of the BSE calculated in other studies, however the behaviour of $\delta^{53}Cr$ during crystallistion means that there is no improvement to the uncertainty.

An alternative approach is to use a weighted average of the flow. While the komatiite flow has undergone differentiation, this occurred after the lava flow was erupted, and so by summing all available parts of the flow, the initial liquid composition can be returned. A weighted average must be used as the Cr concentration varies with $\delta^{53}Cr$ (Figure 4.8.). The composition of the initial komatiite melts calculated from this method are remarkably uniform (Table 4.2.). Although $\delta^{53}Cr$ behaves differently during crystallisation in the different flows, nearly the same value is recreated for all of the flows. This provides support for the view that the weighted average provides an accurate composition of the initial komatiite liquid. The robustness of using komatiite flows versus other archives is also endorsed. Komatiite flows can only be used to estimate the BSE if there is no fractionation during melting. As the same isotopic composition is returned for komatiite flows created from varying degrees of partial melting then this must be the case.

On this basis a more precise value of -0.12 ± 0.03 ‰ of the BSE composition is proposed. This is in agreement with previous estimates taken from peridotites and komatiites ($\delta^{53}Cr$ =-0.12 ± 0.10 ‰., -0.14 ± 0.12 ‰ and -0.11 ± 0.06 ‰) (Schoenberg et al., 2008; Xia et al., 2017; Sossi et al., 2018a)).

Table 4.2.

Method	Victoria Lava Lake	Tony's Flow	Gorgona	Komati	Munro	BSE
Closest Composition	-0.15	-0.14	-0.12	-0.07	-0.17	-0.13 ± 0.07 ‰
Weighted average	-0.15	-0.1	-0.13	-0.1	-0.12	-0.12 ± 0.03 ‰

Table 4.2. Composition of the initial komatiite liquid for the three komatiite localities within this study, as well as two komatiite localities analysed in Sossi et al. (2018a). Two methods for calculating the initial komatiite liquid composition are presented the closest composition and

the weighted average. The weighted average produces remarkably consistent δ^{53}Cr *The initial komatiite liquid compositions are used to calculate a new BSE value.*

The new, more precise, BSE composition can be used to reanalyse variations between previously measured samples and the BSE. The BSE composition is within error of basalts, (δ^{53}Cr= -0.17 to -0.13 ‰ (Schoenberg et al., 2008)), agreeing with previous studies that fractionation does not occur during melting. All classes of chondrites are within error of the new value of the BSE, consistent with no fractionation during core formation (Bonnand et al., 2016b; Schoenberg et al., 2016).

4.6. CONCLUSIONS

The δ^{53}Cr of komatiites from three suites of komatiites, have been collected using high precision techniques. Komatiites show resolvable δ^{53}Cr variations within flows, and variable [Cr] and δ^{53}Cr behaviour between flows.

Chromium isotope and concentration variations in komatiites are controlled by the crystallisation of chromite and olivine, and the conditions under which these minerals form. Victoria Lava Lake samples reflect crystallisation of chromite and olivine throughout the sequence, whereas Tony's Flow had a period of olivine-only crystallisation prior to Cr saturation in the residue.

The Cr isotope composition variations within Tony's Flow are explained by different amounts of isotopically light olivine distributed throughout the flow. This differs from Victoria Lava Lake where there is no change in the δ^{53}Cr. The different behaviour is inferred to be due to a higher $Cr^{2+}/\Sigma Cr_{TOT}$ in Tony's Flow, which creates isotopically light olivine, while Victoria Lava Lake has a lower $Cr^{2+}/\Sigma Cr_{TOT}$.

Using komatiite flows from this study and previous work has enabled a new estimate of the BSE to be calculated. Past methods for calculating the stable isotope composition of komatiites, such as only considering spinifex komatiites, or using komatiites with chemical compositions that are closest to the initial composition, give imprecise values. $\delta^{53}Cr$ does not vary linearly within komatiites and so this selection of samples will not necessarily provide the $\delta^{53}Cr$ value of the initial melt. A weighted average of five komatiite flows provides a well constrained value of $\delta^{53}Cr$ -0.12 ± 0.0 3‰. The agreement between the composition of komatiites and other methods of estimating the composition of the BSE provide additional evidence that melting does not lead to significant changes in $\delta^{53}Cr$.

Chapter 5: The $\delta^{53}Cr$ composition of the enstatite chondrites

5.1. INTRODUCTION

The enstatite meteorites are a group of highly reduced chondrites and achondrites. The oxygen fugacity of the enstatite meteorites has been calculated at -4 ΔIW log units (Brett and Sato, 1984; Cartier et al., 2014), and they have a C/O ratio higher than the solar value of 0.6 (Larimer and Bartholomay, 1979). They are believed to have formed close to the sun, due to their reduced composition (Baedecker and Wasson, 1975; Kallemeyn and Wasson, 1986), which may be the same region as Mercury (Cameron 1978 and Sears 1980), as they have chemical similarities with the planet (Zolotov et al., 2013).

The reduced environment that the enstatite chondrites formed in is reflected in the composition and abundance of the minerals found in these meteorites. Very little FeO is present. The major silicate phase, enstatite (from which this group of meteorites takes there name), is nearly FeO free (<1% Keil, 1968). Iron is contained in Si bearing Fe-Ni metal or a range of abundant sulphides. Enstatite chondrites also contain a plethora of unusual minerals, (e.g. sinoite, osbornite, niningerite etc. (Andersen et al., 1964; Keil and Andersen, 1965; Mason, 1966; Keil, 1968), which could only form under reduced conditions.

Enstatite chondrites have a large range in compositional variations (e.g. Fe from 19 to 32 % (Kallemeyn and Wasson, 1986)). Two distinct groups of enstatite chondrites have been identified, based upon their Fe/Si ratios, EH (high Fe) and EL (low Fe) (Sears et al., 1982), as well as number of anomalous enstatite chondrites that do not fit this classification. The mode of formation of these groups is debated. It has been suggested that the EH and EL chondrites may form a chemical continuum derived from the same parent body (Kong et al., 1997), while others argued that two separate parent bodies were required (Keil, 1989). Recent work has suggested up to eight parent bodies may be needed to account for the enstatite chondrites

alone (Weyrauch et al., 2017). A number of theories have been proposed for the different composition of EH and EL chondrites including:

1. high pressure conditions suppressing the nucleation of iron, followed by high temperature agglomeration to create EL chondrites, (Blander and Abdel-Gawad, 1969; Blander, 1971)
2. mechanical separation, and preferential agglomeration of Fe rich phases (EH chondrites) (Baedecker and Wasson, 1975)
3. different oxygen fugacities, with more reduced conditions creating EH chondrites with higher metal contents (Zhang et al., 1995).

Research on the enstatite chondrites has flourished in recent years, driven by the remarkable similarity of the isotopic compositions to those of Earth, (e.g. O, Ca, Ti, Cr, Ni, Os, (Meisel et al., 1996; Dauphas et al., 2004; Trinquier et al., 2007; Regelous et al., 2008; Dauphas et al., 2014; Young et al., 2016)). The similar isotope composition of Earth and enstatite chondrites suggests that the Earth is created out of enstatite meteorite like material, (Javoy et al., 2010; Warren, 2011; Dauphas, 2017). The accretion of Earth from enstatite chondrites would also provide the reduced conditions pertaining during early core formation (Chabot and Agee, 2003; Wade and Wood, 2005; Wood et al., 2008; Rubie et al., 2011).

Issues exist for an enstatite chondrite model of Earth. Some isotopic systems exhibit resolvable differences between enstatite chondrites and Earth, (Si, Ru, Mo (Georg et al., 2007; Fitoussi and Bourdon, 2012; Zolotov et al., 2013; Fischer-Gödde and Kleine, 2017). Additionally, the chemical composition of the enstatite chondrites is difficult to reconcile with that of the Earth, especially the refractory elements which are fractionated, compared to other material in the solar system (Larimer and Anders, 1970; Baedecker and Wasson, 1975).

Models have been proposed to reconcile the different chemical composition, a silica rich hidden layer in the mantle (Javoy et al., 2010) and extensive vapour loss (Hin et al., 2017).

Heterogeneous Earth accretion models reduce the discrepancies between the chemical composition of enstatite chondrites and the Earth. Dauphas (2017) investigated what proportion of ordinary chondrite material could be added to the Earth, without changing the isotopic composition. This allows 30 - 70 % of the first half of the accreting material to have an ordinary chondrite composition.

Previous $\delta^{53}Cr$ measurements of chondrites have been reported (Moynier et al., 2011b; Schiller et al., 2014; Bonnand et al., 2016b; Schoenberg et al., 2016). In this study we have compared our data with the $\delta^{53}Cr$ values reported in Bonnand et al. (2016b) and Schoenberg et al. (2016), as early studies did not use a double spike, and this may have led to apparently light compositions. The chondrite composition measured in the double spiking studies are ordinary chondrites = -0.11 ± 0.04 ‰ (n=17), carbonaceous chondrites= -0.12 ± 0.05 ‰ (n =11) and enstatite chondrite = -0.08 ± 0.05 ‰ (n=2).

There are only limited $\delta^{53}Cr$ data for enstatite chondrites. Bonnand et al., (2016b) measured two enstatite chondrites, which had compositions heavier than most other chondrites. The $\delta^{53}Cr$ of these meteorites fall towards the heavy end of the BSE, (Indarch EH4 -0.10 ± 0.012 ‰ and Khaipur EL6 -0.05 ± 0.012 ‰). Expanding the available data on this class of meteorites will help to establish if the apparently heavier compositions exist, or the difference is the result of only measuring a limited number of samples. This study expands the available data for the $\delta^{53}Cr$ composition of Earth by measuring an additional 11 enstatite meteorites, which cover a range of petrological types, and represent both EH and EL chondrites.

5.2. SAMPLES

A selection of 11 enstatite chondrites were measured in this study. Samples are taken from the low and high iron enstatite chondrites groups (EH and EL). These meteorites represent a range of petrological types (3 through to 6/7). The petrologic type of the meteorites describes the extent of processing that has occurred following formation on the parent body. The classification was designed to represent increasing degrees of thermal alteration (Van Schmus and Wood, 1967), however, the characteristics of higher petrological types can also be created through shock annealing (Rubin, 2004). The petrological type 3 meteorites are referred to as the unequilibrated meteorites, as they have not experienced significant alteration (McSween, 1979; Scott and Krot, 2003). One unequilibrated meteorite was measured in this study, Kota Kota (EH3). Other meteorites came from petrological type 4, 5 and 6 (Table 5.1.). One anomalous enstatite chondrite, Happy Canyon was also measured, which has been classified as an EL6/7 chondrite. This unusual enstatite meteorite was initially classified as an achondrite (Olsen et al., 1977), but reclassified as an impact melt breccia (McCoy et al., 1995; Rubin et al., 1997), formed on one of the enstatite chondrite parent bodies. It has mineralogical and bulk compositions that tie it to the EL chondrites (McCoy et al., 1995; Boesenberg et al., 2014), although it's Zn isotope composition precludes it from having formed from EL4-6 chondrites (Moynier et al., 2011a).

Two of the EH chondrites in this work have also been classified as melt impact breccias. Adhi Khot and Abee exhibit melting and shock textures, which show the effects of multiple impacts (Rubin, 1983; Rubin and Scott, 1997). These meteorites also contain dark inclusions, rich in silica or oldhamite, which are impact products not in equilibrium with the rest of the rock (Rubin and Scott, 1997).

A mixture of falls and finds were measured. Meteorite falls are able to be quickly recovered while finds may have been on Earth for extensive periods of time and could have undergone terrestrial alteration. Comparisons of falls and find can identify whether terrestrial alteration has led to changes in the $\delta^{53}Cr$ composition of the meteorites.

Enstatite meteorites measured in this study have a range of chemical compositions. The Fe/Mg ratio of the meteorites varies between the two groups, with EL chondrites have values from 1.4 to 2.9 and the EH chondrites having compositions from 2.9 to 4.8. The extent of volatile element depletion is shown by the wide variations in the Zn concentrations from 28 to 457 ppm. Chromium concentrations of the enstatite chondrites range from 1200 to 5500 ppm. Full element compositions are provided in Table 5.1.

5.3. ANALYTICAL TECHNIQUES

Meteorite samples were supplied as small fragments, (50-500 mg). Small amounts of material were treated with caution, as the sample may not be wholly representative of the bulk meteorite. To ensure the sample was homogenised, it was gently hand powdered as this prevented streaking of the soft native metal.

Sample dissolution was carried out on hotplates followed by a more aggressive stage using a high pressure asher. Initial hotplate dissolutions were made using a HF and HNO_3 mix to attack silicates, followed by 6M HCl. In order to ensure full dissolution of resistant grains a higher pressure dissolution followed using an Anton Parr HPA-S high pressure asher. For an asher dissolution, the sample was loaded along with 3 ml of 6M HCl. During one 6 hour run, the chamber was pressurised to 100 bars and the sample carousel heated to temperatures over 200°C.

The chemical composition of each dissolution was measured to provide a true representative composition of the samples. Elemental analysis was carried out using the Perkin Elmer 6100DRC ICP-MS, at Department of Earth Sciences, Oxford University. Element data for the enstatite chondrites are presented in table 5.1.

Two micrograms of Cr were prepared for each measurement. A ^{50}Cr-^{54}Cr double spike was added to the solution prior to Cr purification, so that all experimental fractionations could be corrected. Chromium purification was carried out using a two cation exchange column method, as described in Bonnand et al. (2016b). The first column removed matrix elements, while the second cleaned the isobaric interferences.

Isotopic measurements were made using a Thermo Scientific Triton Thermal Ionisation Mass Spectrometer, at Laboratoire Magams et Volcans, Université Clermont Auvergne. Samples were loaded on to Re filaments along with a Si-B activator. Runs were made at +1275°C, and consisted of 54 blocks of 10 measurements each lasting 8 seconds. After each block a baseline was taken, and the virtual amplifier was rotated. The external reproducibility of the method was calculated using repeated measurements of the geological reference standard JP-1 over an extended period of time. A value of -0.11 ± 0.014 ‰ (2 s.d., n = 8) was obtained, which agrees well with previously published studies.

5.4. RESULTS

The enstatite chondrites in this study have $\delta^{53}Cr$ ranging from -0.12 to +0.02 ‰. The two previous double spiked measurements of enstatite chondrite lie within the range of their respective enstatite chondrite classes (Bonnand et al. 2016b). The EH chondrites vary from $\delta^{53}Cr$= -0.12 to -0.06 ‰ with an average composition of -0.09 ± 0.04 ‰ (2 s.d. n=4), similar to

the previous EH measurement of -0.10 ± 0.012 ‰, (Bonnand et al 2016b). The EL chondrites show a greater variation from $\delta^{53}Cr$= -0.125 to 0.02 ‰ with an average composition of -0.05 ± 0.11 (2 s.d. n=7). The one previous measurement of an EL chondrite, of -0.06 ± 0.012 ‰ (Bonnand et al., 2016b) is consistent with these compositions. The populations of EH and EL chondrites were compared using a two tailed t-test. At the 95% confidence level that there was no difference between their $\delta^{53}Cr$ values.

Table 5.1.

Sample	Abee	Adhi Khot	Atlanta	Blithefield	Daniel's Kuil	Happy Canyon	Hvittis	Kota Kota	Pillistfer	St Marks	Yilmia
δ^{53}Cr (‰)	-0.12	-0.06	-0.15	0.02	-0.10	-0.04	-0.06	-0.08	0.02	-0.08	-0.03
2 s.e.	0.02	0.01	0.01	0.02	0.01	0.03	0.03	0.01	0.02	0.01	0.01
Class	EH4	EH4	EL6	EL6	EL6	EL6/7	EL6	EH3	EL6	EH5	EL6
Fall/Find	Fall	Fall	Find	Find	Fall	Find	Fall	Find	Fall	Fall	Find
Na	0.6	0.7	0.4	0.4	0.5	0.4	0.5	0.5	0.5	0.6	0.5
Mg	6.3	7.1	13.8	13.7	12.0	13.5	16.0	10.4	13.4	9.0	13.0
Mn	0.38	0.42	0.06	0.37	0.17	0.08	0.20	0.22	0.11	0.24	0.11
Fe	19.9	34.4	23.2	25.0	35.2	22.6	22.6	31.1	39.0	27.4	22.6
Ni	1.19	2.41	1.36	1.03	2.41	1.01	1.84	2.00	2.69	1.79	1.58
Al	0.67	0.73	0.99	1.05	0.84	0.85	0.84	0.78	0.81	0.66	0.72
Ca	0.79	0.85	0.86	0.96	1.25	0.90	1.26	1.10	1.39	1.14	0.85
Sc	9.03	8.93	10.88	9.25	8.33	10.02	9.79	10.54	8.54	6.68	9.08
Ti	170	202	308	982	573	405	333	504	266	300	208
V	16	20	29	104	63	38	32	54	25	41	22
Cr	2257	2712	1817	5496	3348	1796	2205	3106	1380	2321	1200
Mn	3526	4174	612	3604	1785	792	2063	2141	1070	2555	1056
Co	558	1126	766	588	1231	635	753	1010	1496	938	850
Cu	138	219	43	145	114	69	80	143	82	148	79
Zn	399	458	23	61	28	59	18	314	34	74	31
Ga	9.15	15.17	12.53	15.87	15.26	47.56	8.22	17.05	16.24	12.79	6.45
Ge	4.47	5.99	5.49	5.19	6.68	5.76	7.17	9.14	8.66	6.10	6.28
Rb	6.05	6.04	4.28	4.91	3.98	2.99	5.46	3.34	4.27	3.04	4.22
Sr	11	12	161	17	23	31	13	26	13	13	17
Zr	13	14	86	22	17	18	12	15	12	12	12
Mo	0.52	1.37	1.28	0.90	1.73	1.31	1.27	1.44	1.53	1.14	1.20
Rh	0.50	0.42	0.36	0.29	0.37	0.33	0.27	0.19	0.43	0.24	0.19
Cd	0.99	1.02	0.13	0.21	0.15	0.32	0.10	0.04	0.30	0.04	0.50
Sn	0.96	0.97	5.26	4.71	4.28	3.55	1.94	4.08	6.51	4.19	5.91
Ir	33	28	26	26	24	22	27	25	73	34	20
Pt	0.93	1.45	1.69	2.80	1.92	0.95	1.04	1.30	2.00	0.93	1.21
Au	13	13	12	12	12	11	12	12	12	11	11
Pb	2.05	2.17	1.14	6.90	42.16	0.53	8.25	1.76	6.08	0.36	0.67

Table 5.1. Enstatite chondrite chemical data. Elemental data was collected using the Perkin Elmer 6100DRC ICP-MS. Isotope data is collected using Triton thermal ionisation mass spectrometers.

5.5. DISCUSSION

5.5.1. Mass independent corrections

Chromium mass independent anomalies in meteorites result from nucleosynthetic anomalies on ^{54}Cr, radiogenic effects on ^{53}Cr and spallation effects on both ^{53}Cr and ^{54}Cr. Spallation effects can generate extreme Cr isotope anomalies, if samples include abundant target ions and have long exposure ages. The size of these anomalies can be very large in iron meteorites which can have anomalies of $\varepsilon^{53}Cr$ >250 and $\varepsilon^{54}Cr$ >1000 (Bonnand and Halliday, 2018; Liu et al., 2019).

The double spike deconvolution technique calculates a deviation from a natural isotopic composition. In terrestrial samples, the natural composition is assumed to be that of the Earth. In extra-terrestrial samples however, the variations in $\varepsilon^{53}Cr$ and $\varepsilon^{54}Cr$ has to be taken into account for the deconvolution (Bonnand et al., 2016b; Bonnand and Halliday, 2018). The difference in the stable isotope composition from mass independent anomalies is highlighted by Bonnand and Halliday, (2018), which shows that spallation can change the $\delta^{53}Cr$ by more than a permil within iron meteorites. Even smaller variations, from nucleosynthetic and radiogenic anomalies, could alter the stable isotope composition. For example, an anomaly of $\varepsilon^{53}Cr = 4.4$ can lead to errors of 0.37‰ (Bonnand and Halliday, 2018).

It is possible to correct for the variations that occur for samples that have $\varepsilon^{54/53}Cr \neq 0$, by using an iterative process (Bonnand et al., 2016b; Bonnand and Halliday, 2018). These

corrections are only necessary if the $\varepsilon^{53}Cr$ and $\varepsilon^{54}Cr$ values are not close to 0. Enstatite chondrites have similar nucleosynethetic $\varepsilon^{54}Cr$ compositions to Earth (Trinquier et al., 2007; Warren, 2011) and do not have large $\varepsilon^{53}Cr$ anomalies (Trinquier et al., 2008b; Qin et al., 2010). The mass independent anomalies in these samples may be small enough that corrections do not need to be applied.

The effects of $\varepsilon^{53}Cr$ and $\varepsilon^{54}Cr$ anomalies of enstatite chondrites were modelled to see if they led to significant change in $\delta^{53}Cr$. The enstatite chondrite Abee was chosen to be modelled as it has anomalies that were greater than average (Table 5.2.) The difference in the stable isotope composition of uncorrected and corrected measurements was only 0.0018 ‰. This is an order of magnitude lower than the external precision in the measurements, and far smaller than the variations seen in the enstatite meteorites. The similarity between the mass independent composition of enstatite chondrites and the Earth, as well as the limits of precision available in our measurements means that using uncorrected data does not affect the accuracy of our data.

Table 5.2.

	$\varepsilon^{53}Cr$	$\varepsilon^{54}Cr$	$\delta^{53}Cr_{uncorrected}$	$\delta^{53}Cr_{corrected}$
Abee	0.26	-0.06	-0.1175	-0.1193
Average Enstatite	0.21±0.13 (n=12)	0.03±0.03 (n=12)	---	---

Comparison of uncorrected and corrected stable isotope compositions of the enstatite chondrites. The average composition of the enstatite chondrites is also shown for comparison. Data from (Trinquier et al., 2007; Trinquier et al., 2008b; Qin et al., 2010; Bonnand et al., 2016b).

5.5.2. Chromium concentration in enstatite chondrites

5.5.2.1. Chromium trends within enstatite chondrites

The small sample sizes available for analysis in this study means that geochemical analyses from other samples of the same meteorites would not necessarily be representative of our sample. To ensure that the chemical composition of the chondrites relates to the chromium isotope measurements, bulk element measurements were carried out on the same aliquots used for the isotope composition (Table 5.1.).

Variations in the Cr content of the EL and EH chondrites are plotted in Figure 5.1. against a number of different elements. The EL chondrites show a positive correlation between the Cr concentration and Ti and V (Figure 5.1.). These two elements have chalcophile behaviour in enstatite chondrites (Allen and Mason, 1973; Crozaz and Lundberg, 1995). The EH chondrites display a positive correlation to Zr and Al (Figure 5.1.). These two elements are both refractory under normal nebular conditions, with half mass condensation temperatures of 1764 and 1677 K respectively (Lodders, 2003). Correlations suggest that within the enstatite chondrites Cr behaves as a refractory chalcophile element.

This behaviour of Cr is unexpected and seemingly contradictory. Sulphides are one of the last phases to condense under normal nebular conditions (Lodders, 2003), and so Cr hosted in sulphides would not normally be refractory. In the following section, the distribution of Cr in enstatite chondrites is investigated in order to understand its behaviour.

Figure 5.1.

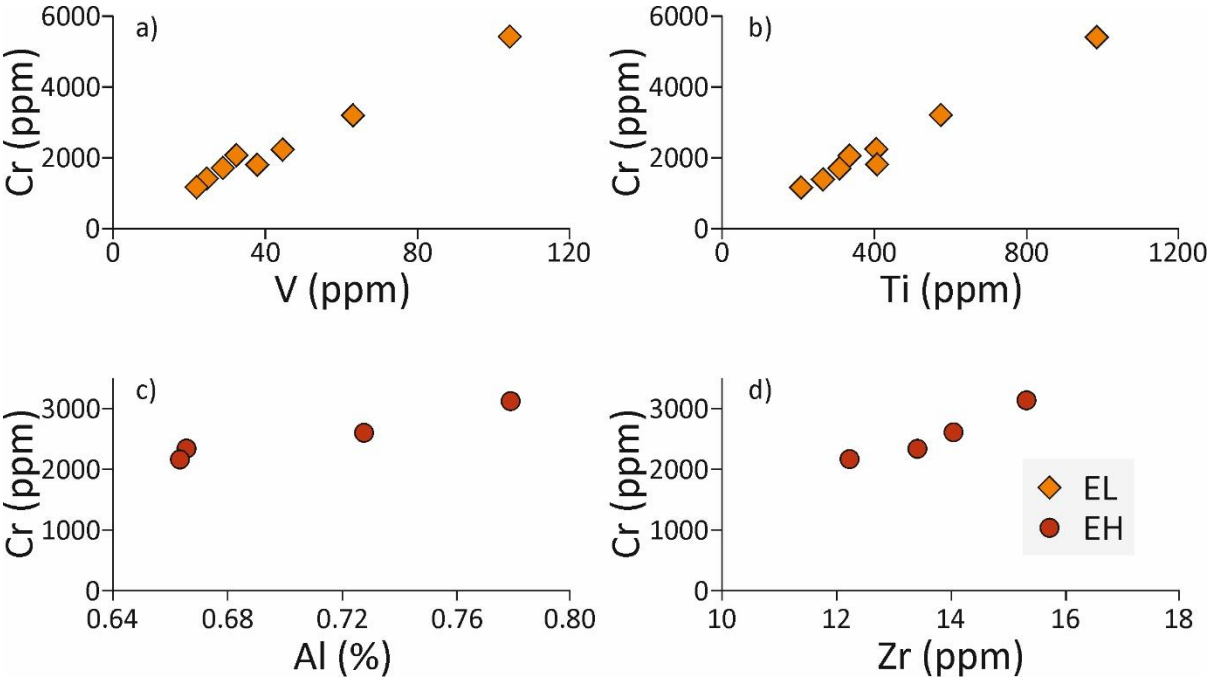

Figure 5.1. Chromium concentration variations in enstatite chondrites. The EL chondrites show variations with elements that are enriched in troilite (Ti and V). The strong correlation shows that Cr is hosted mainly with the sulphide phases. . Chromium in the EH chondrites have strong correlations with refractory elements (Al, Zr), suggesting that condensation of Cr rich phases began early.

5.5.2.2. Chromium distribution in enstatite meteorites

Past studies have provided information on the distribution of Cr in the enstatite chondrites. Chromium is split between sulphides (67%) and silicates (33%), with only a trace amount found in metal phases, (Easton, 1985; Javoy et al., 2010). Enstatite chondrites contain multiple sulphide phases. The most common sulphide is Ti-rich troilite, which has a modal abundance in enstatite chondrites of 5 - 17 % (Keil, 1968). The Ti-rich troilites contain percent levels of Cr (0.2 to 4.1 % Weyrauch et al., 2017), making it a major contributor to the overall Cr abundance. Variations occur in the Cr content of troilite due to exsolution of daubréelite

($FeCr_2S_4$). This creates two populations of troilite; low Cr troilite with exsolved daubréelite and high Cr without exsolved daubréelite (Weyrauch et al., 2017). Exsolution of daubréelite can change the distribution of the Cr in sulphides; however as the daubréelite forms intergrowths within troilite, the bulk Cr content of a meteorite will not be affected. There are other Cr-rich sulphides, Caswellsilverite ($NaCrS_2$, El Goresy et al., 1988), and Heidite ($(Fe,Cr)_{1+x}(Ti,Fe)_2S_4$, Keil and Brett, 1974), which are only found in EH chondrites, (Weisberg and Kimura, 2012). Both minerals are minor phases and will not significantly contribute to the bulk composition of chondrites.

Rock forming minerals, such as silicates and oxides, are the most common phases in the enstatite chondrites and contain around a third of the Cr budget (Easton, 1985; Javoy et al., 2010). Pyroxenes are the most abundant silicate phase. Two types of pyroxenes are commonly found within enstatite chondrites: enstatite, the namesake mineral of this class of chondrites, and a high FeO pyroxene. The enstatite pyroxene is a near end member variety and has low Cr contents (e.g. Cr_2O_3 <0.03 % (Weisberg et al., 1994)). High FeO pyroxenes are found ubiquitously in enstatite chondrites and can contain up to 1.6 % Cr_2O_3 (Lusby et al., 1987; Weisberg et al., 1994; Kimura et al., 2003). Chromium-rich oxides, such as spinel are also found in enstatite chondrites (Weisberg and Kimura, 2012), and may be an important contributor to the overall abundance of Cr.

Available data for the Cr concentration in metal phases of enstatite meteorites are sparse. Measurements are hampered by the low abundance of Cr in the metal, issues with interferences from large Fe signals and the intergrowth of Cr-rich phases. Due to these difficulties, many studies have avoided measuring the Cr content of metal, and those that do struggle with detection limits. Horstmann et al., (2014) provided measurements from

fragments of a chemically diverse polymict breccia (Alhma Sitta meteorite 2008 TC3) along with two other enstatite chondrites. The Alhma Sitta meteorite 2008 TC3 contains clasts of EL and EH chondrite material. Chromium concentrations of metal phases measured in this study are low. The metal composition of the different meteorites is 400 ppm or less, with no difference between the EH and EL chondrites (Horstmann et al., 2014).

The Cr content of metal phases in enstatite chondrites is unexpectedly low. In other chondrites, metal contains abundant Cr (Zanda et al., 1994). Metal alloy is the first Cr bearing phase to form during condensation under normal nebula conditions (Lodders, 2003). When metal condenses, the solar nebula should not be depleted in Cr, and therefore the metal phase is expected to contain high concentrations of Cr. Enstatite chondrites form under reduced conditions, which may be expected to make Cr be more siderophile, as is the case during core formation (Siebert et al., 2011). This is not seen within the enstatite chondrites.

The geochemical behaviour of Cr, as chalcophile and refractory, can be explained be condensation from a reduced solar nebula. The correlations with Ti and V in Figure 5.1. and literature data on the Cr concentration of troilite prove that this phase is the major host of Cr in enstatite chondrites. The correlations between Cr and the refractory elements, Al and Zr, requires troilite to have formed early during the condensation of the enstatite chondrites. In order to explain this behaviour the conditions of condensation from the enstatite chondrite region of the solar nebula must have been different to other regions of the solar nebula.

Under normal conditions Fe-alloy is the first condensing phase that includes Cr (Lodders et al., 1993), however this cannot be the case within the enstatite chondrites. If Fe-alloy was the first condensing phase then Cr would not be depleted in metal phases as there would not be any other phases competing for Cr. As the metal phase is depleted in Cr, another

Cr rich phase must have condensed first. Changes to the conditions of condensation in the solar nebula will alter the half condensation temperatures of elements (e.g. (Larimer, 1975; Larimer and Bartholomay, 1979; Ebel and Alexander, 2011)). Under these more reducing conditions, troilite will condense at higher temperatures ~1250 K (Blander, 1971). If troilite condenses earlier, then it can deplete the nebula in Cr before metal phases form. In this scenario, troilite would behave like a refractory phase and metal will have low Cr contents, which is seen in the enstatite chondrites.

In summary Cr in enstatite chondrites is mainly contained within troilite, with a small fraction split between silicates, oxides and pyroxenes. The low Cr concentration of metal phases and the correlation between Cr and refractory elements is explained by troilite condensing earlier. This different condensation sequence of enstatite chondrite minerals occurs because of the more reducing conditions of the pre-enstatite nebula compared to other chondrites.

5.5.3. Chromium isotope variations

5.5.3.1. Alteration of enstatite chondrites

This study includes meteorites that are both falls and finds. Meteorite finds may have been altered on Earth. The enstatite chondrites formed in conditions that bear little resemblance to those found on the surface of Earth, and the minerals they contain may be unstable in terrestrial conditions. Meteorite 'finds' may have been recovered years after they arrived on Earth and will have been vulnerable to weathering over that time. The δ^{53}Cr of rocks can be fractionated during weathering (Frei et al., 2014), and with the vulnerability of enstatite chondrites to the oxidising conditions on Earth this may have altered their δ^{53}Cr.

There is no evidence of this in our enstatite chondrites samples, no difference exists between the δ^{53}Cr of finds and falls (Figure 5.2.).

Figure 5.2.

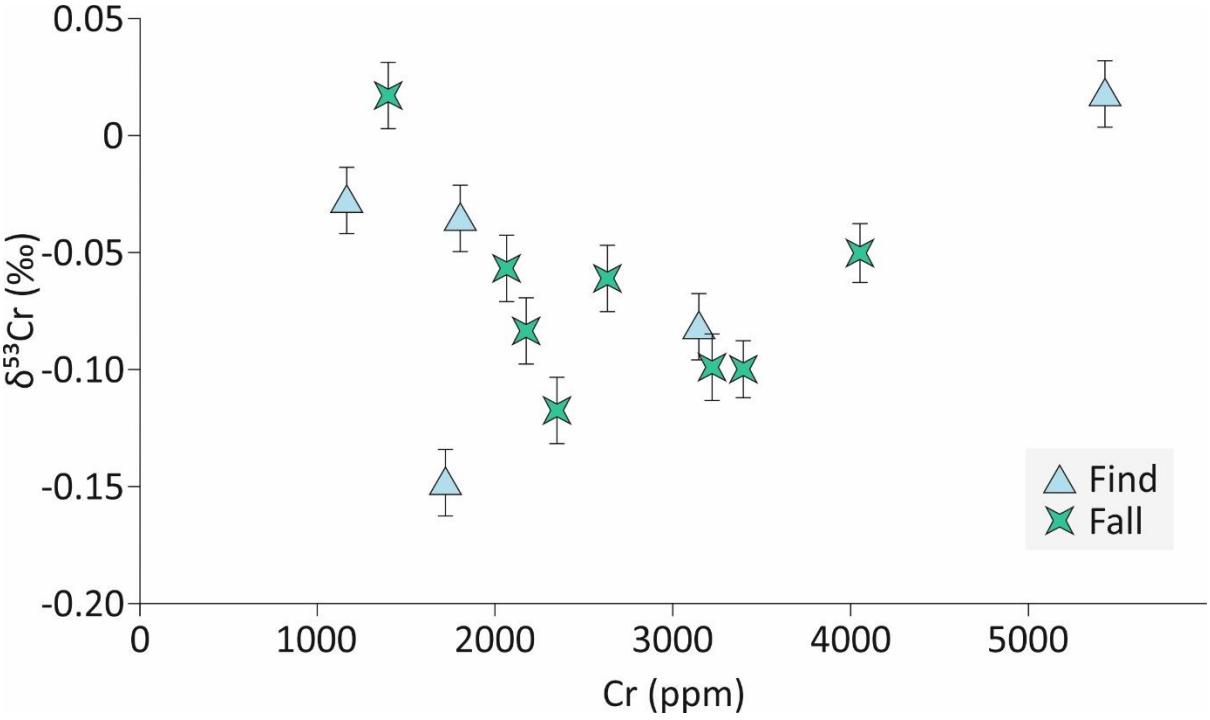

Figure 5.2. No variations in the Cr concentration and stable isotopic composition are seen between enstatites from finds and falls. Enstatite δ^{53}Cr data from this study and Bonnand et al. (2016b).

5.5.3.2 Loss of chromium through thermal processes

Chromium may be lost from meteorites during volatilisation. Chromium is usually classified as transitional element (McDonough and Sun, 1995), however this varies depending upon the conditions, i.e. chromium becomes more volatile under oxidising conditions (Sossi et al., 2018b). Volatility induced δ^{53}Cr fractionations have been identified for lunar samples, where equilibrium fractionation between a cooling post giant impact cloud and the moon, led to loss of heavy Cr (O'Neill, 1991; Sossi et al., 2018b). The enstatite chondrites in this study

have a large range of volatile element loss, as shown in their Zn concentrations (Figure 5.3.). Variations in the Zn content of the enstatite chondrites occur due to loss of Zn during high temperature thermal alteration (Kong et al., 1997). This has produced a wide range of Zn concentrations from the samples analysed in this study from 28 to 457 ppm. No variation is seen in the δ^{53}Cr as Zn concentrations decrease (Fig. 5.3.). The same is true for other volatile elements (e.g. Cd or Sn). The samples measured in this study do not show δ^{53}Cr variations with volatility.

Figure 5.3.

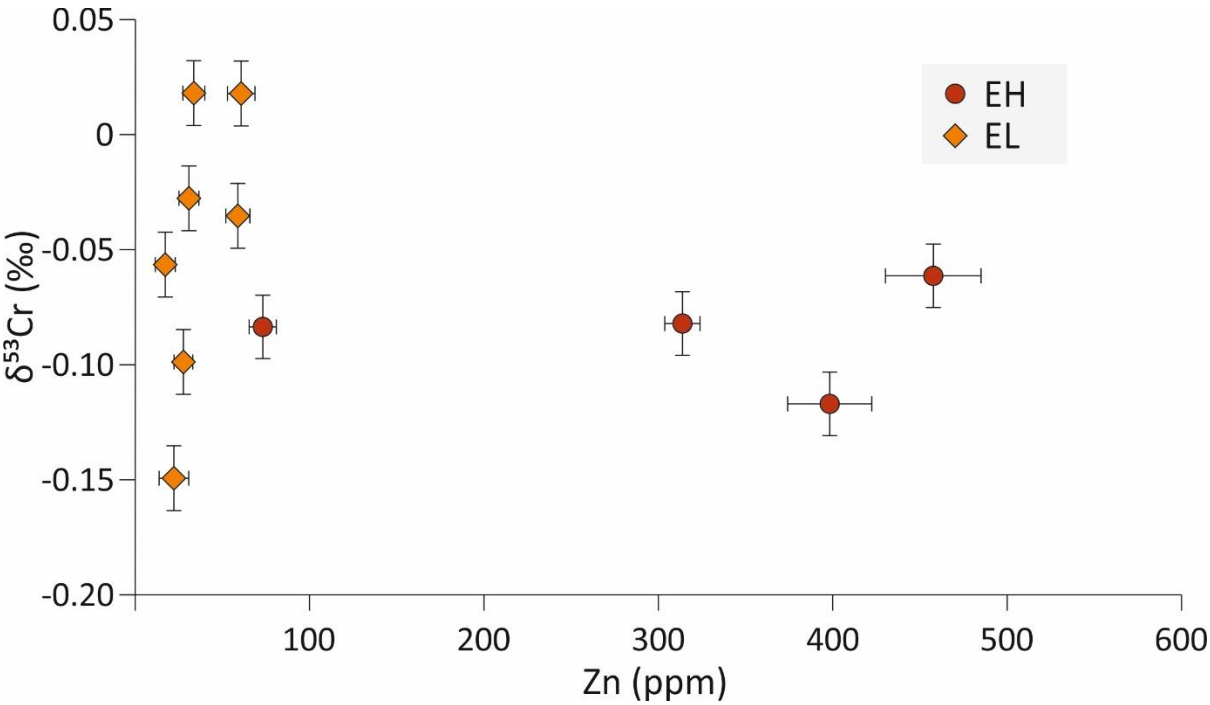

Figure 5.3. The highly volatile element Zn has a wide range of concentrations in enstatite chondrites, with those with higher petrological type containing less Zn. Zinc is lost from enstatite chondrites due to volatilisation, which could also affect δ^{53}Cr. No correlation between δ^{53}Cr and Zn is seen, showing that Cr isotopes have not been affected by volatilisation.

Variations in the petrological type represent samples that have undergone greater degrees of processing, through thermal and shock metamorphism (Keil, 2000; Rubin, 2004). Variations in Zn and S stable isotope occur with petrological type (Moynier et al., 2011a; Defouilloy et al., 2016). Variations in petrological types in this study can only be compared within one class of chondrites (e.g. EH or EL chondrites). This is because the only petrological type 6 meteorites are EL chondrites, therefore it will not be possible to differentiate between the effects of petrological type and enstatite chondrite type. The EH chondrites measured have the range of petrological types from EH3 to EH5, for which there is no variation in the $\delta^{53}Cr$ composition (Figure 5.4.).

Figure 5.4.

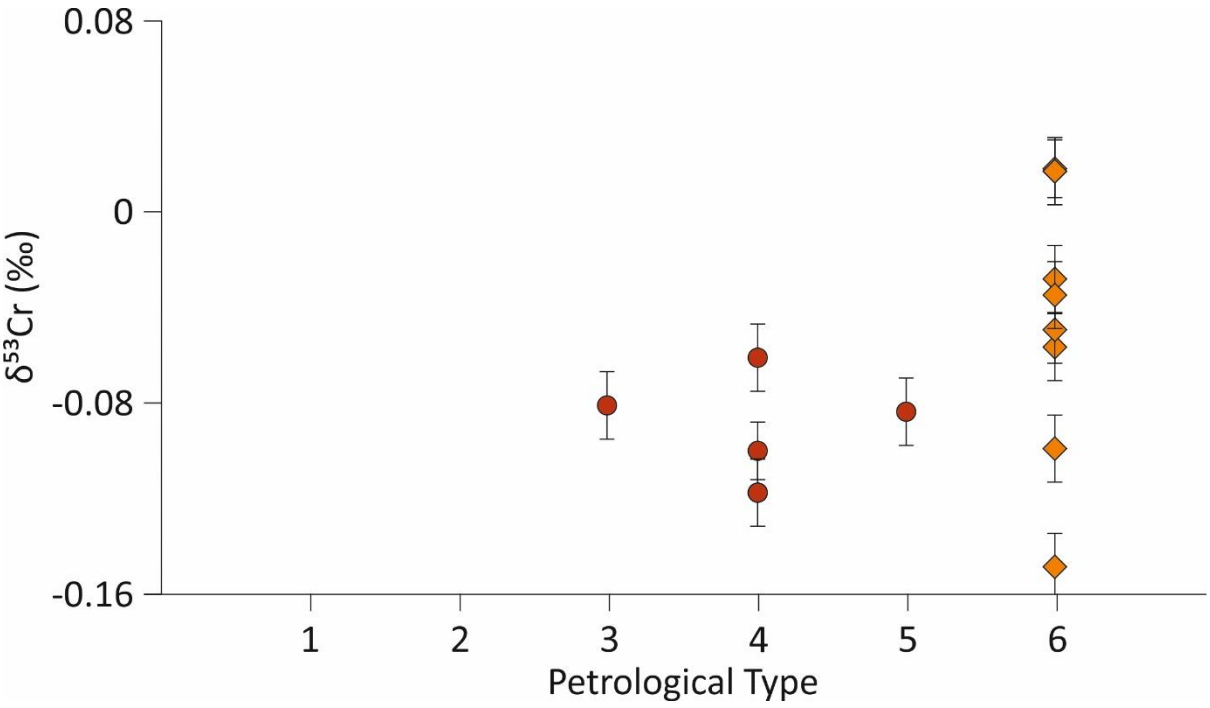

Figure 5.4. Petrological type of the enstatite chondrites plotted against $\delta^{53}Cr$. Comparisons must be made within a class, to avoid confusing the cause of variations. No variations are seen between the Cr stable isotope composition and petrological type in the EH chondrites. The EL

chondrites do not have a range in petrological type, therefore no comparisons can be made. Data taken from this study and Bonnand et al (2016b).

Three of the chondrites measured in this study have been classified as melt breccias, which have been affected by a series of impacts on the parent bodies. However these samples do not have anomalous $\delta^{53}Cr$, with compositions of these meteorites being similar to the EH or EL group that they come from.

5.5.3.3. Chromium stable isotope variations within the EL chondrites

The chromium concentration in the EL chondrites is controlled by sulphides. A negative correlation between $\delta^{53}Cr$ and chalcophile elements (Figure 5.5.) suggest that the same is true for the Cr isotopes as well. A decrease in $\delta^{53}Cr$ of EL chondrites as the chalcophile element increases can be explained by isotopically light troilite.

Figure 5.5.

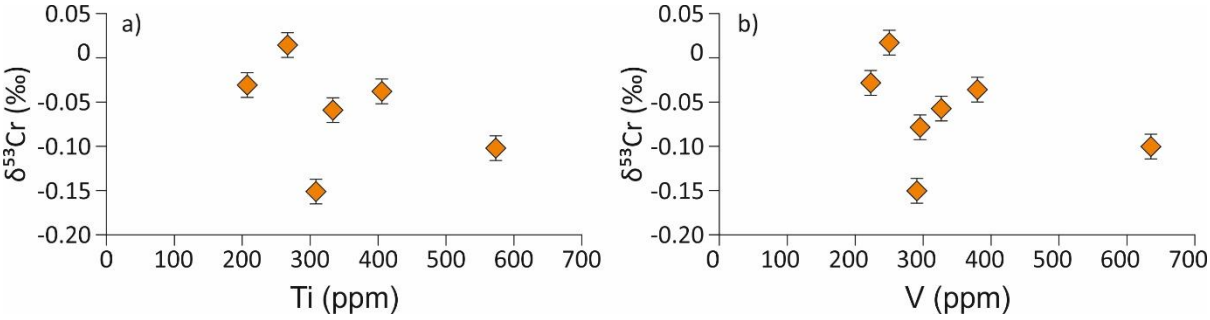

Figure 5.5. The $\delta^{53}Cr$ value of EL chondrites decreases with higher Ti and V abundances. These elements are chalcophiles in the enstatite chondrites. The variations can be explained by the inclusion of isotopically light troilite.

If the increase in V and Ti is assumed to be due to a higher modal abundance of troilite in the meteorite, then a mass balance can be used to calculate the $\delta^{53}Cr$ composition. This returns a value for the troilite of -0.19 ‰, with the non-troilite portion of the meteorite having

a composition of +0.08 ‰ ($\Delta_{troilite\text{-}X}$ = -0.27‰). Two processes can explain the light Cr composition of troilite, either; 1) troilite forms from an isotopically light reservoir, 2) troilite preferentially includes light Cr.

As discussed in section 5.5.2, troilite is stable at much higher temperatures within the pre- enstatite chondrite nebula (e.g. (Larimer, 1975; Larimer and Bartholomay, 1979; Ebel and Alexander, 2011). As troilite condenses early there will not have been previous Cr extraction from the nebula, and the Cr isotope composition will not be fractionated.

The EL meteorites measured in this study are all petrologic type 6. The higher petrologic types have experienced temperatures of 1020 to 1220 K (Keil, 2000). At high temperatures, equilibrium of Cr between minerals will occur, and equilibrium δ^{53}Cr fractionation between phases may occur. The magnitude of equilibrium fractionation at different temperatures has previously been calculated using density functional theory (DFT) (Moynier et al., 2011b). The difference in isotopic composition between troilite and a range of phases and the variation with temperature is shown in Figure 5.6.

Figure 5.6. can be used to see if equilibrium δ^{53}Cr fractionation is a plausible method for the troilite composition within the EL chondrites. The constraints are imposed from the temperature range of equilibration within the EL6 chondrites of 1020 – 1220 K. The difference between phases required to create the isotopically light Cr is -0.27 ‰. These conditions can be met by using a mixture of the phases present in enstatite chondrites. The combined mix of minerals provides a close match to the inter-mineral fractionation required.

Figure 5.6

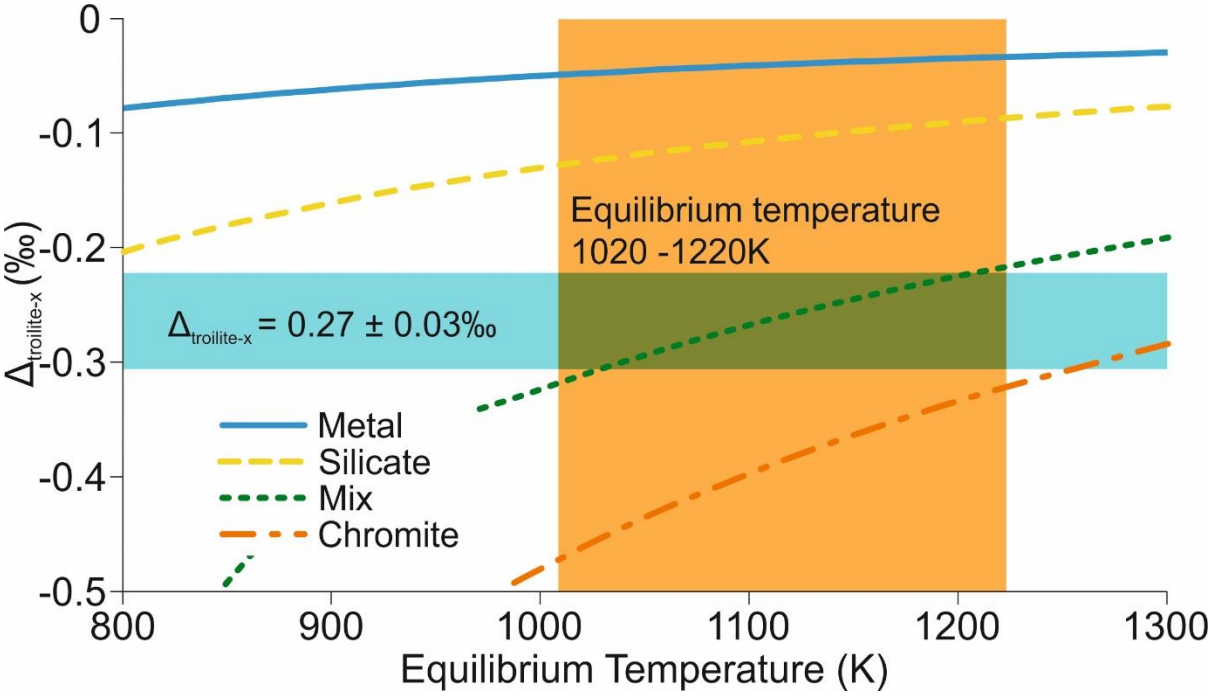

Figure 5.6. Equilbrium fractionations over tempertaures experienced by the EL6 chondrites. The silicate values use that of olivine calculated in Moynier et al. (2011b). Olivine is not a major phase within enstatite chondrites, but we assume that pyroxene will have a similar value, as they have the same valence state and the mineral site coordination. This mix is made of 20 % Metal, 20 % silicate and 60 % chromite as a rough estimate of the distribution of Cr in enstatite chondrites not hosted by in sulphides. The isotopic composition of troilite can be recreated in the temperature range that the EL6 chondrites experienced.

The isotopic composition of troilite is recreated by equilibrium fractionations at realistic conditions in these meteorites. The scatter seen in the EL6 chondrites (Figure 5.5.), can be explained by a combination of different mineral assemblages, (including a greater importance of Daubréelite within some meteorites), as well as heating to a range of different temperatures. Chromium equilibration of the EL chondrites cannot explain the different composition of the bulk chondrites. The equilibration will only result in a redistribution of

chromium isotopes between different phases. The different compositions could have been occurred later during the sampling of available material.

5.5.3.4. Chromium stable isotope variations within the EH chondrites

Strong $\delta^{53}Cr$ correlations occur with the siderophile elements for EH chondrites (Figure 5.7). Positive correlations exist between $\delta^{53}Cr$ chondrites and Fe, Ni, (Figure 5.7.). No correlation is seen with the chalcophile elements, (as identified in the EL chondrites).

Figure 5.7.

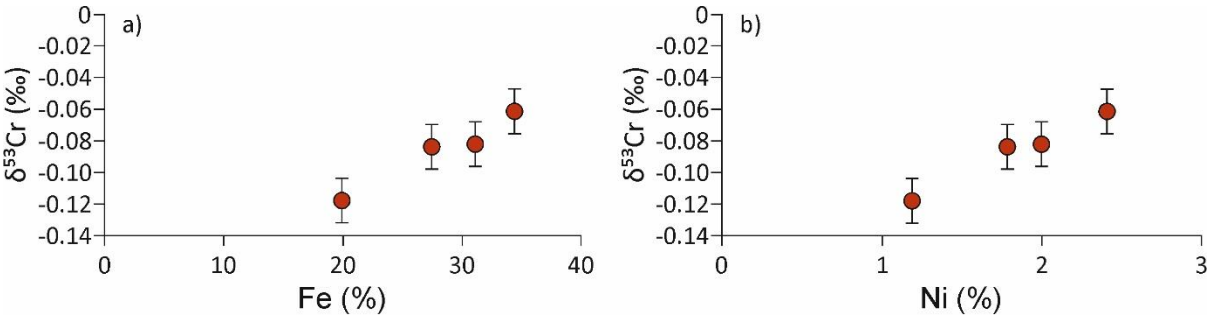

Figure 5.7. The $\delta^{53}Cr$ composition of the EH chondrites varies with the abundance of siderophile phases (Fe, Ni). The correlation suggests that the metal phase in the EH chondrites contains isotopically heavy $\delta^{53}Cr$. Due to the low Cr concentrations in the metal phase, the composition will need to be much heavier than that of the bulk meteorite.

The $\delta^{53}Cr$ isotopic composition of meteorites can be affected the creation of new Cr isotopes through spallation (Leya 2003). The production rate of Cr isotopes will depend upon the concentration of the target nuclei (Fe) within the enstatite meteorite. Spallation will create heavier isotopic compositions 0.2/0.3:1:1:1 compared to natural Cr 0.051859 : 1 : 0.113456 : 0.028211. Therefore, it may explain the correlation between Fe and $\delta^{53}Cr$ seen in Figure 5.7. However spallation can explain the variation in $\delta^{53}Cr$ as it would cause an increase in $\varepsilon^{53}Cr$ and $\varepsilon^{54}Cr$ greater than those seen in enstatite chondrites. Bonnand and

Halliday (2018) showed that an increase of $\delta^{53}Cr$ = 1‰ lead to an increase of $\varepsilon^{53}Cr$ = 10, and due to the smaller initial abundance of ^{54}Cr, an even greater increase in $\varepsilon^{54}Cr$. In order to explain the difference of 0.06‰ across the enstatite chondrites, some EH chondrite would have $\varepsilon^{54}Cr$ >1, which is not seen.

The variation in $\delta^{53}Cr$ with siderophile elements can be explained by addition of an isotopically heavy metal phase. This metal phase controls the isotopic composition, but does not affect the Cr abundance, as it has low Cr concentrations (Horstmann et al., 2014). The low Cr concentration of the metal requires a high $\delta^{53}Cr$ in order to change the overall composition of the chondrites. The $\delta^{53}Cr$ of the metal can be calculated using a mass balance calculation, using the assumption that the concentration of Cr within the metal is 300 ppm, to be ~3.5 ‰. Equilibrium fractionation cannot produce this isotope composition as it is too extreme. The lower temperatures that the EH chondrites reached compared to the EL chondrites, will have also reduced the extent that the Cr within these samples progressed to equilibrium.

As previously discussed, the metal phase within enstatite chondrites contains little Cr as it likely forms from a nebula depleted in Cr. The formation of metal phases from a Cr depleted nebula can explain the high $\delta^{53}Cr$. If an isotopically light phase is condensing out of the solar nebula, then the residue will become isotopically heavy. In order for extreme isotopically heavy metal to condense, the previously accreted material needs to be isotopically light. Isotopically light material may form during condensation, due to equilibrium conditions between an isotopically light Cr phase and a heavy solar nebula; or kinetic fractionation, with light material preferentially included in the condensing phase equilibrium conditions. The effect of condensing an isotopically light phase is shown in Figure 5.8.

Figure 5.8.

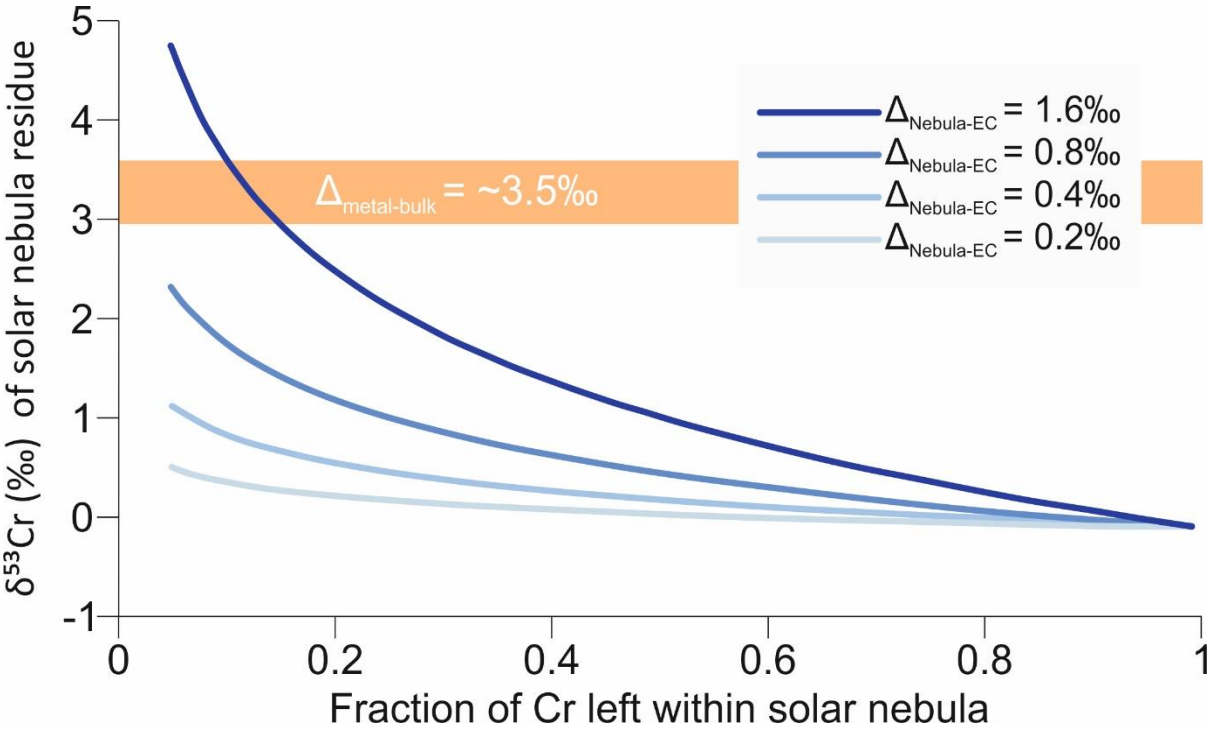

Figure 5.8. Rayleigh fractionation model, illustrating how extreme δ^{53}Cr *can be created in the final few percent of Cr in the solar nebula. Chromium in metal only accounts for a few percent of the overall abundance. If the Cr of the metal phase corresponds, to the last material condensed from the solar nebula then the metal phase could have very heavy* δ^{53}*Cr values*.

Rayleigh fractionation of Cr isotopes during condensation will lead to the last Cr that condenses being highly fractionated, as illustrated in Figure 5.8. The composition of the metal can be recreated through Rayleigh fractionation. If the metal phase condenses from the last few percent of Cr left in the solar nebula then it will inherit this extreme isotope composition. The lower temperatures experienced by the EH3-5 chondrites, means that this disequilibrium metal phase will be preserved.

5.5.4. An enstatite chondrite model for Earth

The isotopic similarities between Earth and the enstatite chondrites has led many studies to propose that they are the main building blocks of the Earth (Javoy et al., 2010; Dauphas, 2017). Of the two enstatite chondrite groups, the EH chondrites have a composition that is closest to the BSE, of -0.09 ± 0 .04 ‰ (2 s.d. n =5), although EL chondrites, -0.05 ± 0.10 ‰ (2 s.d. n=8), are also within error of the BSE (-0.12 ± 0.03 ‰, Chapter 4 of this thesis).

The enstatite chondrites are similar to the Earth in many isotopic systems, but some elements Si, Mo and Ru have resolvable isotope composition from Earth (Georg et al., 2007; Fitoussi and Bourdon, 2012; Zolotov et al., 2013; Fischer-Gödde and Kleine, 2017). There are also variations in the chemical composition, namely the excess Si in enstatite chondrites and the refractory element fractionations. Dauphas (2017) approached this problem by seeing how heterogeneous accretion could relax the constraints imposed by isotopes. Dauphas (2017) produced a model with an initial period of reduced planetary formation, during which the mantle received only a small portion of its siderophile elements (Ni, Cr, Mo and Ru). This allowed between 30 and 70 % of ordinary chondrites to be added to the Earth during the first 60 % of accretion.

The δ^{53}Cr of the BSE was recreated using the same model outlined in Dauphas (2017), using average partition coefficients of Cr from, Rubie et al., (2011). Metal silicate segregation does not lead to δ^{53}Cr fractionations (Bonnand et al., 2016b), so the composition of the mantle and core is inherited from the chondrites. The BSE composition used is taken from chapter 4 of this thesis (-0.12 ± 0.03 ‰). The composition of ordinary chondrites is -0.11 ± 0.04 ‰ n =17 (Bonnand et al., 2016b; Schoenberg et al., 2016). The results of this model are shown in Figure 5.9.

Figure 5.9.

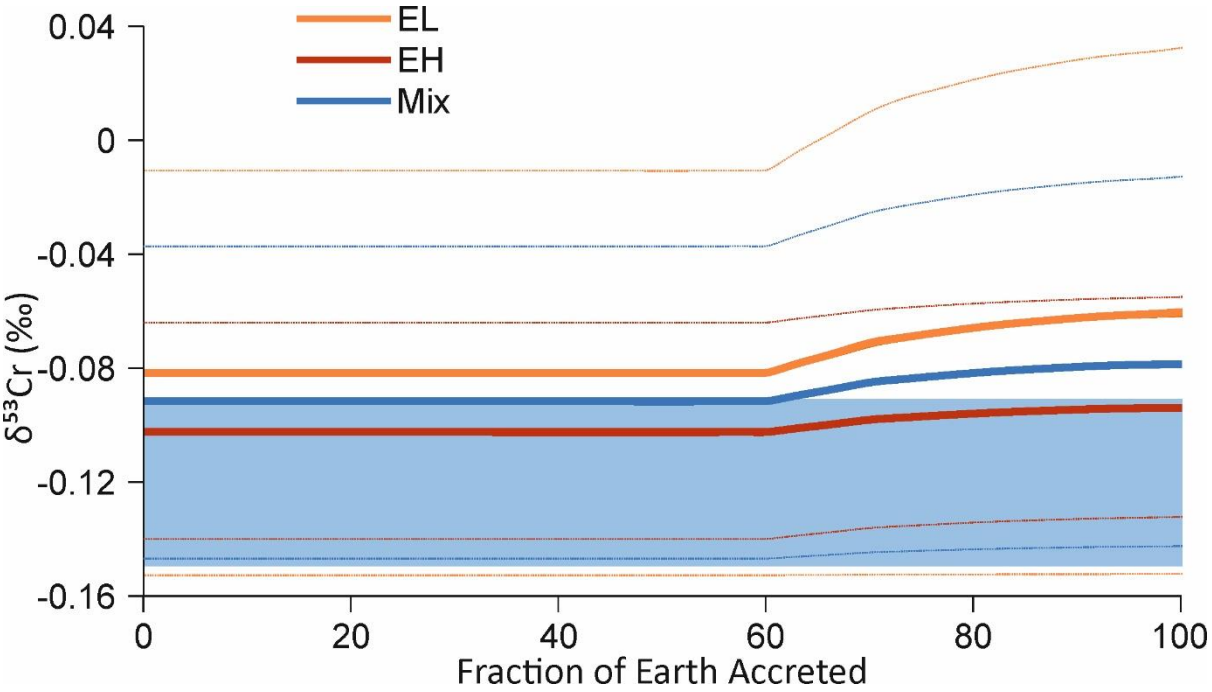

Figure 5.9. The $\delta^{53}Cr$ evolution of the BSE during accretion. The composition of the BSE -0.12 ± 0.03‰ is taken from Chapter 4 of this thesis and shown by the light blue shaded area. The uncertainty of the modelled lines is shown by dotted lines. The first 60 % of accretion is "reduced", with the Cr partition factor (metal/silicate) of 6.6, followed by 40% of "oxidised" conditions with a partition factor of 1.1. The accreting material over the first 60 % of Earth's accretion is an equal mix of ordinary chondrite and enstatite chondrite. Ordinary chondrite composition is -0.11 ± 0.04 ‰ (Bonnand et al., 2016b; Schoenberg et al., 2016)*. The enstatite material starting composition varies from EL (-0.05 ± 0.10 ‰), EH (-0.09 ± 0.04 ‰) and a mixture (-0.07 ‰). An Earth accretion model using EH chondrites, is best able to recreate the final $\delta^{53}Cr$ composition of the BSE.*

The Dauphas (2017) model is able to recreate the $\delta^{53}Cr$ of the mantle through a mix of enstatite and ordinary chondrites. The best estimate of the Earth's $\delta^{53}Cr$ is given by an enstatite chondrite composition that is mainly made from EH chondrites. The composition is

within the range of the BSE. The models using the EL chondrites are within error of the BSE, but have a larger uncertainty due to the variation within this class of chondrites, with an average value slightly heavier than that of the BSE. Both models, while within error of the BSE are slightly heavier. The EH chondrite $\delta^{53}Cr$ varies with the Fe content (Figure 5.7.a.). If the Earth formed from EH chondrites with relatively low Fe contents, this would provide a composition more in line with that of the Earth. Alternatively, the slight discrepancy could be reconciled if a small amount of Cr lost through volatilisation under oxidised conditions (Sossi et al., 2018a).

5.5.5. Similar $\delta^{53}Cr$ of the EH and EL chondrites

The EH and EL chondrites in this study show different $\delta^{53}Cr$ behaviour, with the EL chondrites having experienced higher temperatures leading to equilibrium fractionation between phases. This process is only believed to rearrange $\delta^{53}Cr$ in the chondrite and should not change the bulk composition of the parent meteorite. No variation is seen between the petrological types in the EH chondrites (Figure 5.3.), therefore thermal processing does not lead to loss of light / heavy Cr isotopes from the parent body. The variation in $\delta^{53}Cr$ of the EL chondrites is explained by heterogeneous distribution of troilite. As the variation is due to sampling then $\delta^{53}Cr$ values should have a normal distribution. Therefore, the average composition of the EL chondrites represents that of the parent body and is not due to later processes.

The two populations of EH and EL chondrites have no significant statistical difference. This may be unexpected as the formation of the two types of enstatite chondrites has previously been explained through condensing at different times (e.g. Blander and Abdel-

Gawad, 1969; Blander, 1971). In this chapter, we have shown how condensation from the enstatite nebular can lead to heavier $\delta^{53}Cr$ values of later formed material. This would then plausibly lead to one population of enstatite chondrites that are heavier than the other. However, Figure 5.8. shows that there is no significant variation in the $\delta^{53}Cr$ of condensing material until the nebula is almost completely fractionated.

5.6. CONCLUSIONS

This study has greatly expanded the number of measurements of Cr stable isotope compositions of enstatite chondrites, through measuring an additional 11 samples. These samples cover both EH and EL chondrites and include a greater range of petrological types. Enstatite chondrite with a lower petrological grade have $\delta^{53}Cr$ compositions controlled by condensation processes, while those meteorites, which have been heated, have equilibrium $\delta^{53}Cr$ fractionations between phases.

During condensation of the enstatite chondrites, troilite forms earlier. During condensation, light Cr phases condenses first increasing the $\delta^{53}Cr$ of the remaining nebular gas. This leaves a Cr depleted and fractionated nebula when metal phases form. The EH chondrites in this study show $\delta^{53}Cr$ variations related to the amount of isotopically light metal. Variations between the EH and EL chondrite can be explained by EL chondrites forming later from a slightly heavier solar nebular gas.

Meteorites that have reached equilibrium show $\delta^{53}Cr$ variations with the amount of troilite. Variations are explained by equilibrium fractionations of Cr, with troilite -0.27 ‰ lighter than coexisting phases. Variations in meteorites are due to small sampling of heterogeneous material.

A heterogeneous accretion model with the early formed material composed of ordinary and enstatite chondrites, followed by enstatite chondrite only material, can recreate the $\delta^{53}Cr$ composition of the BSE. The EH chondrites are the enstatite chondrite type that is best able to recreate the composition of the Earth.

Chapter 6: Summary and Outlook

The objective of this work was to constrain the $\delta^{53}Cr$ of the BSE, and appraise the role of enstatite chondrites in the formation of Earth. This was achieved using high precision Cr isotope measurement techniques and analysis of the behaviour of Cr stable isotopes in different geological settings.

In order to obtain an accurate composition of the BSE, the behaviour of $\delta^{53}Cr$ needs to be understood. The behaviour of stable Cr isotopes in the mantle has been a topic of contention, with the impact of partial melting debated (Schoenberg et al., 2008; Xia et al., 2017). Variations in the mantle were first identified by Schoenberg et al. (2008), who showed a similar composition of mantle peridotites to basalts, which contradicts later studies that showed that $\delta^{53}Cr$ varies with melt indicators, suggesting that the $\delta^{53}Cr$ of the mantle is affected by partial melting (Xia et al., 2017; Shen et al., 2018). This work has provided further insights into this problem by measuring a large data set of well characterised mantle samples. This set combined with previous measurements show that the $\delta^{53}Cr$ of the mantle does not vary with degree of partial melting. Partial melting models show that $\delta^{53}Cr$ in the mantle is not expected to change with melting. This is because there is only a small fractionation between mantle and melts means and Cr behaves compatibly in the mantle therefore no significant change in the mantle $\delta^{53}Cr$ can occur during melting.

Metasomatism has previously been proposed as a method to explain heavy $\delta^{53}Cr$ values of mantle peridotites (Xia et al., 2017). Within the mantle metasomatism is indeed able to alter $\delta^{53}Cr$ of peridotites. Some mantle peridotites with high $\delta^{53}Cr$, have low Ti/Eu and high La/Yb trace element ratios. These trace element indicators taken together are a sign of carbonatite metasomatism (Nelson et al., 1988; Rudnick et al., 1993). Carbonatite liquids can have created the heavy $\delta^{53}Cr$ values through non-equilibrium exchange of Cr, due to a transfer of Cr into

these undersaturated melts. Other Cr undersaturated melts will lead to similar variations. Metasomatic $\delta^{53}Cr$ variations described within this study as well as other examples previously identified, are the major control of Cr stable isotopes in the mantle. The effects of metasomatism in mantle peridotites can be hard to identify, and so it is difficult to account for its effect on $\delta^{53}Cr$ of mantle samples. Therefore, using mantle peridotites to calculate the $\delta^{53}Cr$ of the BSE will not provide a well constrained value.

An alternative method for calculating the BSE is to use komatiites. These high degree partial melts allow a larger volume of the mantle to be sampled, which reduces the effect of localised heterogeneities. Komatiites have proven a useful tool in calculating the composition of the BSE for other isotope system as the high degree of melting leads them to have similar compositions to the mantle, and the high temperatures of melting reduces the isotope fractionation. A combination of komatiites and other ultramafic rocks has previously been used to provide the best constrained $\delta^{53}Cr$ BSE value to date, of -0.11 ± 0.06 ‰ (Sossi et al., 2018a).

During fractional crystallisation the $\delta^{53}Cr$ varies due to crystallisation of isotopically heavy or light phases (Bonnand et al., 2016a, in review). In komatiite melts, variations occur during crystallisation due to excesses or deficits of isotopically light olivine. These variations were not identified within every flow. The crystallisation of isotopically light olivine only occurs in liquids with a high $Cr^{2+}/\Sigma Cr_{TOT}$, due to high temperatures (Li et al., 1995). Different methods to recreate the initial composition of the komatiite flows were used, with a weighted average able to best account for the variations during crystallisation. The initial $\delta^{53}Cr$ composition of three komatiite localities measured in this study, along with two komatiite flows from Sossi et al. (2018a), were used to calculate a new BSE value of -0.12 ± 0.03 ‰ (n=5). This agrees

with the values of other studies, but provides at least a twofold improvement in the uncertainty. The new composition of the BSE can be used in the future to clearly identify variations that occur in the mantle and comparisons to other planets.

Using the new improved composition of the BSE, it is possible to identify variations between the Earth and other solar system bodies. This is useful for identifying the material that created Earth. Metal silicate segregation does not fractionate $\delta^{53}Cr$, so no $\delta^{53}Cr$ changes are expected during core formation (Bonnand et al., 2016b). The material that formed Earth will have the same composition as the BSE. The enstatite chondrites are the class of chondrites that most closely match the mass independent Cr isotopic composition of Earth (Trinquier et al., 2007; Warren, 2011). Previous work however, has shown that the enstatite chondrites have a $\delta^{53}Cr$ composition that is heavy compared to the BSE (Bonnand et al., 2016b). Further study of this class of chondrites is required to see if this difference is due to the small sample size (n=2) or is a resolvable difference from Earth.

Measurements of 11 enstatite chondrites were obtained. Different $\delta^{53}Cr$ compositions and behaviour in the two classes of enstatites were seen, due to the different petrological types sampled within each class. During condensation isotopically light Cr phases condense first, leaving behind a nebula with increasing $\delta^{53}Cr$ values. The EH chondrites in this study have not been equilibrated and retain metal with isotopically heavy $\delta^{53}Cr$, which formed from a Cr depleted nebula. The EL chondrite in this study were all petrological type 6 and show evidence of equilibrium fractionation between phases, resulting in light troilite. Light troilite in the EL chondrites occurs during equilibrium of Cr. The different $\delta^{53}Cr$ of EH and EL chondrites, is explained by EL chondrites forming later from a slightly heavier solar nebula.

The enstatite chondrites cannot recreate the Earth alone, as they have chemical compositions that show significant different to the BSE. Dauphas (2017) presented a model that included ordinary and enstatite chondrites during the initial 60% of accretion, which is able to satisfy the isotopic composition of Earth for a number of isotope systems. Using this model the class of enstatite chondrite that provided the closest match to Earth, EH, EL or a mixture of both, was assessed. The composition of the BSE is best recreated by using the EH chondrites.

We have proposed a model for the enstatite chondrites where the different conditions of condensation alter the Cr content of the condensing phases. Unfortunately available data on condensation and volatility of the elements have a restricted range of conditions, under terrestrial conditions, and during condensation of the solar nebula under normal conditions. To fully understand the behaviour of Cr within enstatite chondrites, and the implications for Earth requires a greater understanding of these processes.

Enstatite chondrite like materials remain a possibility for the material that formed the Earth. However, the behaviour of $\delta^{53}Cr$ during core formation of enstatite chondrite like material is not yet fully understood. Metal-silicate experiments were carried out within mixtures that did not include sulphides, which, for the enstatite chondrites is a major reservoir. The effect of sulphide on $\delta^{53}Cr$ in metal silicate differentiations is currently unknown.

Appendices

Appendix 1- Additional figures for Chapter 3: Mantle

Supplementary information providing additional figures to support the main text. These include geochemical data, melting models and models of equilibrium interactions between carbonatites and the mantle.

Figures S1, S2 and S3, show additional geochemical data. Figure S1 uses a range of indicators of partial melting in order to see if there is any variation in the $\delta^{53}Cr$ of the mantle during melting. Figure S2 provides more information on whether the variation in $(La/Yb)_n$ is due to a change in the La concentrations, Yb concentrations, or both. Figure S3 presents available data for other stable isotope systems, which have been affected by a range of processes, to see if any variations in the $\delta^{53}Cr$ composition correlate with these.

A melting model is presented in Figure S4 to highlight the effects of compatibility on the Cr stable isotope composition of the residue. This is used to explain the different results from the models presented in this paper and those of Xia et al., (2017).

The interactions between carbonatiites and mantle at equilibrium or shown in Figures S5 and S6. These interactions show the end members, where variations may be entirely due to equilibrium fractionations, or due to mixing of different starting compositions. The models show whether or not these interactions are likely, or if the $\delta^{53}Cr$ values required would be too extreme, or if the amount of carbonatite required be unrealistic.

Figure A1

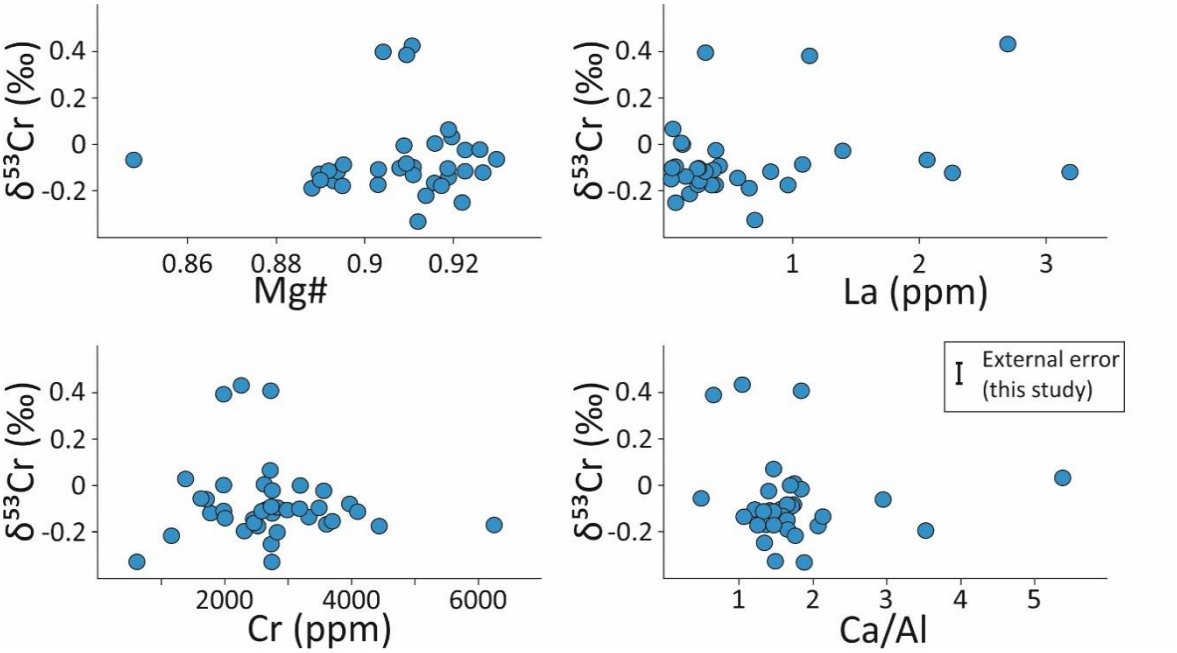

Figure A1.

$\delta^{53}Cr$ plotted against a number of indicators of partial melting, mg# (3a), La (3b), Cr (3c) and Ca/Al (3d). These melt geochemical proxies have different compatibilities so between them will identify correlations with $\delta^{53}Cr$ that is not seen in others. No trends are identified. Geochemical data is taken from previously mentioned references.

Figure A2

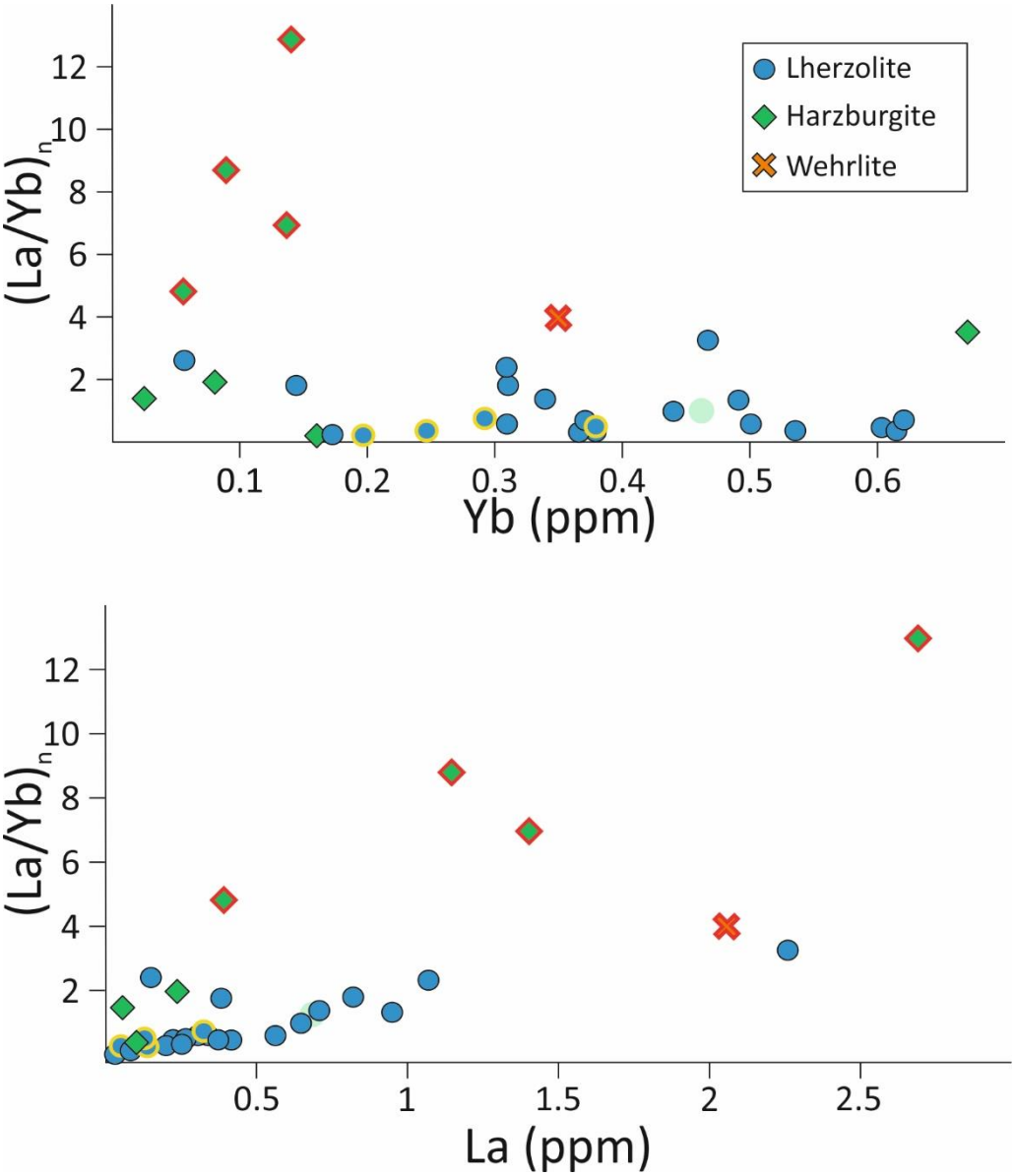

Figure A2.

$(La/Yb)_n$ plotted against the concentrations of La (Fig 2a) and Yb (Fig 2b). The axis have been chosen to provide further information on the $(La/Yb)_n$ ratio. Data points with red outlines and yellow outlines are group 1 and group 2 peridotites respectively, as defined by Figure 5. The group 1 peridotites have high La and low Yb concentrations, which combine to give a high $(La/Yb)_n$ ratio. Group 2 peridotites show no variation in their REE concentrations compared to

unaltered mantle peridotites. The group 2 peridotites must have had changes to the $\delta^{53}Cr$ compositions without changes to the REE composition.

Figure S3

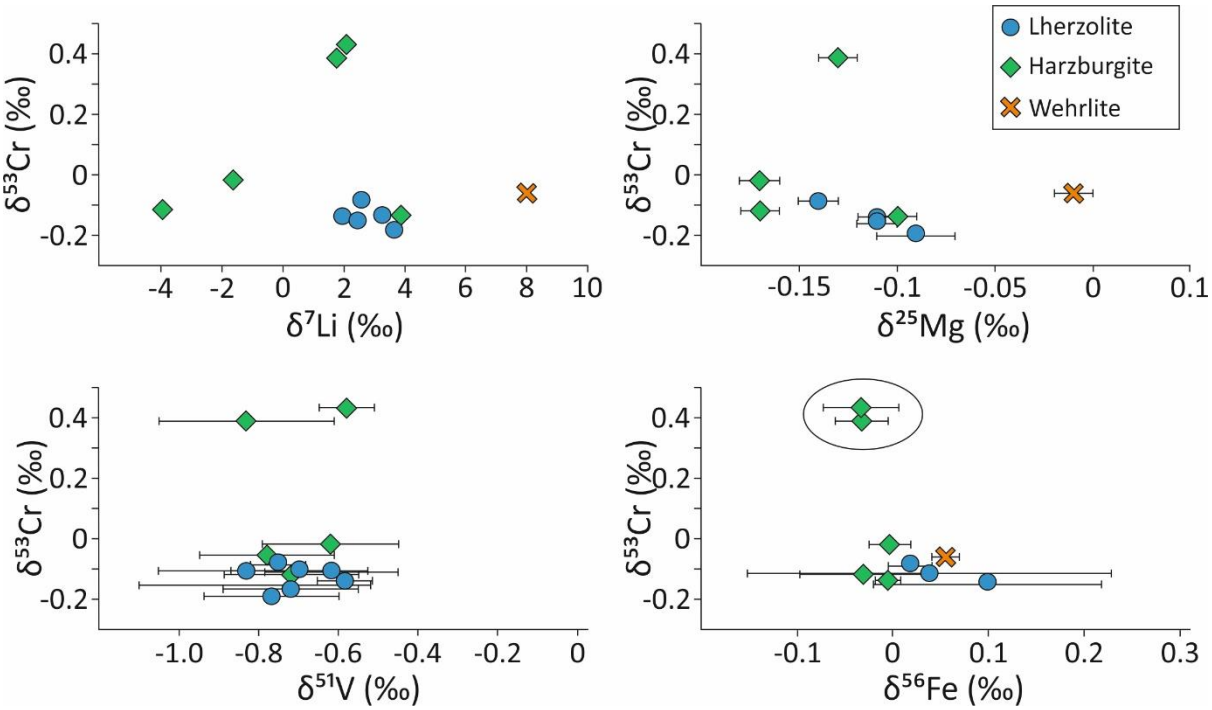

Figure A3.

Comparisons of $\delta^{53}Cr$ and other stable isotope data available on these samples. Magnesium and lithium stable isotope variations are related to diffusion. Vanadium isotopes are altered due to partial melting. No variation is seen with these isotopes. Iron stable isotopes are fractionated by partial melting. The iron isotope composition and mg# of two samples, 8530-24 and 8531-40 have previously been used to show metasomatism, and are highlighted (Weyer and Ionov, 2007). The $\delta^{53}Cr$ of these samples also show that these samples have been affected by metasomatism. Isotope data for other elements comes from (Williams et al., 2005; Weyer and Ionov, 2007; Pogge von Strandmann et al., 2011; Prytulak et al., 2013).

Figure A4

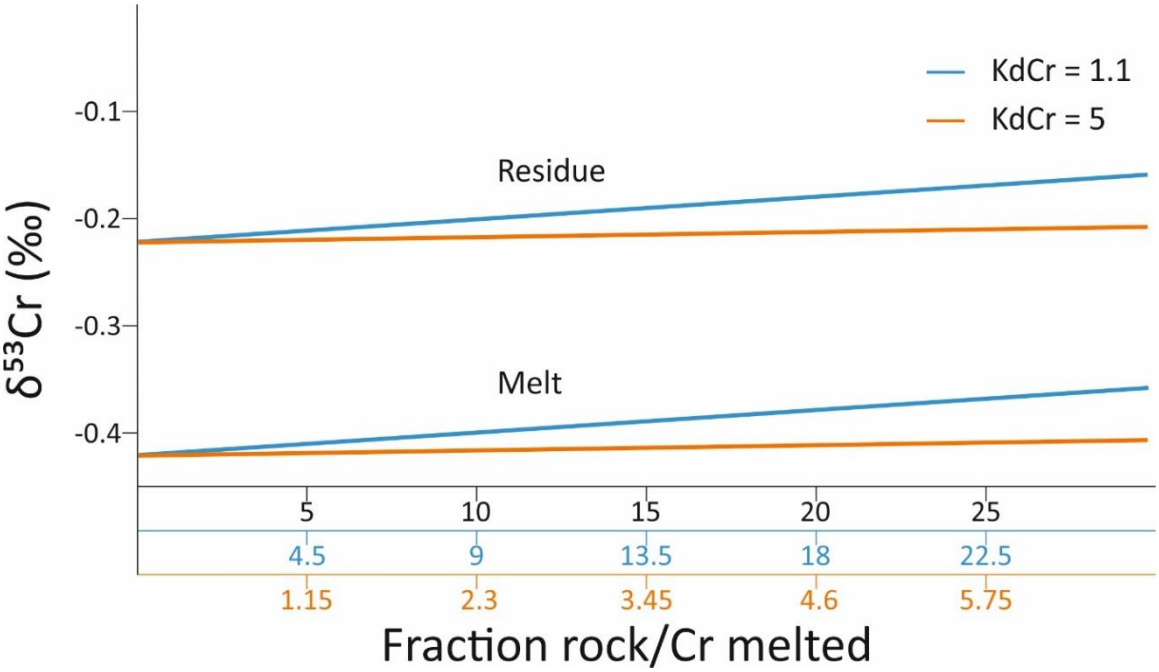

Figure A4

This model illustrates the change of the $\delta^{53}Cr$ composition using different bulk distribution coefficient. Models are created using Rayleigh fractionation, and use an α value of 1.0002 The axis show the amount of rock melted in black, and the amount of Cr removed using a KD_{Cr} of 1.1 (blue) and 5 (orange). Less than a quarter of the Cr is removed from the mantle over 30% melting when using a KD_{Cr} of 5 compared to 1.1. The change in the $\delta^{53}Cr$ of the mantle using the higher KD_{Cr} is much lower, due to the smaller amount of Cr removed over the same degree of melting.

Figure A5.

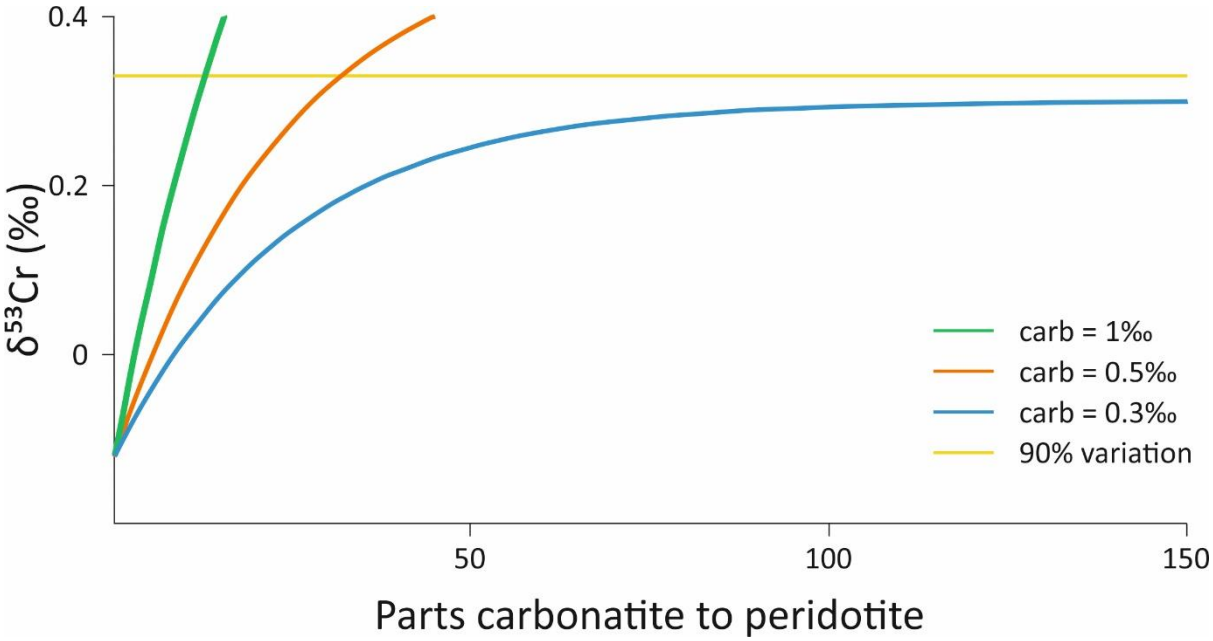

Figure A5.

Modelled interactions between carbonatite with heavy $\delta^{53}Cr$ and the mantle. Interactions between the two phases is modelled to lead to a composition where the Cr from mantle and the melt has equilibrated with a fractionation factor of $\alpha = 1$, and so the composition of the mantle is increased. Each interaction includes one part of carbonatite melt to one part mantle. The rate of change in the mantle composition becomes less, as the mantle composition becomes closer to the composition of carbonatite. In order to increase the starting mantle to 90% of the variation seen, a composition of carbonatite material of 1‰ requires 14 parts of carbonatite to 1 part mantle, 0.5‰, 32 parts of carbonatites, and a starting composition of 0.3‰ will never reach the 90% limit.

Figure S6

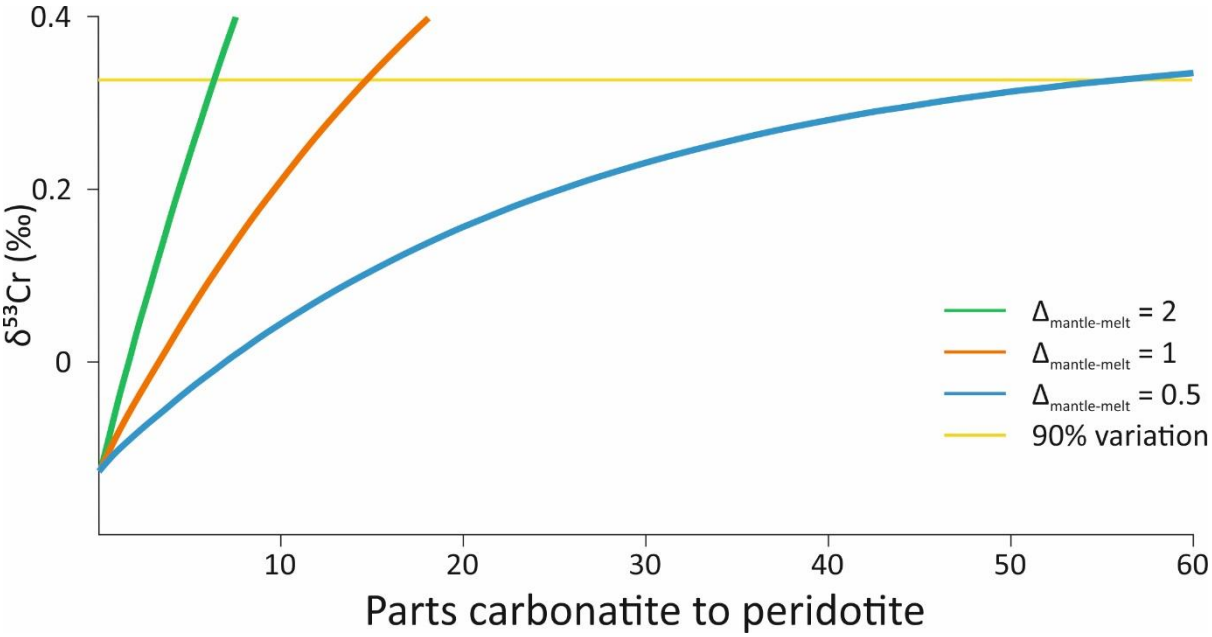

Figure A6.

Modelled interactions between carbonatite and the mantle. Interactions between the phases are assumed to equilibrium = 0.5, 1 and 2‰, with the starting composition of the mantle and carbonatitie melts at -0.12‰. The rate of change in the mantle composition becomes less, as the mantle composition increases, as the mantle and carbonatites require smaller changes to reach equilibrium. In order to increase the starting mantle to 90% of the variation seen, a fractionation $\Delta_{Mantle\text{-}melt}$ of 2‰ requires 7 parts of carbonatite material to every part of the mantle, 1‰ requires 15 parts of carbonatite, and 0.5‰ requires 57.

Appendix 2 - Komatiite bulk chemical data

Table A1

Sample	GOR 94-3	GOR 94-17	GOR 94-19	GOR 94-43	GOR 94-44	12001	12101	12105
SiO2	45.1	45.8	45.8	47.8	45.5	45.8	51.0	45.8
TiO2	0.49	0.63	0.58	0.55	0.57	0.38	0.67	0.38
Al203	8.1	10.7	9.8	9.2	9.6	7.4	13.3	7.4
Fe2O3	11.6	12.2	12.0	11.8	11.8	12.4	11.7	12.3
MnO	0.17	0.18	0.18	0.17	0.18	0.20	0.20	0.20
MgO	28.6	20.9	23.9	23.4	24.7	26.4	10.1	26.6
CaO	6.56	9.1	8.12	n.d.	8.02	5.85	10.4	5.88
Na2O	0.31	0.89	0.53	0.51	0.51	0.94	1.92	0.92
K2O	0.05	0.03	0.04	0.01	0.02	0.22	0.36	0.18
P2O5	0.04	0.05	0.04	0.04	0.04	0.06	0.09	0.06
V	173	188	101	209	167	134	216	138
Cr	2745	932	514	1340	2598	3146	607	3170
Co	n.d.	n.d.	n.d.	n.d.	n.d.	105	54	90
Ni	1018	1079	1201	935	1050	1172	241	1185
Cu	n.d.	n.d.	n.d.	n.d.	n.d.	60	99.7	57.8
LOI	n.d.	n.d.	n.d.	n.d.	n.d.	2.99	0.74	3.21

Table A1 cont.

Sample	12106	12110	12117	12124	TN-01	TN-03	TN-05	TN-06
SiO2	47.7	50.6	50.9	52.5	46.9	48.3	48.4	48.6
TiO2	0.48	0.59	0.65	0.70	0.37	0.41	0.42	0.44
Al203	9.2	11.7	13.1	14.3	7.3	8.1	8.3	8.8
Fe2O3	11.8	11.7	11.5	11.1	12.7	12.9	13.1	13.4
MnO	0.19	0.19	0.19	0.19	0.22	0.21	0.21	0.22
MgO	21.5	13.7	11.2	7.4	24.0	20.2	19.5	18.1
CaO	7.43	9.04	10.3	11	7.22	7.86	8.48	8.58
Na2O	1.07	1.84	1.98	2.19	0.54	0.97	1.12	1.25
K2O	0.22	0.33	0.10	0.53	0.14	0.08	0.07	0.08
P2O5	0.07	0.09	0.09	0.09	0.02	0.02	0.02	0.02
V	153	200	206	249	156	183	184	188
Cr	1933	1277	818	372	2332	2455	2369	2191
Co	72	27	44	21	97	79	82	84
Ni	1005	332	306	86	1371	1006	880	758
Cu	68.7	90.3	98.3	107	67	75	n.d.	n.d.
LOI	1.06	2.25	0.58	0.25	6.61	3.85	3.3	2.95

Table A1 cont

Sample	TN-16	TN-19	ZV-10	ZV-14
SiO2	45.0	45.3	46.2	49.4
TiO2	0.26	0.28	0.31	0.46
Al203	5.2	5.3	6.2	9.3
Fe2O3	n.d.	11.8	12.2	13.4
MnO	0.19	0.19	0.20	0.22
MgO	31.0	30.3	27.5	16.5
CaO	5.21	5.48	6.11	9.02
Na2O	0.61	0.63	0.66	1.16
K2O	0.01	0.01	0.02	0.06
P2O5	0.01	0.01	0.02	0.02
V	116	122	137	203
Cr	2247	2223	2284	2023
Co	114	96	108	74
Ni	2245	2131	1804	541
Cu	47	n.d.	52	n.d.
LOI	3.07	2.68	2.16	2.79

Table A1- Geochemical data from the

References

Aitken B. G. and Echeverria L. M. (1984) Petrology and geochemistry of komatiites and tholeiites from Gorgona Island, Colombia. *Contrib. to Mineral. Petrol.* **86**, 94–105.

Albaréde F. and Beard B. (2004) Analytical Methods for Non-Traditional Isotopes. *Rev. Mineral.* **55**, 74.

Allègre C. J. ., Poirer J.-P., Humler E. and Hofmann A. W. (1995) The chemical composition of the Earth. *Earth Planet. Sci. Lett.* **134**, 515–523.

Allen R. O. and Mason B. (1973) Minor and trace elements in some meteoritic minerals. *Geochim. Cosmochim. Acta* **37**, 1435–1456.

Andersen C. A., Keil K. and Mason B. (1964) Silicon Oxynitride : A Meteoritic Mineral. *Science (80-.).* **146**, 256–257.

Armytage R. M. G., Georg R. B., Savage P. S., Williams H. M. and Halliday A. N. (2011) Silicon isotopes in meteorites and planetary core formation. *Geochim. Cosmochim. Acta* **75**, 3662–3676. Available at: http://dx.doi.org/10.1016/j.gca.2011.03.044.

Arndt N. T. (1986) Differentiation of komatiite flows. *J. Petrol.* **27**, 279–301.

Arndt N. T. (2008) *Komatiite*., Cambridge University Press.

Arndt N. T. (1976) Melting relations of ultramafic lacas (komatiites) at 1 atm and high pressure. *Carnegie Inst. Washingt. Yearb.* **75**, 555–562.

Arndt N. T., Ginibre C., Chauvel C., Albarède F., Cheadle M. J., Herzberg C., Jenner G. and Lahaye Y. (1998) Were komatiites wet? *Geology* **26**, 739–742.

Arndt N. T, Kerr A. C., Arndt Nicholas T, Kerr A. C. and Tarney J. (1997) Dynamic melting in plume heads : The formation of Gorgona komatiites and basalts Dynamic melting in plume heads : the formation of Gorgona komatiites and basalts. *Earth Planet. Sci. Lett.* **146**, 289–301.

Asafov E. V., Sobolev A. V., Gurenko A. A., Arndt N. T., Batanova V. G., Portnyagin M. V., Garbe-Schönberg D. and Krasheninnikov S. P. (2018) Belingwe komatiites (2.7Ga) originate from a plume with moderate water content, as inferred from inclusions in olivine. *Chem. Geol.* **478**, 39–59. Available at: https://doi.org/10.1016/j.chemgeo.2017.11.002.

Badro J., Brodholt J. P., Piet H., Siebert J. and Ryerson F. J. (2015) Core formation and core composition from coupled geochemical and geophysical constraints. *Proc. Natl. Acad. Sci.* **112**, 12310–12314.

Badullovich N., Moynier F., Creech J., Teng F.-Z. and Sossi P. A. (2017) Tin isotopic fractionation during igneous differentiation and Earth's mantle composition. *Geochemical Perspect. Lett.*, 24–28. Available at: http://www.geochemicalperspectivesletters.org/article1741.

Baedecker P. A. and Wasson J. T. (1975) Elemental fractionations among enstatite chondrites. *Geochim. Cosmochim. Acta* **39**, 735–765.

Barnes S. J. (1998) Chromite in Komatiites, 1. Magamatic Controls on Crystallization and Composition. *J. Petrol.* **39**, 1689–1720.

Berry A. J. and O'Neill H. S. C. (2004) A XANES determination of the oxidation state of chromium in silicate glasses. *Am. Mineral.* **89**, 790–798.

Berry A. J., O'Neill H. S. C., Scott D. R., Foran G. J. and Shelley J. M. G. (2006) The effect of composition on Cr 2 + / Cr 3 + in silicate melts. *Am. Mineral.* **91**, 1901–1908.

Berry A. J., Shelley J. M. G., Garry J., O'Neill H. S. C. and Scott D. R. (2003) A furnace design for XANES spectroscopy of silicate melts under controlled oxygen fugacities and temperatures to 1773 K research papers. *J. Synchrotron Radiat.* **10**, 332–336.

Bickle M. J. (1982) The magnesium contents of komatiitic liquids. In *Komatiites* (eds. N. T. Arndt and E. G. Nisbet). George Allen and Unwin, London. pp. 479–494.

Bigeleisen J. and Mayer M. G. (1947) Calculation of Equilibrium Constants for Isotopic Exchange Reactions. *J. Chem. Phys.* **15**, 261–267. Available at: http://aip.scitation.org/doi/10.1063/1.1746492.

Birch F. (1964) Density and Composition of Mantle and Core. *J. Geophyiscal Res.* **59**, 4377–4388.

Birck J.-L. and Allègre C. J. . (1984) Chromium Isotopic Anomalies in Allende Refractory Inclusions. *Geophys. Res. Lett.* **11**, 943–946.

Birck J.-L. and Allègre C. J. . (1985) *Isotopic Ratios in the Solar System*., Cepadues-Editions, Toulouse.

Birck J. L., Richard L. P. and Allégre C. J. (1980) Chromium isotopes in meteorites and terrestrial samples. *Meteoritics* **16**.

Blander M. (1971) The constrained equilibrium theory: Sulphide phases in meteorites. *Geochim. Cosmochim. Acta* **35**, 61–76.

Blander M. and Abdel-Gawad M. (1969) The origin of meteorites and the constrained equilibrium condensation theory. *Geochim. Cosmochim. Acta* **33**, 701–716.

Blum J. D. and Bergquist B. A. (2007) Reporting of variations in the natural isotopic composition of mercury. In *Analytical and Bioanalytical Chemistry* pp. 353–359.

Boesenberg J. S., Weisberg M. K., Greenwood R. C., Gibson J. M. and Franchi I. A. (2014) The anomalous enstatite meteorites- Part 2: the recrystallisze EL meteorites. *Lunar Planet. Sci. Conf.* **45**, 1468–1467.

Bonnand P., Doucelance R., Boyet M., Bachèlery P., Bosq C., Auclair D. and Schiano P. The influence of igneous processes on the chromium isotopic compositions of terrestrial basalts.

Bonnand P. and Halliday A. N. (2018) Oxidized conditions in iron meteorite parent bodies. *Nat. Geosci.* **11**, 2–6. Available at: http://dx.doi.org/10.1038/s41561-018-0128-2.

Bonnand P., James R. H., Parkinson I. J., Connelly D. P. and Fairchild I. J. (2013) The chromium isotopic composition of seawater and marine carbonates. *Earth Planet. Sci. Lett.* **382**, 10–20. Available at: http://dx.doi.org/10.1016/j.epsl.2013.09.001.

Bonnand P., Parkinson I. J. and Anand M. (2016a) Mass dependent fractionation of stable chromium isotopes in mare basalts: Implications for the formation and the differentiation of the Moon. *Geochim. Cosmochim. Acta* **175**, 208–221.

Bonnand P., Parkinson I. J., James R. H., Karjalainen A.-M. and Fehr M. A. (2011) Accurate and precise determination of stable Cr isotope compositions in carbonates by double spike MC-ICP-MS. *J. Anal. At. Spectrom.* **26**, 528–535.

Bonnand P., Williams H. M., Parkinson I. J., Wood B. J. and Halliday A. N. (2016b) Stable chromium isotopic composition of meteorites and metal-silicate experiments: Implications for

fractionation during core formation. *Earth Planet. Sci. Lett.* **435**, 14–21.

Brett R. and Sato M. (1984) Intrinsic oxygen fugacity measurements on seven chondrites, a pallasite, and a tektite and the redox state of meteorite parent bodies. *Geochim. Cosmochim. Acta* **48**, 111–120.

Brooks C. and Hart S. R. (1974) On the Significance of Komatiite. *Geology*, 107–110.

Canil D. (1997) Vanadium partitioning and the oxidation state of Archaean komatiite magmas. *Nature* **389**, 842–845.

Canil D. (1999) Vanadium partitioning between orthopyroxene, spinel and silicate melt and the redox states of mantle source regions for primary magmas. *Geochim. Cosmochim. Acta* **63**, 557–572.

Cartier C., Hammouda T., Doucelance R., Boyet M., Devidal J. and Moine B. (2014) Experimental study of trace element partitioning between enstatite and melt in Enstatite-Chondrites at low oxygen fugacities and 5 GPa. *Geochim. Cosmochim. Acta* **130**, 167–187. Available at: http://dx.doi.org/10.1016/j.gca.2014.01.002.

Chabot N. L. and Agee C. B. (2003) Core formation in the Earth and Moon : New experimental constraints from V , Cr , and Mn. *Geochim. Cosmochim. Acta* **67**, 2077–2091.

Chabot N. L., Saslow S. A., Donough W. F. M. C. and Jones J. H. (2009) An investigation of the behavior of Cu and Cr during iron meteorite crystallization. *Meteorit. Soc.* **519**, 505–519.

Chase M. (1998) NIST-JANAF thermochemical tables. *J. Phys. Chem. Ref. Data Monogr. (National Inst. Stand. Technol. Gaithersburg, MD),* **4**.

Chauvel C., Dupré B. and Arndt N. T. (1993) Pd and Nd isotopic correlation in Belingwe komatiites and basalts. In *The Geology of the Belingwe Greenstone Belt, Zimbabwe. A Study of the Evolution of Archean Continental Crust. A.A. Balkema, Rotterdam/Brookfield* pp. 205–220.

Cheng Z., Zhang Z., Hou T., Santosh M., Zhang D. and Ke S. (2015) Petrogenesis of nephelinites from the Tarim Large Igneous Province, NW China: Implications for mantle source characteristics and plume-lithosphere interaction. *Lithos* **220–223**, 164–178. Available at:

http://dx.doi.org/10.1016/j.lithos.2015.02.002.

Clayton D. D. (2003) *Handbook of isotopes in the Cosmos*., Cambridge University Press, Cambridge.

Coath C. D., Elliott T. and Hin R. C. (2017) Double-spike inversion for three-isotope systems. *Chem. Geol.* **451**, 78–89.

Coleman R. G. and Keith T. E. (1971) A Chemical Study of Serpentinization — Burro Mountain, California. *J. Petrol.* **12**, 311–328.

Condie K. C. (1993) Chemical composition and evolution of the upper continental crust : Contrasting results from surface samples and shales. *Chem. Geol.* **104**, 1–37.

Crawford A. J., Falloon T. J. and Green D. H. (1989) Classification, petrogenesis and tectonic setting of boninites. In *Bonitites* (ed. A. J. Crawford). Unwin Hyman, London. pp. 1–49.

Crozaz G. and Lundberg L. L. (1995) The origin of oldhamite in unequilibrated enstatite chondrites. *Geochim. Cosmochim. Acta* **59**, 3817–3831.

Dann J. C. (2001) Vesicular komatiites, 3.5-Ga Komati Formation, Barberton Greenstone Belt, South Africa: Inflation of submarine lavas and origin of spinifex zones. *Bull. Volcanol.* **63**, 462–481.

Dasgupta R., Hirschmann M. M., McDonough W. F., Spiegelman M. and Withers A. C. (2009) Trace element partitioning between garnet lherzolite and carbonatite at 6.6 and 8.6 GPa with applications to the geochemistry of the mantle and of mantle-derived melts. *Chem. Geol.* **262**, 57–77. Available at: http://dx.doi.org/10.1016/j.chemgeo.2009.02.004.

Dauphas N. (2017) The isotopic nature of the Earth's accreting material through time. *Nature* **541**, 521–524. Available at: http://dx.doi.org/10.1038/nature20830.

Dauphas N., Chen J. H., Zhang J., Papanastassiou D. A., Davis A. M. and Travaglio C. (2014) Calcium-48 isotopic anomalies in bulk chondrites and achondrites: Evidence for a uniform isotopic reservoir in the inner protoplanetary disk. *Earth Planet. Sci. Lett.* **407**, 96–108. Available at: http://dx.doi.org/10.1016/j.epsl.2014.09.015.

Dauphas N., Davis A. M., Marty B. and Reisberg L. (2004) The cosmic molybdenum-ruthenium isotope correlation. *Earth Planet. Sci. Lett.* **226**, 465–475.

Davies R., Nixon P. H., Pearson G. and Obata M. (1993) Tectonic implications of graphitized diamonds from the Ronda peridotite massif , southern Spain. *Geology* **21**, 2–5.

Dawson J. B. (1984) Kimberlites II: The Mantle and Crust-Mantle Relationship. In (ed. J. Kornprobst). Elsevier Science Publishers, Holland. p. 289.

Defouilloy C., Cartigny P., Assayag N., Moynier F. and Barrat J. (2016) High-precision sulfur isotope composition of enstatite meteorites and implications of the formation and evolution of their parent bodies. *Geochim. Cosmochim. Acta* **172**, 393–409. Available at: http://dx.doi.org/10.1016/j.gca.2015.10.009.

Deng Z., Moynier F., Zuilen K. Van, Sossi P. A., Pringle E. A. and Chaussidon M. (2018) Lack of resolvable titanium stable isotopic variations in bulk chondrites. *Geochim. Cosmochim. Acta* **239**, 409–419.

Dodson M. H. (1963) A theoretical study of the use of internal standards for precise isotopic analysis by the surface ionization technique : Part I - General first-order algebraic solutions A theoretical study of the use of internal standards for precise isotopic analysis by. *J. Sci. Instrum.* **40**, 289–295.

Donaldson C. H. (1982) Spinifex-textured komatiites: a review of textures, compositions and layering. In *Komatiites* (eds. N. T. Arndt and E. G. Nisbet). George Allen and Unwin. pp. 211–244.

Easton A. J. (1985) E-Chondrites: Significance of the Partition of Elements between “Silicate” and “Sulphide.” *Meteoritics* **20**, 89–101.

Ebel D. S. and Alexander C. M. O. D. (2011) Equilibrium condensation from chondritic porous IDP enriched vapor : Implications for Mercury and enstatite chondrite origins. *Planet. Space Sci.* **59**, 1888–1894. Available at: http://dx.doi.org/10.1016/j.pss.2011.07.017.

Echeverria L. M. (1980) Mineralogy and Petrology Tertiary or Mesozoic Komatiites From Gorgona Island , Colombia : Field Relations and Geochemistry. *Contrib. to Mineral. Petrol.* **266**, 253–266.

Ellis A. S., Johnson T. M. and Bullen T. D. (2002) Chromium Isotopes and the Fate of Hexavalent Chromium in the Environment. *Science (80-.).* **295**, 2060–2062.

Ellis A. S., Johnson T. M. and Bullen T. D. (2004) Using Chromium Stable Isotope Ratios to Quantify Cr(VI) Reduction: Lack of Sorption Effects. *Environ. Sci. Technol.* **38**, 3604–3607.

Farkaš J., Chrastný V., Novák M., Čadkova E., Pašava J., Chakrabarti R., Jacobsen S. B., Ackerman L. and Bullen T. D. (2013) Chromium isotope variations (??53/52Cr) in mantle-derived sources and their weathering products: Implications for environmental studies and the evolution of ??53/52Cr in the Earth's mantle over geologic time. *Geochim. Cosmochim. Acta* **123**, 74–92.

Faure F., Arndt N. I. and Libourel G. (2006) Formation of spinifex texture in komatiites: An experimental study. *J. Petrol.* **47**, 1591–1610.

Fischer-Gödde M. and Kleine T. (2017) Ruthenium isotopic evidence for an inner Solar of the late veneer. *Nature* **541**, 525–527.

Fischer R. A., Nakajima Y., Campbell A. J., Frost D. J., Harries D., Langenhorst F., Miyajima N., Pollok K. and Rubie D. C. (2015) High pressure metal-silicate partitioning of Ni, Co, V, Si and O. *Geochim. Cosmochim. Acta* **167**, 177–194.

Fitoussi, C; Bourdon B. (2012) Silicon Isotope Evidence Against an Enstatite Chondrite Earth. *Science (80-.).* **335**, 1477–1480.

Fitoussi C. and Bourdon B. (2012) Silicon Isotope Evidence Against an Enstatite Chondrite Earth. *Science (80-.).* **335**, 1477–1480.

Frei R., Gaucher C., Døssing L. N. and Sial A. N. (2011) Chromium isotopes in carbonates — A tracer for climate change and for reconstructing the redox state of ancient seawater Author ' s personal copy. *Earth Planet. Sci. Lett.* **312**, 114–125.

Frei R., Gaucher C., Poulton S. W. and Canfield D. E. (2009) Fluctuations in Precambrian atmospheric oxygenation recorded by chromium isotopes. *Nature* **461**, 250–253. Available at: http://dx.doi.org/10.1038/nature08266.

Frei R., Gaucher C., Stolper D. and Canfield D. E. (2013) Fluctuations in late Neoproterozoic atmospheric oxidation — Cr isotope chemostratigraphy and iron speciation of the late Ediacaran lower Arroyo del Soldado Group (Uraguay). *Gondwana Res.* **23**, 797–811.

Frei R., Poiré D. and Frei K. M. (2014) Weathering on land and transport of chromium to the ocean in a subtropical region (Misiones, NW Argentina): A chromium stable isotope perspective. *Chem. Geol.* **381**, 110–124.

Fujii T., Moynier F., Agranier A., Ponzevera E., Abe M., Uehara A. and Yamana H. (2013) Nuclear field shift effect in isotope fractionation of thallium. *J. Radioanal. Nucl. Chem.* **296**, 261–265.

Gall L., Williams H. M., Halliday A. N. and Kerr A. C. (2017) Nickel isotopic composition of the mantle. *Geochim. Cosmochim. Acta* **199**, 196–209. Available at: http://dx.doi.org/10.1016/j.gca.2016.11.016.

Georg R. B., Halliday A. N., Schauble E. a and Reynolds B. C. (2007) Silicon in the Earth's core. *Nature* **447**, 1102–1106.

Goldstein J. I., Scott E. R. D. and Chabot N. L. (2009) Iron meteorites : Crystallization, thermal history, parent bodies, and origin. *Chemie der Erde* **69**, 293–325. Available at: http://dx.doi.org/10.1016/j.chemer.2009.01.002.

El Goresy A., Yabuki H., Ehlers K., Woolum D. and Pernicka E. (1988) Qingzhen and Yamato-691: A tentative alphabet for the EH chondrites. *Proc. NIPR symp. Antarct. Meteorites* **1**, 65–101.

Greber N. D., Puchtel I. S., Nägler T. F. and Mezger K. (2015) Komatiites constrain molybdenum isotope composition of the Earth's mantle. *Earth Planet. Sci. Lett.* **421**, 129–138. Available at: http://dx.doi.org/10.1016/j.epsl.2015.03.051.

Green D. H. and Wallace M. E. (1988) Mantle metasomatism by ephemeral carbonatite melts. *Nature* **336**, 459–462.

Grove L., Parman W. and Dann J. (1999) Conditions of magma generation for Archean komatiites from the Barberton Mountainland, South Africa. *Geochemical Soc. Spec. Publ.*, 155–168.

Grove T. L., De Wit M. J. and Dann J. C. (1997) Komatiites from the komati type section, Barberton, South Africa. *Oxford Monogr. Geol. Geophys.* **35**, 438–456.

Hallis L. J., Anand M. and Strekopytov S. (2014) Trace-element modelling of mare basalt parental melts: Implications for a heterogeneous lunar mantle. *Geochim. Cosmochim. Acta* **134**, 289–

316. Available at: http://dx.doi.org/10.1016/j.gca.2014.01.012.

Hanson B. and Jones J. H. (1998) The systematics of Cr3+ and Cr2+ partitioning between olivine and liquid in the presence of spinel. *Am. Mineral.* **83**, 669–684.

Hartmann D. ., Woosley S. E. . and El Eid M. F. . (1985) Nucleosynthesis in Neutron-Rich Supernova Ejecta. *Astrophys. J.* **297**, 837–845.

Harvey J., König S. and Luguet A. (2015) The effects of melt depletion and metasomatism on highly siderophile and strongly chalcophile elements: S-Se-Te-Re-PGE systematics of peridotite xenoliths from Kilbourne Hole, New Mexico. *Geochim. Cosmochim. Acta* **166**, 210–233.

Harvey J., Yoshikawa M., Hammond S. J. and Burton K. W. (2012) Deciphering the Trace Element Characteristics in Kilbourne Hole Peridotite Xenoliths : Melt ^ Rock Interaction and Metasomatism beneath the Rio Grande Rift , SW USA. *J. Petrol.* **53**, 1709–1742.

Herzberg C. (2004) Geodynamic Information in Peridotite Petrology. *J. Petrol.* **45**, 2507–2530.

Hevey P. J. and Sanders I. S. (2006) A model for planetesimal meltdown by 26 Al and its implications for meteorite parent bodies. *Meteorit. Planet. Sci.* **41**, 95–106.

Hibbert K. E. J., Williams H. M., Kerr A. C. and Puchtel I. S. (2012) Iron isotopes in ancient and modern komatiites: Evidence in support of an oxidised mantle from Archean to present. *Earth Planet. Sci. Lett.* **321**–**322**, 198–207. Available at: http://dx.doi.org/10.1016/j.epsl.2012.01.011.

Hin R. C., Coath C. D., Carter P. J., Nimmo F., Lai Y. J., Pogge von Strandmann P. A. E., Willbold M., Leinhardt Z. M., Walter M. J. and Elliott T. (2017) Magnesium isotope evidence that accretional vapour loss shapes planetary compositions. *Nature* **549**, 511–527. Available at: http://dx.doi.org/10.1038/nature23899.

de Hoffmann E. and Stroobant V. (2007) *Mass Spectrometry, Principles and Applications*. Third., Wiley.

Honda M. and Imamura M. (1971) Half-Life of Mn53. *Phys. Rev. C* **4**, 1182–1188. Available at: http://link.aps.org/doi/10.1103/PhysRevC.4.1182.

Horstmann M., Humayun M. and Bischoff A. (2014) Clues to the origin of metal in Almahata Sitta EL

and EH chondrites and implications for primitive E chondrite thermal histories. *Geochim. Cosmochim. Acta* **140**, 720–744. Available at: http://dx.doi.org/10.1016/j.gca.2014.04.041.

Ionov D. (2004) Chemical Variations in Peridotite Xenoliths from Vitim , Siberia : Inferences for REE and Hf Behaviour in the Garnet-Facies Upper Mantle. *J. Petrol.* **45**, 343–367.

Ionov D. A. (2010) Petrology of Mantle Wedge Lithosphere : New Data on Supra-Subduction Zone Peridotite Xenoliths from the Andesitic AvachaVolcano , Kamchatka. *J. Petrol.* **51**, 327–361.

Ionov D. A., Chanefo Æ. I. and Bodinier J. (2005) Origin of Fe-rich lherzolites and wehrlites from Tok , SE Siberia by reactive melt percolation in refractory mantle peridotites Origin of Fe-rich lherzolites and wehrlites from Tok , SE Siberia by reactive melt percolation in refractory mantle peridotites. *Contrib. to Mineral. Petrol.* **150**, 335–353.

Ionov D. A., Chazot G., Chauvel C., Merlet C. and Bodinier J. (2006) Trace element distribution in peridotite xenoliths from Tok , SE Siberian craton : A record of pervasive , multi-stage metasomatism in shallow refractory mantle. *Geochim. Cosmochim. Acta* **70**, 1231–1260.

Ionov D. A. and Hofmann A. W. (2007) Depth of formation of subcontinental off-craton peridotites. *Earth Planet. Sci. Lett.* **261**, 620–634.

Izbicki J. A., Ball J. W., Bullen T. D. and Sutley S. J. (2008) Occurrence of Hexavalent Chromium in Ground Water in the Western Mojave Desert , California. *Appl. Geochemistry* **23**, 1325–1352.

Jagoutz E., Palme H., Baddenhausen H., Blum K., Cendales M., Dreibus G. E., Spettel B., Lorez V. and Wanke H. (1979) The abundances of major, minor and trace elements in the earth's mantle as derived from primitive ultramafic nodules. *Earth Planet. Sci. Lett.* **10**, 2031–2050.

Javoy M., Kaminski E., Guyot F., Andrault D., Sanloup C., Moreira M., Labrosse S. and Jambon A. (2010) Author ' s personal copy The chemical composition of the Earth : Enstatite chondrite models. *Earth Planet. Sci. Lett.* **293**, 259–268.

Jones J. H. and Palme H. (2000) Geochemical constraints on the origin of the Earth and Moon. In *The Origin of the Earth and the Moon* (eds. R. Canup and K. Righter). University of Arizona Press, Tucson, AZ. pp. 197–216.

Kallemeyn G. W. and Wasson J. T. (1986) Compositions of enstatite (EH3 , EH4 , 5 and EM) chondrites : Implications regarding their formation. *Geochim. Cosmochim. Acta* **50**, 2153–2164.

Keil K. (1989) Enstatite meteorites and their parent bodies. *Meteoritics* **24**, 195–208.

Keil K. (1968) Mineralogical and Chemical Relationships among Enstatite Chondrites. *J. Geophys. Res.* **73**, 6945–6976.

Keil K. (2000) Thermal alteration of asteroids: evidence from meteorites. *Planet. Space Sci.* **48**, 887–903.

Keil K. (1969) Titanium distribution in enstatite chondrites and achondrites, and its bearing on their origin. *Earth Planet. Sci. Lett.* **7**, 243–248.

Keil K. and Andersen C. A. (1965) Occurence of Sinoite, Si2N2O, in Meteorites. *Nature*, 1965.

Keil K. and Brett R. (1974) Heidite, (Fe,Cr)1+x(Ti,Fe)2S4, A New Mineral in Achondrite the Bustee Enstatite. *Am. Mineral.* **59**, 465–470.

Kerr A. C. (2005) La Isla de Gorgona, Colombia: A petrological enigma? *Lithos* **84**, 77–101.

Kimura M., Hiyagon H., Lin Y. and Weisberg M. K. (2003) FeO-rich silicates in the Sahara 97159 (EH3) enstatite chondrite : Mineralogy, oxygen isotopic compositions, and origin. *Meteorit. Planet. Sci.* **38**, 389–398.

Kleine T., Mezger K., Palme H. and Münker C. (2004) The W isotope evolution of the bulk silicate Earth : constraints on the timing and mechanisms of core formation and accretion. *Earth Planet. Sci. Lett.* **228**, 109–123.

Klemme S., Gensk F. S., Berndt J., Rohrbach A. and Sossi P. A. (2018) Cr isotope fractionation during the degassing of silicate melts. In *American Geophysical Union, Fall Meeting*

Klemme S. and O'Neill H. S. C. . (2000) The near-solidus transition from garnet lherzolite to spinel lherzolite. *Contrib. to Mineral. Petrol.*, 237–248.

Kong P., Mori T. and Ebihara M. (1997) Compositional continuity of enstatite chondrites and implications for heterogeneous accretion of the enstatite parent body. *Geochim. Cosmochim. Acta* **61**.

Konhauser K., Lyons T. W., Mojzsis S. J. and Rouxel O. (2011) Aerobic bacterial pyrite oxidation and acid rock drainage during the Great Oxidation Event. *Lett. to Nat.* **478**, 369–374.

Kushiro I. and Yoder H. S. (1969) No Title. *Carangie Inst. Yearb.* **67**, 153–158.

Lamoreaux R. H., Hildenbrand D. L. and Brewer L. (1987) High-Temperature Vaporization Behaviour of Oxide II. Oxides of Be, Mg, Ca, Sr, Ba, B, Al, Ga, In, Tl, Si, Ge, Sn, Pb, Zn, Cd and Hg. *J. Phys. Chem. Ref. Data* **16**, 419–443.

Larimer J. W. (1975) The effect of C / O ratio on the condensation of planetary material. *Geochim. Cosmochim. Acta* **39**, 389–392.

Larimer J. W. and Anders E. (1970) Chemical fractionations in meteorites-III. Major element fractionations in chondrites. *Geochim. Cosmochim. Acta* **34**, 367–387.

Larimer J. W. and Bartholomay M. (1979) The role of carbon and oxygen in cosmic gases : some applications to the chemistry and mineralogy of enstatite chondrites. *Geochim. Cosmochim. Acta* **43**.

Larsen K. K., Trinquier A., Paton C., Schiller M., Wielandt D., Ivanova M. A., Connelly J. N., Nordlund Å., Krot A. N. and Bizzarro M. (2011) Evidence for magnesium isootpe heterogeneity in the solar protoplanetary disk. *Astrophys. J. Lett.* **37**, 1–7.

Leya I., Wieler R. and Halliday A. N. . (2003) The influence of cosmic-ray production on extinct nuclide systems. *Geochim. Cosmochim. Acta* **67**, 529–541.

Li J.-P., O'Neill H. S. C. . and Seifert F. (1995) Subsolidus Phase Relations in the System MgO-SiO2-Cr-O in Equilibrium with Metallic Cr, and their Significance for the Petrochemistry of Chromium. *J. Petrol.* **36**, 107–132.

Liang Y. and Elthon D. (1990) Evidence from chromium abundances in mantle rocks for extraction of picrite and komatiite melts. *Lett. to Nat.* **348**, 551–553.

Liu J., Qin L., Xia J., Carlson R. W., Leya I., Dauphas N. and He Y. (2019) Cosmogenic effects on chromium isotopes in meteorites. *Geochim. Cosmochim. Acta* **251**, 73–86. Available at: https://doi.org/10.1016/j.gca.2019.01.032.

Liu X. I. and O'Neill H. S. C. (2004) The Effect of Cr2O3 on the Partial Melting of Spinel Lherzolite in the System CaO – MgO – Al2O3 – SiO2 – Cr2O3 at 1.1 GPa. *J. Petrol.* **45**, 2261–2286.

Lodders K. (2003) Solar System Abundances and Condensation Temperatures of the Elements. *Astrophys. J.* **591**, 1220–1247. Available at: http://adsabs.harvard.edu/abs/2003ApJ...591.1220L.

Lodders K., Palme H. and Wlotzka F. (1993) Trace elements in mineral separates of the Pena Blanca Spring aubrite: Implications for the evolution of the aubrite parent body. *Meteoritics* **28**, 539–551.

Lugmair G. W. and Shukolyukov A. (1998) Early solar system timescales according to 53Mn-53Cr systematics. *Geochim. Cosmochim. Acta* **62**, 2863–2886.

Lusby D., Scott E. R. D. and Keil K. (1987) Ubiquitous High-FeO Silicates in Enstatite Chondrites. *Proc. Lunar Planet. Sci. Conf.* **92**, 679–695.

Macris C. A., Manning C. E. and Young E. D. (2015) Crystal chemical constraints on inter-mineral Fe isotope fractionation and implications for Fe isotope disequilibrium in San Carlos mantle xenoliths. *Geochim. Cosmochim. Acta* **154**, 168–185. Available at: http://dx.doi.org/10.1016/j.gca.2015.01.024.

Mason B. (1966) The enstatite chondrites. *Geochim. Cosmochim. Acta* **30**, 23–39.

McCoy T. J., Keil K., Bogard D. D., Garrison D. H., Casanova I., Lindstrom M. M., Brearley A. J., Kehm K., Nichols R. H. and Hohenberg C. M. (1995) Origin and history of impact-melt rocks of enstatite chondrite parentage. *Geochim. Cosmochim. Acta* **59**, 161–175.

McDonough W. F. (1990) Constraints on the composition of the continental lithospheric mantle. *Earth Planet. Sci. Lett.* **101**, 1–18.

McDonough W. F. and Sun S. (1995) The composition of the Earth '. *Chem. Geol.* **2541**, 223–253.

McSween H. Y. J. (1979) Are Carbonaceous Chondrites Primitive or Processed? A Review. *Rev. Geophys. Sp. Phys.* **17**, 1059–1078.

Meisel T., Walker R. J. and Morgan J. W. (1996) The osmium Isotopic composition of the Earth's

primitive upper mantle. *Nature* **383**, 517–520.

Menzies M. A. and Hawkesworth C. J. (1987) *Mantle Metasomatism*., Academic Press, London.

Morrison C. W. (1980) Characteristics and tectonic setting of the shoshonite rock association. *Lithos* **13**, 97–108.

Mougel B., Moynier F., Göpel C. and Koeberl C. (2017) Chromium isotope evidence in ejecta deposits for the nature of Paleoproterozoic impactors. *Earth Planet. Sci. Lett.* **460**, 105–111.

Moynier F., Paniello R. C., Gounelle M., Albare F., Beck P., Podosek F. and Zanda B. (2011a) Nature of volatile depletion and genetic relationships in enstatite chondrites and aubrites inferred from Zn isotopes. *Geochim. Cosmochim. Acta* **75**, 297–307.

Moynier F., Yin Q.-Z. and Jacobsen B. (2007) DATING THE FIRST STAGE OF PLANET FORMATION Frederic Moynier, Qing-zhu Yin, and Benjamin Jacobsen. *Astrophys. J.* **671**, 54–56.

Moynier F., Yin Q.-Z. and Schauble E. (2011b) Isotopic evidence of Cr partitioning into Earth's core. *Science* **331**, 1417–1420.

Murck B. W. and Campbell I. H. (1986) The effects of temperature, oxygen fugacity and melt composition on the behaviour of chromium in basic and ultrabasic melts. *Geochim. Cosmochim. Acta* **50**, 1871–1887. Available at: http://petrology.oxfordjournals.org/content/40/5/831%5Cnhttp://petrology.oxfordjournals.org/content/40/5/831.full.pdf%5Cnhttp://petrology.oxfordjournals.org/content/40/5/831.short.

Nelson D. R., Chivas A. R., Chappell B. W. and Mcculloch M. T. (1988) Geochemical and isotopic systematics in carbonatites and implications for the evolution of ocean-island sources. *Geochim. Cosmochim. Acta* **52**, 1–17.

Nicklas R. W., Puchtel I. S. and Ash R. D. (2016) High-precision determination of the oxidation state of komatiite lavas using vanadium liquid-mineral partitioning. *Chem. Geol.* **433**, 36–45. Available at: http://dx.doi.org/10.1016/j.chemgeo.2016.04.011.

Nicklas R. W., Puchtel I. S. and Ash R. D. (2018) Redox state of the Archean mantle: Evidence from V partitioning in 3.5–2.4 Ga komatiites. *Geochim. Cosmochim. Acta* **222**, 447–466. Available at:

https://doi.org/10.1016/j.gca.2017.11.002.

Niederer F. R., Papanastassiou D. A. and Wasserburg G. J. (1981) The isotopic composition of titanium in the Allende and Leoville meteorites. *Geochim. Cosmochim. Acta* **45**, 1017–1031.

Nisbet E. G., Arndt N. T., Bickle M. J., Chauvel C., Cheadle M., Martin A., Renner R., Roedder E., Hegner E. and Kyser T. K. (1987) Uniquely fresh 2 . 7 Ga komatiites from the Belingwe greenstone belt , Zimbabwe. *Geology* **15**, 1147–1150.

Nisbet E. G., Cheadle M. J., Arndt N. T. and Bickle M. J. (1993) Constraining the Potential Temperature of the Archean Mantle - a Review of the Evidence from Komatiites. *Lithos* **30**, 291–307.

Ntoumbé M., Déruelle B., Bertrand I., Mbowou G. and Ngounouno I. (2016) New Petrological and Geochemical Data of the Nephelinitic Lavas and Geodynamic Implications of Mount Etinde (Cameroon). *Int. J. Geosci.* **7**, 1452–1470.

O'Neill H. S. . (1991) The origin of the Moon and the early history of the Earth- A chemical model Part 1: The Moon. *Geochim. Cosmochim. Acta* **55**, 1135–1157.

Olsen E. J., Bunch T. E., Jarosewich E., Noonan A. F. and Huss G. I. (1977) Happy Canyon: a New Type of Enstatite Achondrite. *Meteoritics* **12**, 109–124.

Palme H. and O'Neill H. S. C. (2014) Cosmochemical Estimates of Mantle Composition. *Treatise Geochemistry 2nd Ed.* **3**, 1–37.

Papike J., Karner J. and Shearer C. (2005) O 2 conditions that range from IW-2 (Moon) to IW+6 (Earth) with Mars somewhere between at IW to IW+2. In this range of. *Lunar Planet. Sci.* **34**, 2004–2005.

Parman S. W., Dann J. C., Grove T. L. and Wit M. J. De (1997) Emplacement conditions of komatiite magmas from the 3 . 49 Ga Komati Formation, Barberton Greenstone Belt, South Africa. *Earth Planet. Sci. Lett.* **150**, 303–323.

Parman S. W., Grove T. L., Dann J. C. and Wit M. J. De (2004) A subduction origin for komatiites and cnitonic lithospheric mantle. *South African J. Geol.* **107**, 107–118.

Paul C. Hess (1989) *Origins of Igneous Rocks*.,

Plank T. and Langmuir C. H. (1998) The chemical composition of subducting sediment and its consequences for the crust and mantle. *Chem. Geol.* **145**, 325–394.

Pogge von Strandmann P. A. E., Elliott T., Marschall H. R., Coath C., Lai Y. J., Jeffcoate A. B. and Ionov D. A. (2011) Variations of Li and Mg isotope ratios in bulk chondrites and mantle xenoliths. *Geochim. Cosmochim. Acta* **75**, 5247–5268. Available at: http://dx.doi.org/10.1016/j.gca.2011.06.026.

Project B. V. S. (1981) *Basaltic Volcanism on the Terrestrial Planets.* ed. Pergamon,

Prytulak J., Nielsen S. G., Ionov D. A., Halliday A. N., Harvey J., Kelley K. A., Niu Y. L., Peate D. W., Shimizu K. and Sims K. W. W. (2013) The stable vanadium isotope composition of the mantle and mafic lavas. *Earth Planet. Sci. Lett.* **365**, 177–189. Available at: http://dx.doi.org/10.1016/j.epsl.2013.01.010.

Puchtel I. S., Haase K. M., Hofmann A. W., Chauvel C., Kulikov V. S., Garbe-Schönberg C. D. and Nemchin A. A. (1997) Petrology and geochemistry of crustally contaminated komatiitic basalts from the Vetreny Belt, southeastern Baltic Shield: Evidence for an early Proterozoic mantle plume beneath rifted Archean continental lithosphere. *Geochim. Cosmochim. Acta* **61**, 1205–1222.

Puchtel I. S., Hofmann A. W., Mezger K., Shchipansky A. A., Kulikov V. S. and Kulikova V. V. (1996) Petrology of a 2.41 Ga remarkably fresh komatiitic basalt lava lake in Lion Hills, central Vetreny Belt, Baltic Shield. *Contrib. to Mineral. Petrol.* **124**, 273–290.

Puchtel I. S., Toubal M., Blichert-Toft J., Walker R. J., Brandon A. D., Nicklas R. W., Kulikov V. S. and Samsonov A. V. (2016a) Lithophile and siderophile element systematics of Earth ' s mantle at the Archean – Proterozoic boundary : Evidence from 2.4 Ga komatiites. *Geochim. Cosmochim. Acta* **180**, 227–255.

Puchtel I. S., Touboul M., Blichert-Toft J., Walker R. J., Brandon A. D., Nicklas R. W., Kulikov V. S. and Samsonov A. V. (2016b) Lithophile and siderophile element systematics of Earth's mantle at the

Archean-Proterozoic boundary: Evidence from 2.4 Ga komatiites. *Geochim. Cosmochim. Acta* **180**, 227–255.

Puchtel I. S., Walker R. J., Brandon A. D. and Nisbet E. G. (2009) Pt-Re-Os and Sm-Nd isotope and HSE and REE systematics of the 2.7 Ga Belingwe and Abitibi komatiites. *Geochim. Cosmochim. Acta* **73**, 6367–6389. Available at: http://dx.doi.org/10.1016/j.gca.2009.07.022.

Pyke D. R., Naldretty A. J. and Eckstrand O. R. (1973) Archean Ultramafic Flows in Munro Township , Ontario. *Geol. Soc. Am. Bull.* **84**, 955–978.

Qin L., Alexander C. M. O. D., Carlson R. W., Horan M. F. and Yokoyama T. (2010) Contributors to chromium isotope variation of meteorites. *Geochim. Cosmochim. Acta* **74**, 1122–1145. Available at: http://dx.doi.org/10.1016/j.gca.2009.11.005.

Qin L., Nittler L. R., Alexander C. M. O. D., Wang J., Stadermann F. J. and Carlson R. W. (2011) Extreme 54 Cr-rich nano-oxides in the CI chondrite Orgueil – Implication for a late supernova injection into the solar system. *Geochim. Cosmochim. Acta* **75**, 629–644. Available at: http://dx.doi.org/10.1016/j.gca.2010.10.017.

Regelous M., Elliott T. and Coath C. D. (2008) Nickel isotope heterogeneity in the early Solar System. *Earth Planet. Sci. Lett.* **272**, 330–338.

Reid A. M., Donaldson C. H., Brown R. W., Ridleyt W. I. and Dawson B. (1975) MINERAL CHEMISTRY OF PERIDOTITE XENOLITHS FROM THE LASHAINE VOLCANO ,Tanzania. *Phys. Chem. Earth* **9**, 525–543.

Renner R., Nisbet E. G., Cheadle M. J., Arndt N. T., Bickle M. J. and Cameron W. E. (1994) Komatiite Flows from the Reliance Formation , Belingwe Belt , Zimbabwe : I . Petrography and Mineralogy. *J. Petrol.* **35**, 361–400.

Révillon S., Arndt N. T., Chauvel C. and Hallot E. (2000) Geochemical study of ultramafic volcanic and plutonic rocks from Gorgona Island, Colombia: The plumbing system of an oceanic plateau. *J. Petrol.* **41**, 1127–1153.

Rhodes J. M. . and Dawson J. B. (1975) MAJOR AND TRACE ELEMENT CHEMISTRY OF PERIDOTITE

INCLUSIONS FROM THE LASHAINE VOLCANO , TANZANIA. *Phys. Chem. Earth* **9**, 545–557.

Richter F. M., Davis A. M., Ebel D. S. and Hashimoto A. (2002) Elemental and isotopic fractionation of type B calcium-, aluminum-rich inclusions: Experiments, theoretical considerations, and constraints on their thermal evolution. *Geochim. Cosmochim. Acta* **66**, 521–540.

Roeder P. L. and Reynolds I. (1991) Crystallization of Chromite and Chromium Solubility in Basaltic Melts. *J. Petrol.*, 909–934.

Rubie D. C., Frost D. J., Mann U., Asahara Y., Nimmo F., Tsuno K., Kegler P., Holzheid A. and Palme H. (2011) Heterogeneous accretion , composition and core – mantle differentiation of the Earth. *Earth Planet. Sci. Lett.* **301**, 31–42.

Rubin A. E. (2004) Postshock annealing and postannealing shock in equilibrated ordinary chondrites: Implications for the thermal and shock histories of chondritic asteroids. *Geochim. Cosmochim. Acta* **68**, 673–689.

Rubin A. E. (1983) The Adhi Kot breccia and implications for the origin of chondrules and silica-rich clasts in enstatite chondrites. *Earth Planet. Sci. Lett.* **64**, 201–212.

Rubin A. E. and Scott E. R. D. (1997) Abee and related EH chondrite impact-melt breccias. *Geochim. Cosmochim. Acta* **61**, 425–435.

Rubin A. E., Scott E. R. D. and Keil K. (1997) Shock metamorphism of enstatite chondrites. *Geochim. Cosmochim. Acta* **61**, 847–858.

Rudge J. F., Reynolds B. C. and Bourdon B. (2009) The double spike toolbox. *Chem. Geol.* **265**, 420–431. Available at: http://dx.doi.org/10.1016/j.chemgeo.2009.05.010.

Rudnick R. L. and Gao S. (2003) Composition of the Continental Crust. In *The Crust* Elsevier Science Publishers, New York. pp. 1–64.

Rudnick R. L., McDonough W. F. and Chappell B. W. (1993) Carbonatite metasomatism in the northern Tanzanian mantle: petrographic and geochemical characteristics. *Earth Planet. Sci. Lett.* **114**, 463–475.

Santos J. F., Scha U. and Girardeau J. (2002) Genesis of Pyroxenite-rich Peridotite at Cabo Ortegal (

NW Spain): Geochemical and Pb – Sr – Nd Isotope Data. *J. Petrol.* **43**, 17–43.

Schauble E. (2004) Applying stable isotope fractionation theory to new systems. *Rev. Mineral. Geochemistry* **55**, 65. Available at: papers://dee23da0-e34b-4588-b624-f878b46d7b3d/Paper/p132.

Schauble E. A., Ghosh P. and Eiler J. M. (2006) Preferential formation of 13C – 18O bonds in carbonate minerals, estimated using first-principles lattice dynamics. *Geochim. Cosmochim. Acta* **70**, 2510–2529.

Schiller M., Van Kooten E., Holst J. C., Olsen M. B. and Bizzarro M. (2014) Precise measurement of chromium isotopes by MC-ICPMS. *J. Anal. At. Spectrom.* **29**, 1406. Available at: http://xlink.rsc.org/?DOI=C4JA00018H.

Van Schmus W. R. and Wood J. A. (1967) A chemical-petrologic classification for the chondritic meteorites. *Geochim. Cosmochim. Acta* **31**, 747–765.

Schoenberg R., Merdian A., Holmden C., Kleinhanns I. C., Haßler K., Wille M. and Reitter E. (2016) The stable Cr isotopic compositions of chondrites and silicate planetary reservoirs. *Geochim. Cosmochim. Acta* **183**, 14–30.

Schoenberg R., Zink S., Staubwasser M. and von Blanckenburg F. (2008) The stable Cr isotope inventory of solid Earth reservoirs determined by double spike MC-ICP-MS. *Chem. Geol.* **249**, 294–306.

Schreiber H. D. and Haskin L. A. (1976) Chromium in basalts: Experimental determination of redox staets and partitioning among synthetic silicate phases. *Proc. Lunar Planet. Sci. Conf.* **7**, 1221–1259.

Scott E. R. D. and Krot A. N. (2003) Chondrites and their components. *Treatise on geochemistry*, 63–115.

Sears D. W., Kallemeyn G. W. and Wasson J. T. (1982) The compositional classification of chondrites: II The ensatite chondrite groups. *Geochim. Cosmochim. Acta* **46**, 597–608.

Shahar A., Ziegler K., Young E. D., Ricolleau A., Schauble E. A. and Fei Y. (2009) Experimentally

determined Si isotope fractionation between silicate and Fe metal and implications for Earth's core formation. *Earth Planet. Sci. Lett.* **288**, 228–234. Available at: http://dx.doi.org/10.1016/j.epsl.2009.09.025.

Shaw D. M. (1970) Trace element fractionation during anatexis. *Geochim. Cosmochim. Acta* **34**, 237–243.

Shen J., Fang Z., Qin L., Zhang Q., Xiao Y. and Yu H. (2016) High temperature inter-mineral Cr isotope fractionation : ionic model constraint and implication for mantle xenoliths from North China Craton. *Goldschmidt Conf. Abstr.*, 2816.

Shen J., Liu J., Qin L., Wang S.-J., Li S., Xia J., Ke S. and Yang J. (2015) Chromium isotope signature during continental crust subduction recorded in metamorphic rocks. *Geochemistry, Geophys. Geosystems* **16**, 1–15.

Shen J., Qin L., Fang Z., Zhang Y., Liu J., Liu W., Wang F., Xiao Y., Yu H. and Wei S. (2018) High-temperature inter-mineral Cr isotope fractionation : A comparison of ionic model predictions and experimental investigations of mantle xenoliths from the North China Craton. *Earth Planet. Sci. Lett.* **499**, 278–290. Available at: https://doi.org/10.1016/j.epsl.2018.07.041.

Shields W. R., Murphy T. J., Catanzaro E. J. and Garner E. (1966) Absolute Isotopic Abundance Ratios and the Atomic Weight of a Reference Sample of Chromium. *J. Res. Natl. Bur. Stand. A. Phys. Chem.* **70**, 193–197.

Shikari K. (1997) Geochemical Behaviour of Chromium. *Resour. Geol.* **47**, 319–330.

Shimizu K., Komiya T., Hirose K., Shimizu N. and Maruyama S. (2001) Cr-spinel, an excellent micro-container for retaining primitive melts - implications for a hydrous plume origin for komatiites. *Earth Planet. Sci. Lett.* **189**, 177–188.

Shore M. (1996) Cooling and crystallisation of komatiite lava flows (PhD thesis).

Shukolyukov A. and Lugmair G. . (2004) Manganese-chromium isotope systematics of enstatite meteorites. *Geochim. Cosmochim. Acta* **68**, 2875–2888. Available at: http://linkinghub.elsevier.com/retrieve/pii/S0016703704000675.

Siebert J., Corgne A. and Ryerson F. J. (2011) Systematics of metal – silicate partitioning for many siderophile elements applied to Earth ' s core formation. *Geochim. Cosmochim. Acta* **75**, 1451–1489. Available at: http://dx.doi.org/10.1016/j.gca.2010.12.013.

Snow J. E. and Dick H. J. B. (1995) Pervasive magnesium loss by marine weathering of peridotite. *Geochim. Cosmochim. Acta* **59**, 4219–4235.

Sobolev A. V., Asafov E. V., Gurenko A. A., Arndt N. T., Batanova V. G., Portnyagin M. V., Garbe-Schönberg D. and Krasheninnikov S. P. (2016) Komatiites reveal a hydrous Archean deep-mantle reservoir. *Lett. to Nat.* **531**, 628–632. Available at: http://dx.doi.org/10.1038/nature17152.

Sossi P. A., Eggins S. M., Nesbitt R. W., Nebel O., Hergt J. M., Campbell I. H., O'Neill H. S. C., Kranendonk M. Van and Rhodri Davies D. (2016) Petrogenesis and geochemistry of Archean Komatiites. *J. Petrol.* **57**, 147–184.

Sossi P. A., Klemme S., O'Neill H. S. C., Berndt J. and Moynier F. (2019) Evaporation of moderately volatile elements from silicate melts: experiments and theory. *Geochim. Cosmochim. Acta* **260**, 204–231. Available at: https://doi.org/10.1016/j.gca.2019.06.021.

Sossi Paolo A, Moynier F. and Zuilen K. Van (2018) Volatile loss following cooling and accretion of the Moon revealed by chromium isotopes. *PNAS* **115**, 10920–10925.

Sossi Paolo A., Nebel O., O'Neill H. S. C. and Moynier F. (2018) Zinc isotope composition of the Earth and its behaviour during planetary accretion. *Chem. Geol.* **477**, 73–84. Available at: https://doi.org/10.1016/j.chemgeo.2017.12.006.

Streckeisen A. (1976) To each plutonic rock its proper name. *Earth Sci. Rev.* **12**, 1–33.

Sugiura N. and Fujiya W. (2014) Correlated accretion ages and e 54 Cr of meteorite parent bodies and the evolution of the solar nebula. *Meteorit. Planet. Sci.* **787**, 772–787.

Sun S. -s. and McDonough W. F. (1989) Chemical and isotopic systematics of oceanic basalts: implications for mantle composition and processes. *Geol. Soc. London, Spec. Publ.* **42**, 313–345.

Sweeney R. J., Green D. H. and Sie S. H. (1992) Trace and minor element partitioning between garnet

and amphibole and carbonatitic melt. *Earth Planet. Sci. Lett.* **113**, 1–14.

Trinquier A., Birck J.-L. and Allègre C. J. (2008a) High-precision analysis of chromium isotopes in terrestrial and meteorite samples by thermal ionization mass spectrometry. *J. Anal. At. Spectrom.* **23**, 1565–1574.

Trinquier A., Birck J.-L. and Allègre C. J. (2007) Widespread 54Cr Heterogeneity in the Inner Solar System. *Astrophys. J.* **655**, 1179–1185.

Trinquier A., Birck J.-L., Allègre C. J., Gopel C. and Ulfbeck D. (2008b) Mn – 53 Cr systematics of the early Solar System revisited. *Geochim. Cosmochim. Acta* **72**, 5146–5163.

Trinquier A., Birck J. and Alle C. J. (2006) The nature of the KT impactor . A 54Cr reappraisal. *Earth Planet. Sci. Lett.* **241**, 780–788.

Urey H. C. (1947) The Thermodynamic Properties of Isotopic Substances. *J. Chem. Soc.*, 562–581.

Viljoen M. J. and Viljoen R. P. (1969) Evidence for the existence of a mobile extrusive peridotitic magma from the Komati Formation of the Onverwacht Group. *Trans. Geol. Soc. S. Afr. Spec.* **2**, 88–112.

Wade J. and Wood B. J. (2005) Core formation and the oxidation state of the Earth. *Earth Planet. Sci. Lett.* **236**, 78–95.

Walker R. J. ., Storey M., Kerr A. C. ., Tarney J. and Arndt N. T. (1999) Implications of 187Os isotopic heterogeneities in a mantle plume : Evidence from Gorgona Island and Curacao. *Geochim. Cosmochim. Acta* **63**, 713–728.

Walter M. J. (1998) Melting of garnet peridotite and the origin of komatiite and depleted lithosphere. *J. Petrol.* **39**, 29–60.

Warren P. H. (2011) Stable-isotopic anomalies and the accretionary assemblage of the Earth and Mars : A subordinate role for carbonaceous chondrites. *Earth Planet. Sci. Lett.* **311**, 93–100. Available at: http://dx.doi.org/10.1016/j.epsl.2011.08.047.

Wasson J. T., Choi B. G., Jerde E. A. and Ulff-Møller F. (1998) Chemical classification of iron meteorites: XII. New members of the magmatic groups. *Geochim. Cosmochim. Acta* **62**, 715–

724.

Wasson J. T. and Kallemeyn G. W. (1988) Compositions of Chondrites. *Philos. Trans. R. Soc.* **325**, 535–544. Available at: http://rsta.royalsocietypublishing.org/cgi/doi/10.1098/rsta.1988.0066.

Wasson J. T. and Richardson J. W. (2001) Fractionation frends among IVA iron meteorites: Constrast with IIIAB trends. *Geochim. Cosmochim. Acta* **65**, 951–970.

Wasson J. T. and Wang J. (1984) A nonmagmatic origin of group-IIE iron meteorites. *Geochim. Cosmochim. Acta* **50**, 725–732.

Weisberg M. K. and Kimura M. (2012) The unequilibrated enstatite chondrites. *Chemie der Erde* **72**, 101–115. Available at: http://dx.doi.org/10.1016/j.chemer.2012.04.003.

Weisberg M. K., Prinz M. and Fogel R. A. (1994) The evolution of enstatite and chondrules in unequilibrated enstatite chondrites : Evidence from iron-rich pyroxene. *Meteoritics* **313**, 362–373.

Weyer S., Anbar A. D., Brey G. P., Münker C., Mezger K. and Woodland A. B. (2005) Iron isotope fractionation during planetary differentiation. *Earth Planet. Sci. Lett.* **240**, 251–264.

Weyer S. and Ionov D. A. (2007) Partial melting and melt percolation in the mantle: The message from Fe isotopes. *Earth Planet. Sci. Lett.* **259**, 119–133.

Weyrauch M., Horstmann M. and Bischoff A. (2017) Chemical variations of sulfides and metal in enstatite chondrites — Introduction of a new classification scheme. *Meteorit. Planet. Sci.* **22**, 1–22.

Wieser M. E. and Schwieters J. B. (2005) The development of multiple collector mass spectrometry for isotope ratio measurements. *Int. J. Mass Spectrom.* **242**, 97–115.

Williams H. M., Peslier A. H., Mccammon C. and Halliday A. N. (2005) Systematic iron isotope variations in mantle rocks and minerals : The effects of partial melting and oxygen fugacity. **235**, 435–452.

Wilson A. H., Versfeld J. A. and Hunter D. R. (1989) Emplacement , crystallization and alteration of spinifex-textured komatiitic basalt flows in the Archaean Nondweni greenstone belt , southern

Kaapvaal Craton , South Africa. *Contrib. to Mineral. Petrol.* **101**, 301–317.

Wood B. J., Wade J. and Kilburn M. R. (2008) Core formation and the oxidation state of the Earth: Additional constraints from Nb, V and Cr partitioning. *Geochim. Cosmochim. Acta* **72**, 1415–1426. Available at: http://dx.doi.org/10.1016/j.gca.2007.11.036.

Wooley A. R. and Kempe D. (1989) Carbonatites: nomenclature, average chemical compositions and element distributions. In *Carbonatites Genesis and Evolution* (ed. K. Bell). Unwin Hyman, London. pp. 1–14.

Woosley S. E. ., Heger A. and Weaver T. A. (2002) On the evolution and explosion of massive stars. *Rev. Mod. Phys.* **74**, 1051–1071.

Xia J., Carlson R. W. and Zhang Q. (2015) Chromium Stable Isotope Composition of Meteorites. *Lunar Planet. Sci. Conf.* **46**, 0–1.

Xia J., Qin L., Shen J., Carlson R. W. and Ionov D. A. (2017) Chromium isotope heterogeneity in the mantle. *Earth Planet. Sci. Lett.* **464**, 103–115. Available at: http://dx.doi.org/10.1016/j.epsl.2017.01.045.

Yamakawa A., Yamashita K., Makishima A. and Nakamura E. (2010) CHROMIUM ISOTOPE SYSTEMATICS OF ACHONDRITES : CHRONOLOGY AND ISOTOPIC. *Astrophys. J.*, 150–154.

Yamashita K., Maruyama S., Yamakawa A. and Nakamura E. (2010) Mn – 53 Cr CHRONOMETRY OF CB CHONDRITE : EVIDENCE FOR UNIFORM DISTRIBUTION OF 53 Mn IN THE EARLY SOLAR SYSTEM. *53Mn-53Cr Chronom. CB chondrite Evid. unifrom Distrib. 53Mn Early Sol. Syst.* **3**, 20–24.

Yaxley G. M., Green D. H. and Kamenetsky V. (1998) Carbonatite Metasomatism in the Southeastern Australian Lithosphere. *J. Petrol.* **39**, 1917–1930. Available at: http://www.petrology.oxfordjournals.org/cgi/doi/10.1093/petroj/39.11-12.1917.

Yin Q., Jacobsen B., Moynier F. and Hutcheon I. D. (2007) Towars consistent chronology in the early Solar System. *Astrophys. J.* **662**, L43–L46.

Young E. D., Kohl I. E., Warren P. H., Rubie D. C., Jacobson S. A. and Morbidelli A. (2016) Oxygen

isotopic evidence for vigorous mixing during the Moon-forming giant impact. *Science (80-.).* **351**, 493–496.

Young E. D., Manning C. E., Schauble E. A., Shahar A., Macris C. A., Lazar C. and Jordan M. (2015) High-temperature equilibrium isotope fractionation of non-traditional stable isotopes: Experiments, theory, and applications. *Chem. Geol.* **395**, 176–195.

Zanda B., Bourot-Denise M., Perron C. and Hewins R. H. (1994) Origin and metamorphic redistribution of silicon, chromium, and phosphorus in the metal of chondrites. *Science (80-.).* **265**, 1846–1849.

Zhang Y., Benoit P. H. and Sears D. W. G. (1995) The classification and complex thermal history of the enstatite meteorites. *J. Geophyiscal Res.* **100**, 9417–9438.

Zhu K., Sossi P. A., Siebert J. and Moynier F. (2018) Chromium Stable Isotopic Insights into the Origin of the Volatile Element Depletion of Vesta. In *Lunar and Planetary Science Conference 50*

Zolotov M. Y., Sprague A. L., Hauck S. A., Nittler L. R., Solomon S. C. and Weider S. Z. (2013) The redox state, FeO content, and origin of sulfur-rich magmas on Mercury. *J. Geophys. Res.* **118**, 138–146.